UNIVERSITY OF CALIFORNIA,
IRVINE

Pincer Ligands for the Control of Metal Coordination Spheres

THESIS

submitted in partial satisfaction of the requirements
for the degree of

MASTER OF SCIENCE

in Chemistry

by

Francisco Joseph Gomez

Dissertation Committee:
Professor Andy S. Borovik, Chair
Professor Alan F. Heyduk
Associate Professor Jenny Y. Yang

2020

Table of Contents

List of Figures

List of Tables

Acknowledgements

First, and foremost, I must thank Prof. Dr. Andy S. Borovik for his mentorship during the time that I have been in his research group, despite my many faults.

I have learned a great deal of chemistry from many other professors in my time at the University of California, Irvine: Prof. Heyduk, Prof. Yang, Prof. Evans, Prof. Green, Prof. Van Vranken, Prof. Law, and Prof. Ribbe (in no particular order). I am especially grateful at this moment to Prof. Heyduk and Prof. Yang for their place in my thesis committee. The lessons I learned from Dir. Joe Ziller, Dir. Phillip Dennison, Dir. Felix Grun, and Benjamin Katz were no less important.

The work presented in Chapter 2 would not have been possible without the work of Dr. Qiang Yu. The work presented in Chapter 3 would not have been possible without the work of Dr. Sarah Cook. The work presented in Chapter 4 would not have been possible without the work of Prof. Dr. Justin “the Legend” Bogart.

Finalmente, presento unas gracias a mi sangre y a mi corazoncita. Las ofrendas de mi sangre para el futuro que sería en actual son sin número. Gracias a la otra parte de mi por su paciencia y por el junto viaje que viene. Oro por nuestras salud y por nuestras salvamento, en el nombre.

ABSTRACT OF THE THESIS

Pincer Ligands for the Control of Metal Coordination Spheres

by

Francisco Joseph Gomez

Master of Science in Chemistry

University of California, Irvine, 2020

Professor Andy S. Borovik, Chair

.

Metalloenzymes are efficient catalysts, operating both stereo- and regioselectively with high reaction rates at ambient temperatures in aqueous conditions. In order to generate synthetic catalysts which operate in similarly efficient pathways, it is useful to study biomimetic complexes which incorporate the techniques used by biological systems. In this report, several pincer ligand frameworks are used to incorporate the interplay between primary coordination sphere effects and secondary coordination sphere effects observed in metalloenzyme active sites. H_4dippy, which combines appendant dipeptides to create a chiral environment as well as distal hydrogen-bonding groups was prepared and used to generate $Cu^{II}H_2$dippy. Further experiments probed the oxidation of $Cu^{II}H_2$dippy with aqueous H_2O_2. A new phosphonamide bis(aminophenyl)amine ligand, H_3tap, was used to prepare a cobalt(II) complex with optical features consistent with a $[Co_2N_2]$ diamond core structure. Reaction with oxidants generated species with spectroscopic characteristics consistent with ligand oxidation and retention of a dinuclear complex. Finally, the redox-active sulfonamide bis(aminophenyl)amine, H_3ibaps, as

well as H_3tap, were used to generate putative iron(III) thiolate complexes. These complexes were studied by reaction with the oxo-transfer reagent isopropyl iodoxybenzoate and subsequent reaction with substrates.

Chapter 1

Introduction

There are several differences between the catalytic functions of metalloproteins and synthetic complexes. Metalloenzymes are efficient: they can operate both stereo- and regioselectively with high reaction rates at ambient temperatures in aqueous conditions. Synthetic complexes are more easily modified and scalable, and current high throughput plants based on synthetic catalysts operate at much higher yields than plants based on enzymatic or whole cell reactors.[1,2] The economies of scale inherent to industrial chemistry and manufacturing have necessitated the use of high volume synthetic metal complex systems, though study into biomimetic complexes present a pathway to adopting the techniques used successfully by enzymes in biological systems.

Biological metalloenzymes have evolved over millions of years across every form of life; because they arise from terrestrial elements, the nine most prevalent metal ions (Fe, Mn, Mg, Zn, Cu, Co, Ni, Mo, and W) are also inexpensive and relatively abundant in the earth's crust and/or seawater.[3–5] The process of evolution has resulted in enzymes whose structure and metal coordination permit highly efficient and selective reactivity while avoiding cytotoxicity. Industrial chemistry, on the other hand, relies heavily on metal or metal oxide heterogeneous catalysts.[6] While these are easily made on large scales, and permit facile separation from products and flow processes, many involve the use of precious metals (Table 1).

These catalysts tend to rely on precious metals because of their propensity to readily undergo two-electron oxidation and reduction processes, which are vital in organometallic chemistry. The more earth abundant first-row transition metal ions, however, are more likely to proceed via one-electron processes, which lead to unproductive radical processes. In biological

systems, radical processes are avoided through several factors, including site isolation, controlled stepwise one-electron processes, and redox-active cofactors. Site isolation in metalloenzymes prevents the premature quenching of reactive intermediates: for example, while ferric porphyrins readily dimerize to form μ-oxo bridged dimers, the same does not occur in iron hemeproteins because the ferric heme cofactor is immobilized in the protein superstructure.[7] Because many chemical processes proceed through two-electron steps, subsequent one-electron steps must be coupled for first-row transition metals.

Table 1. Some industrially important catalytic processes involving heterogeneous metal catalysts.[6]

Process	Main uses	Key Reaction	Typical catalyst(s)
Olefin Hydrogenation	Oil Refining	$C_2H_4 + H_2 \rightarrow C_2H_6$	Ni, Pt
Ammonia oxidation	Nitric Acid	$4NH_3 + 5O_2 \rightarrow 4NO + 6H_2O$	90% Pt-10% Rh wire gauze
Ethylene Oxide Production	Antifreeze	$C_2H_4 + ½O_2 \rightarrow (CH_2)_2O$	Ag on Al_2O_3
Catalytic reforming	Fuels	$n\text{-}C_6H_{14} \rightarrow i\text{-}C_6H_{14}$	Pt, Pt-Re, or Pt-Sn on acidic Al_2O_3 or zeolite
Vinyl acetate Production	Polymers	$C_2H_4 + CH_3COOH + ½O_2 \rightarrow CH_3COOCH{=}CH_2 + H_2O$	Pd on SiO_2 or Al_2O_3

One way that proteins accommodate large redox changes is through a combination of metal-based and redox-active ligand-based oxidation state changes. Cytochrome P450 is a classic example: during the hydroxylation of substrate, dioxygen binds to a ferrous heme cofactor to give a ferric superoxido complex.[8–10]

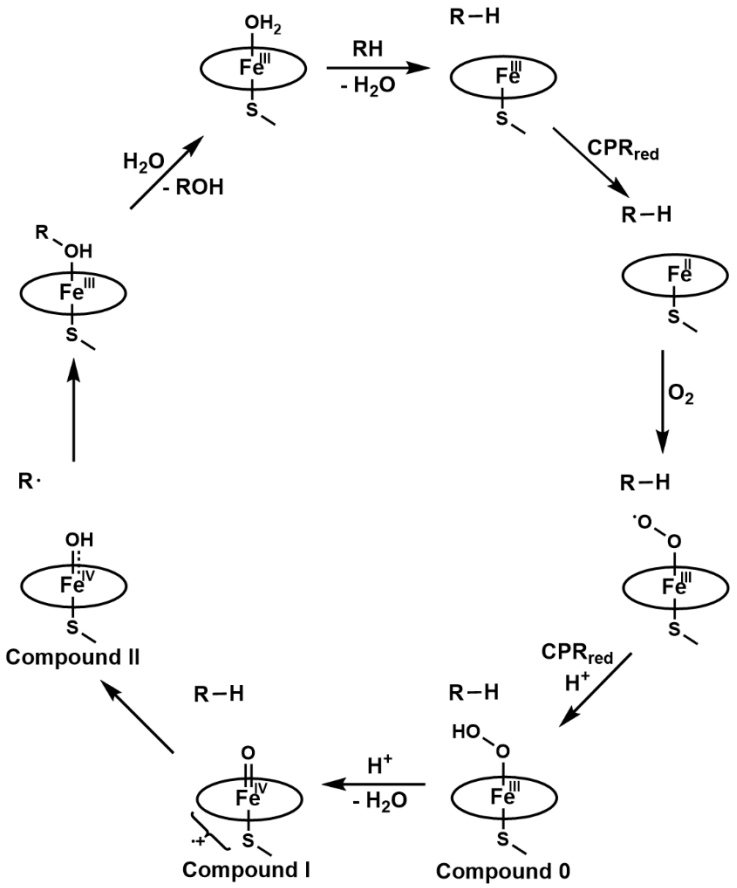

Scheme 1. Consensus mechanism of reaction for the reaction of Cytochrome P450 with substrate. CPR_{red} refers to reduced cytochrome P450 reductase, which acts as an electron shuttle from NADPH to cytochrome P450.[11]

One-electron reduction and subsequent protonation of this complex gives a ferric hydroperoxido complex which reacts through O—O bond cleavage to generate a formal perferryl oxido species. This perferryl species, however, is more accurately described as a ferryl center coupled to a ligand radical.[12] Ribonucleotide reductase is another example: ribonucleotides are converted to deoxyribonucleotides through a process catalyzed by a proximal thiyl radical.[13,14] This thiyl radical is generated by long-range electron transfer to a stable tyrosine radical generated during the reduction of dioxygen to water by a diiron cofactor. During the four-electron process of dioxygen reduction, three electrons are abstracted from the iron centers,

forming a mixed valence ferryl-ferric complex, while the last electron is believed to come from a nearby tryptophan residue.

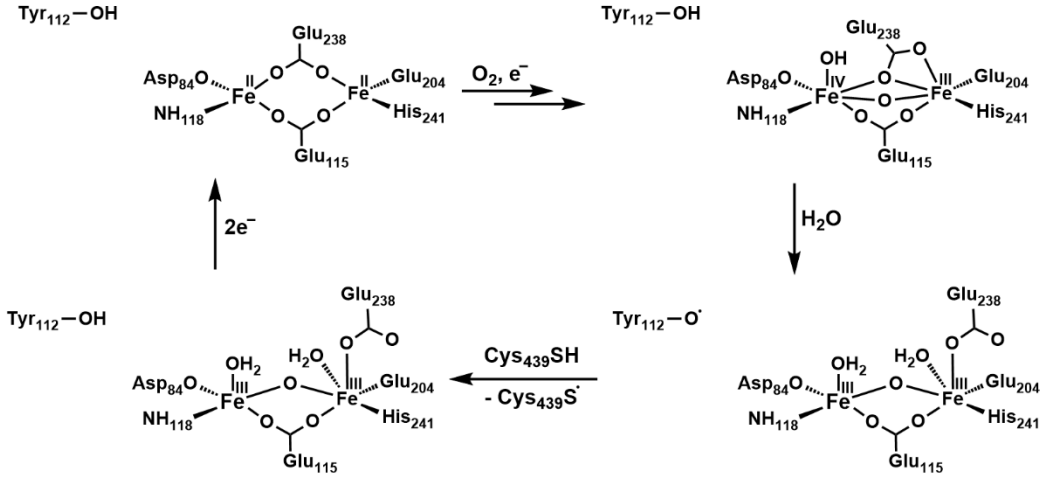

Scheme 2. Consensus mechanism of reaction for the reaction of the diiron cofactor of ribonucleotide reductase with dioxygen to form the stable tyrosine radical to generate the thiyl radical intermediate.

Previous work in the Borovik group has focused on the ability to secondary sphere effects to control the stability and reactivity of metal complexes. The characterization of $[Fe^{III}(O)]^{-2}$, $[Fe^{IV}(O)]^{-}$, $[Mn^{III}(O)]^{-2}$, $[Mn^{IV}(O)]^{-}$, $[Mn^{V}(O)]^{0}$ were aided by the use of hydrogen-bonding interaction in the secondary coordination sphere to stabilize the metal-oxido species.[15–21]

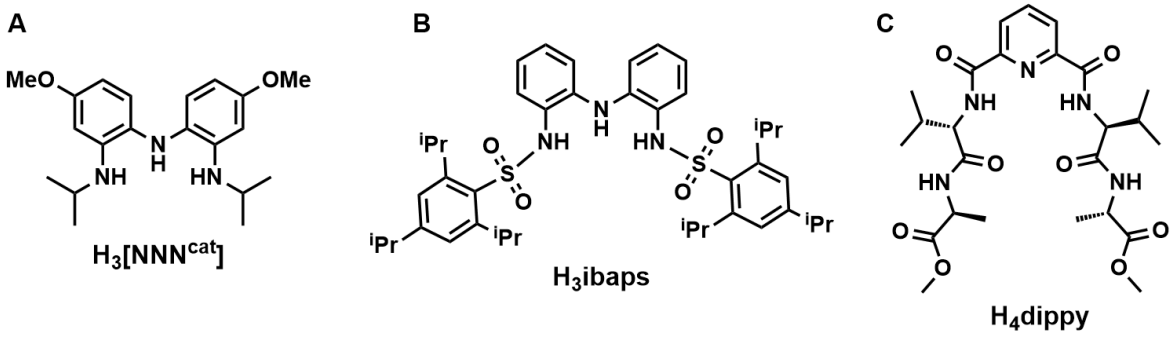

Scheme 3. (A) The bis(amidophenyl)amide ligand framework studied by the Heyduk group. (B) H_3ibaps, developed and studied by Cook and Bogart. (C) 2,6-dicarbonyl-L-valyl-L-methylalanine pyridine (here, H_4dippy), developed by Yu and studied further in this report.

Recent efforts have focused on incorporating hydrogen-bonding interactions into a tridentate redox-active ligand based on the bis(amidophenyl)amide ligand framework studied by the Heyduk group:[22–24] the ligand developed by Cook and further studied by Bogart included bulky aryl sulfonamido arms to prevent complex dimerization and to position hydrogen bond accepting groups in the secondary coordination sphere.[25] Several ligands designed to form supramolecular structures have also been developed, based on a pyridine dicarboxyamide ligand framework, which rely on intramolecular and intermolecular hydrogen bonding interactions to create chiral structures.

Chapter 2: Pursuit of a High-Valent Copper Pyridine Dicarboxyamide Complex

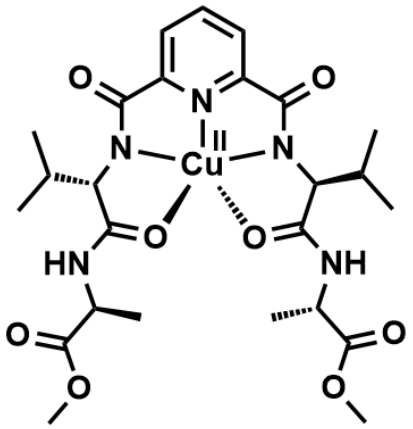

Scheme 4. $Cu^{II}H_2$dippy, studied in this chapter.

Lytic polysaccharide monooxygenases (LPMO) are a diverse class of enzymes that cleave polysaccharides through hydroxylation of the C–H bond geminal to a glycosidic bond, resulting in formation of a geminal diol which undergoes further hydrolysis.[26] These enzymes utilize a copper-based active site with T-shaped coordination provided by three endogenous N-atom donors, referred to as the "histidine brace". LPMO is traditionally understood to catalyze this reaction through reduction of dioxygen and formation of a reactive oxygen species; however, the mechanism is still unknown.[27] In modeling the copper complex of LPMOs, a pyridine

dicarboxyamide ligand with appendant dipeptide arms was investigated. This compound, 2,6-dicarbonyl-L-valyl-L-methylalanine pyridine, has been previously studied in the Borovik group, but its metal-binding properties were unknown.[28] This compound had several attractive qualities: the dipeptide arms contain both hydrogen bond accepting and hydrogen bond donating groups; alternate peptides may be incorporated to investigate various ligand properties; finally, the dianionic nature of the ligand may help to stabilize a high-valent copper complex. Therefore, this chapter focuses on the properties of a copper complex of 2,6-dicarbonyl-L-valyl-L-methylalanine pyridine (from here on, H_4dippy) and determine its ability to bind exogenous ligands and to stabilize higher oxidation states.

Chapter 3: Investigation of a Cobalt(II) Complex of a Redox-Active Phosphinamide Ligand

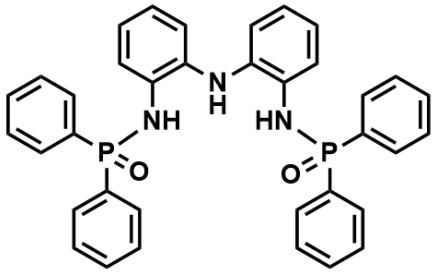

H_3tap

Scheme 5. H_3tap ligand developed and investigated in this chapter.

Previous work by Cook and Bogart resulted in the development of monometallic cobalt(II) and iron(II/III) complexes in a sulfonamide bis(aminophenyl)amine framework which exhibited reversible oxidations and reductions. Furthermore, these redox events demonstrated the redox non-innocence of this bis(aminophenyl)amine framework. In extending this work, the sulfonamides were replaced with phosphonamides, based on the work done in tripodal systems which showed that higher oxidation states could be supported with phosphonamide-based ligands than sulfonamide-based ligands.[29,30] This chapter describes work undertaken to study the

properties of a phosphonamide bis(aminophenyl)amine ligand and the preparation of a cobalt(II) complex in this ligand framework.

Chapter 4: Efforts towards Generation of High-Valent Iron-Thiolate Complexes in Redox-Active Bis(amidophenyl)amide Ligands

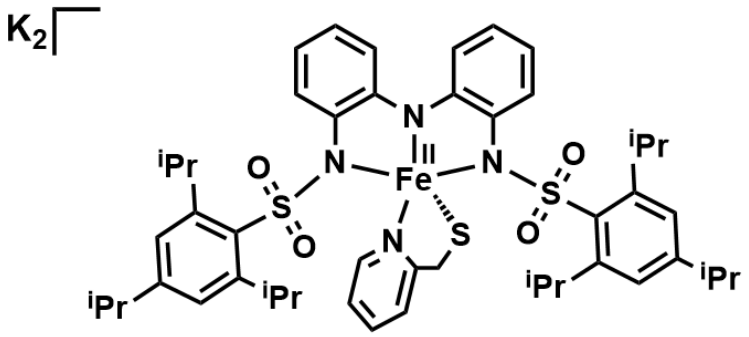

Scheme 6. $K_2[Fe^{II}ibaps(pyCH_2S)]$ complex synthesized by Bogart.

In further studies of the iron complexes of the H_3ibaps system, Bogart synthesized an iron(III) thiolate complex through synthesis of the $K_2[Fe^{II}ibaps(pyCH_2S)]$ followed by oxidation with ferrocenium tetrafluoroborate. This putative $[Fe^{III}ibaps(pyCH_2S)]^{-}$ species was characterized as having a $S = 5/2$ ground state by perpendicular-mode EPR spectroscopy at 77 K and exhibited two features in the visible spectrum at λ_{max} = 485 nm and 675 nm. This species was reactive with O_2 and was also noted to react with IBX-^{i}Pr, generating a complex with an intense feature in the visible spectrum at λ_{max} = 980 nm and an intense perpendicular-mode EPR signal at g = 2. This chapter aims to further investigate the properties of this iron(III)-thiolate complex and to compare them with the properties of the analogous complex prepared in the H_3tap ligand framework.

References

(1) Noe, S. A. Ammonia Synthesis Converter. 4,696,799, 1987.

(2) Schmid, A.; Dordick, J. S.; Hauer, B.; Kiener, A.; Wubbolts, M.; Witholt, B. Industrial

Biocatalysis Today and Tomorrow. *Nature* **2001**, *409* (6817), 258–268.

(3) Banci, L.; Bertini, I. Metallomics and the Cell: Some Definitions and General Comments. In *Metal Ions in Life Sciences*; Springer, Dordrecht, 2013; Vol. 12, pp 1–13.

(4) Buccella, D.; Lim, M. H.; Morrow, J. R. Metals in Biology: From Metallomics to Trafficking. *Inorg. Chem.* **2019**, *58* (20), 13505–13508.

(5) Williams, R. J. P.; da Silva, J. J. R. F. *The Chemistry of Evolution*; Elsevier, 2006.

(6) Ma, Z.; Zaera, F. Heterogeneous Catalysis by Metals. *Encycl. Inorg. Bioinorg. Chem.* **2006**, 1–18.

(7) McCandlish, E.; Miksztal, A. R.; Nappa, M.; Sprenger, A. Q.; Valentine, J. S.; Stong, J. D.; Spiro, T. G. Reactions of Superoxide with Iron Porphyrins in Aprotic Solvents. A High Spin Ferric Porphyrin Peroxo Complex. *J. Am. Chem. Soc.* **1980**, *102* (12), 4268–4271.

(8) Mansuy, D. Cytochrome P450 and Synthetic Models. *Pure Appl. Chem* **1987**, *59* (6), 759–770.

(9) Behan, R. K.; Hoffart, L. M.; Stone, K. L.; Krebs, C.; Green, M. T. Evidence for Basic Ferryls in Cytochromes P450. *J. Am. Chem. Soc*. **2006**, *128* (35), 11471–11474.

(10) Behan, R. K.; Green, M. T. On the Status of Ferryl Protonation. *J. Inorg. Biochem.* **2006**, *100* (4), 448–459.

(11) Lu, A. Y.; Junk, K. W.; Coon, M. J. Resolution of the Cytochrome P-450-Containing Omega-Hydroxylation System of Liver Microsomes into Three Components. *J. Biol. Chem.* **1969**, *244* (13), 3714–3721.

(12) Rittle, J.; Green, M. T. Cytochrome P450 Compound I: Capture, Characterization, and C-H Bond Activation Kinetics. *Science (80-.).* **2010**, *330* (6006), 933–937.

(13) Kolberg, M.; Strand, K. R.; Graff, P.; Kristoffer Andersson, K. Structure, Function, and Mechanism of Ribonucleotide Reductases. *Biochim. Biophys. Acta - Proteins Proteomics* **2004**, *1699* (1–2), 1–34.

(14) Nordlund, P.; Sjoberg, B.-M.; Eklund, H. Three-Dimensional Structure of the Free Radical Protein of Ribonucleotide Reductase. *Nature* **1990**, *345*, 593–598.

(15) Shirin, Z.; Hammes, B. S.; Young, V. G.; Borovik, A. S. Hydrogen Bonding in Metal Oxo Complexes: Synthesis and Structure of a Monomeric Manganese(III) - Oxo Complex and Its Hydroxo Analogue. *J. Am. Chem. Soc.* **2000**, *122* (8), 1836–1837.

(16) MacBeth, C. E.; Golombek, A. P.; Young, J.; Yang, C.; Kuczera, K.; Hendrich, M. P.; Borovik, A. S. O2 Activation by Nonheme Iron Complexes: A Monomeric Fe(III)-Oxo Complex Derived from O_2. *Science (80-.).* **2000**, *289* (5481), 938–941.

(17) MacBeth, C. E.; Gupta, R.; Mitchell-Koch, K. R.; Young, V. G.; Lushington, G. H.; Thompson, W. H.; Hendrich, M. P.; Borovik, A. S. Utilization of Hydrogen Bonds to Stabilize M-O(H) Units: Synthesis and Properties of Monomeric Iron and Manganese Complexes with Terminal Oxo and Hydroxo Ligands. *J. Am. Chem. Soc.* **2004**, *126* (8), 2556–2567.

(18) Parsell, T. H.; Behan, R. K.; Green, M. T.; Hendrich, M. P.; Borovik, A. S. Preparation and Properties of a Monomeric Mn^{IV}-Oxo Complex. *J. Am. Chem. Soc.* **2006**, *128* (27), 8728–8729.

(19) Lacy, D. C.; Gupta, R.; Stone, K. L.; Greaves, J.; Ziller, J. W.; Hendrich, M. P.; Borovik, A. S. Formation, Structure, and EPR Detection of a High Spin Fe^{IV}-Oxo Species Derived from Either an Fe^{III}-Oxo or Fe^{III}-OH Complex. *J. Am. Chem. Soc.* **2010**, *132* (35), 12188–12190.

(20) Taguchi, T.; Gupta, R.; Lassalle-Kaiser, B.; Boyce, D. W.; Yachandra, V. K.; Tolman, W. B.; Yano, J.; Hendrich, M. P.; Borovik, A. S. Preparation and Properties of a Monomeric High-Spin Mn^{V}-Oxo Complex. *J. Am. Chem. Soc.* **2012**, *134* (4), 1996–1999.

(21) Mann, S. I.; Heinisch, T.; Ward, T. R.; Borovik, A. S. Coordination Chemistry within a Protein Host: Regulation of the Secondary Coordination Sphere. *Chem. Commun* **2018**, *54*, 4413.

(22) Nguyen, A. I.; Blackmore, K. J.; Carter, S. M.; Zarkesh, R. A.; Heyduk, A. F. One- and Two-Electron Reactivity of a Tantalum(V) Complex with a Redox-Active Tris(Amido) Ligand. *J. Am. Chem. Soc.* **2009**, *131* (9), 3307–3316.

(23) Nguyen, A. I.; Zarkesh, R. A.; Lacy, D. C.; Thorson, M. K.; Heyduk, A. F. Catalytic Nitrene Transfer by a Zirconium(IV) Redox-Active Ligand Complex. *Chem. Sci.* **2011**, *2* (1), 166–189.

(24) Wong, J. L.; Sánchez, R. H.; Logan, J. G.; Zarkesh, R. A.; Ziller, J. W.; Heyduk, A. F. Disulfide Reductive Elimination from an Iron(III) Complex. *Chem. Sci.* **2013**, *4*, 1906–1910.

(25) Cook, S. A.; Bogart, J. A.; Levi, N.; Weitz, A. C.; Moore, C.; Rheingold, A. L.; Ziller, J. W.; Hendrich, M. P.; Borovik, A. S. Mononuclear Complexes of a Tridentate Redox-Active Ligand with Sulfonamido Groups: Structure, Properties, and Reactivity. *Chem. Sci.*

2018, *9* (31), 6540–6547.

(26) Beeson, W. T.; Vu, V. V; Span, E. A.; Phillips, C. M.; Marletta, M. A. Cellulose Degradation by Polysaccharide Monooxygenases. *Annu. Rev. Biochem* **2015**, *84*, 923–946.

(27) Kjaergaard, C. H.; Qayyum, F.; Wong, S. D.; Xu, F.; Hemsworth, G. R.; Walton, D. J.; Young, N. A.; Davies, G. J.; Walton, P. H.; Johansen, K. S.; et al. Spectroscopic and Computational Insight into the Activation of O_2 by the Mononuclear Cu Center in Polysaccharide Monooxygenases. *Proc. Natl. Acad. Sci.* **2014**, *111* (24), 8797–8802.

(28) Yu, Q.; Baroni, T. E.; Liable-Sands, L.; Rheingold, A. L.; Borovik, A. S. Synthesis and Structure of Chiral 2,6-Bis[(2-Carbamoylphenyl)Carbamoyl]Pyridine Ligands. *Tetrahedron Lett.* **1998**, *39* (38), 6831–6834.

(29) Oswald, V. F.; Weitz, A. C.; Biswas, S.; Ziller, J. W.; Hendrich, M. P.; Borovik, A. S. Manganese-Hydroxido Complexes Supported by a Urea/Phosphinic Amide Tripodal Ligand. *Inorg. Chem.* **2018**, *57* (21), 13341–13350.

(30) Oswald, V. F. Tripodal Phosphoryl Amide Farmeworks: Investigating the Relationship Between High Valent Metal-Oxido and Metal-Hydroxido Complexes., University of California, Irvine, 2018.

Chapter 2

Pursuit of a High-Valent Copper Pyridine Dicarboxyamide Complex

Abstract

The ability of lytic polysaccharide monooxygenases to utilize hydrogen peroxide (H_2O_2) as a cosubstrate for polysaccharide hydroxylation has inspired the development of a synthetic functional mimic. A ligand scaffold, H_4dippy, which combines appendant dipeptides to create a chiral environment, distal hydrogen-bonding groups to stabilize reactive intermediates, and a meridional metal binding pocket was synthesized and characterized. The copper complex of this ligand, $Cu^{II}H_2$dippy, was prepared and characterized through UV-vis, IR, and EPR spectroscopies, as well as cyclic voltammetry. A putative azide complex of $Cu^{II}H_2$dippy was prepared and characterized by UV-vis, IR, and EPR spectroscopies. A putative hydroxido complex of $Cu^{II}H_2$dippy was prepared and characterized by UV-vis, IR, and EPR spectroscopies. Reactivity studies of $Cu^{II}H_2$dippy with aqueous H_2O_2 resulted in the observation of a new spectral feature at λ_{max} = 420 nm, similar to the spectral features of $[NBu_4][Cu^{II}H_2dippy(N_3)]$. Subsequent EPR studies showed that over the course of the reaction between $Cu^{II}H_2$dippy and H_2O_2, a signal centered at g = 2 in the perpendicular-mode EPR spectrum significantly decreases in intensity, discounting the formation of a monomeric copper(II) peroxide species, while Evan's method studies support the formation of an S = 1 product.

Introduction

Lytic polysaccharide monooxygenases (LPMO) are a diverse class of enzymes that cleave polysaccharides through hydroxylation of the C–H bond geminal to a glycosidic bond, resulting in formation of a geminal diol which undergoes further hydrolysis.[1] These enzymes

utilize a copper-based active site with T-shaped coordination provided by three endogenous N-atom donors, referred to as the "histidine brace" (Figure 1).

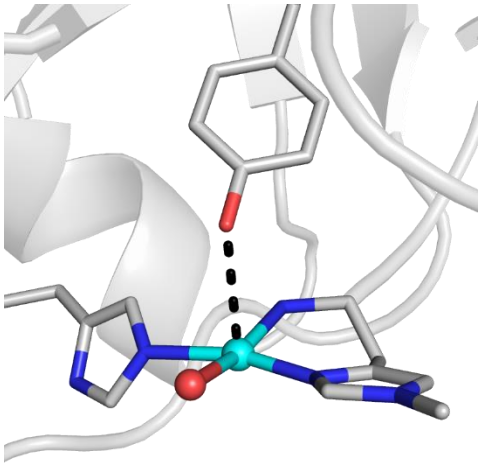

Figure 1. The active site of the oxidized form of *N. crassa* LPMO (PDB: 4EIS).

LPMOs are traditionally understood to catalyze this reaction through reduction of dioxygen and formation of a reactive oxygen species; however, the mechanism is still unknown.[2] A recent report by Bissaro and Eijsink suggest that H_2O_2 is the catalytically relevant substrate which performs the hydroxylation of the polysaccharide.[3] Moreover, computational studies by Walton and Hedegard support the viability of this pathway and invoke a copper oxyl species as the active intermediate (Figure 2).[4,5] A recent report by Marletta has attempted to discount this pathway, but more extensive studies will be required to fully resolve this issue.[6] In any case, the ability to use H_2O_2 as an oxidant to stereoselectively and regioselectively hydroxylate substrates is a subject of considerable interest.

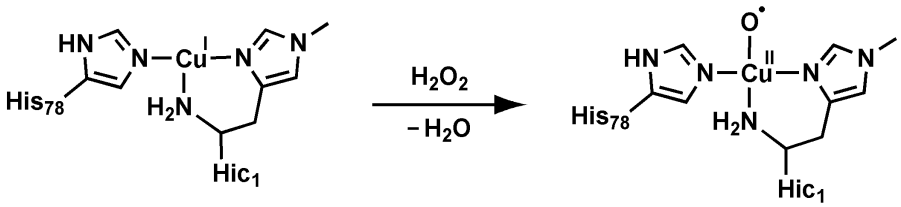

Figure 2. Proposed reaction between LPMO-Cu and H_2O_2 to form a copper(II) oxyl radical. Hic_1 represents the methylated N-terminal histidine.

A synthetic copper complex that can mimic this reactivity is an attractive target for several reasons: 1) the copper ion has three accessible oxidation states (copper(I), copper(II), and copper(III)); 2) copper complexes readily form coordinatively unsaturated species;[7,8] and 3) by electron paramagnetic resonance (EPR) spectroscopy, copper(II) has a g = 2 signal with a distinct four-line hyperfine splitting pattern and copper(I) and copper(III) are amenable to characterization by nuclear magnetic resonance (NMR) spectroscopy. A large body of work has accumulated in the realm of monomeric copper complexes of reactive oxygen species, both through reduction of dioxygen (O_2) and through binding of H_2O_2. Copper(II)-superoxido complexes have been investigated by both Karlin and Itoh, and the former observed hydrogen-atom abstraction of weak C–H bonds.[9,10] Moreover, both hydroperoxo and alkylperoxo complexes of copper(II) have been investigated, and in both cases hydrogen-atom abstraction chemistry was invoked.[11,12] Recent work by Tolman has explored the ability of copper(III) hydroxido complexes to activate C–H bonds.[13–15] Moreover, Margerum has reported numerous copper(III)-tripeptide complexes which are stable in aqueous solution at room temperature for extended periods of time.[16,17]

Previous work in the Borovik group has investigated a series of pyridine dicarboxyamide complexes with respect to ability to form supramolecular structures, and a number of copper(II) complexes, both fully chelated by the ligand as well as with bound exogenous ligands, were characterized.[18,19] A pyridine dicarboxyamide compound which incorporates appendant dipeptides has been previously prepared by the Borovik group, 2,6-dicarbonyl-L-valyl-L-methylalanine pyridine.[20] This compound, however, has not been extensively studied with respect to its metal-binding properties, despite several attractive qualities. The dipeptide arms may rotate to accommodate hydrogen-bond acceptance through the peptidyl carbonyls as well as

hydrogen-bond donation by the peptidyl amides. Additionally, these dipeptide arms are inherently chiral, which may assist in stereoselective reactivity. Finally, alternate peptides may be incorporated to examine various properties such as the influence of redox-active amino acid sidechains on reactivity or the interaction between hydrogen-bonding amino acid sidechains with substrate molecules. Therefore, this research proposes to investigate the properties of a copper complex of 2,6-dicarbonyl-L-valyl-L-methylalanine pyridine (from here on, H_4dippy) and determine its ability to bind exogenous ligands and its reactivity with H_2O_2.

Results and Discussion

Generation and Characterization of Metal Complexes of H_4dippy.

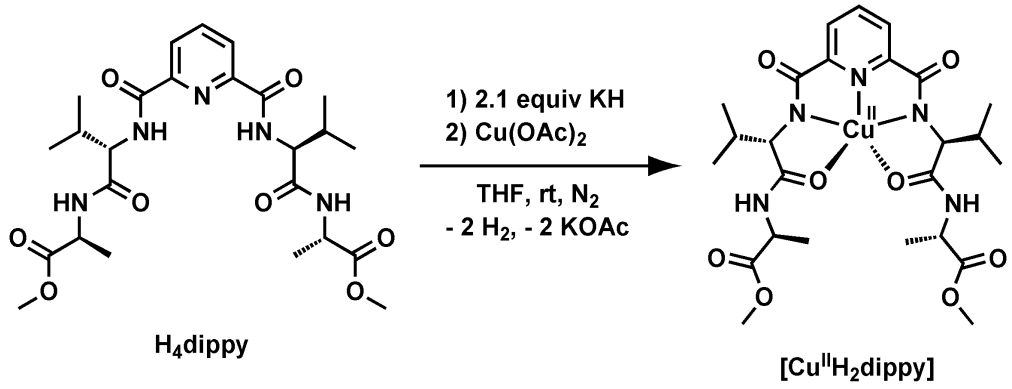

Scheme 1. Preparation of $Cu^{II}H_2$dippy.

H_4dippy was prepared through the coupling of N-Boc-L-valine and L-alanine methyl ester hydrochloride using pentafluorophenyl trifluoroacetate, followed by deprotection with trifluoroacetic acid. Finally, the dipeptide was reacted with 2,6-dicarbonyl-pyridine dichloride to give the ligand precursor, H_4dippy. H_4dippy was then used to prepare the metal complex synthon, $Cu^{II}H_2$dippy (Scheme 1). H_4dippy was deprotonated with potassium hydride (KH), followed by metalation with $Cu(OAc)_2$. $Cu^{II}H_2$dippy was characterized by UV-visible (UV-vis), Infrared (IR), and EPR spectroscopies. The optical spectrum of $Cu^{II}H_2$dippy contains one feature in the visible region with λ_{mas} = 640 nm (ε_M = 63 M^{-1} cm^{-1}) that is assigned as a *d-d* transition

based on the low value for its molar absorptivity. The EPR spectrum of $Cu^{II}H_2$dippy was fit as a rhombic S = ½ system with $g_1 = 2.022$, $g_2 = 2.085$, $g_3 = 2.226$, and $A_{Cu} = 430$ MHz (Figure 4).

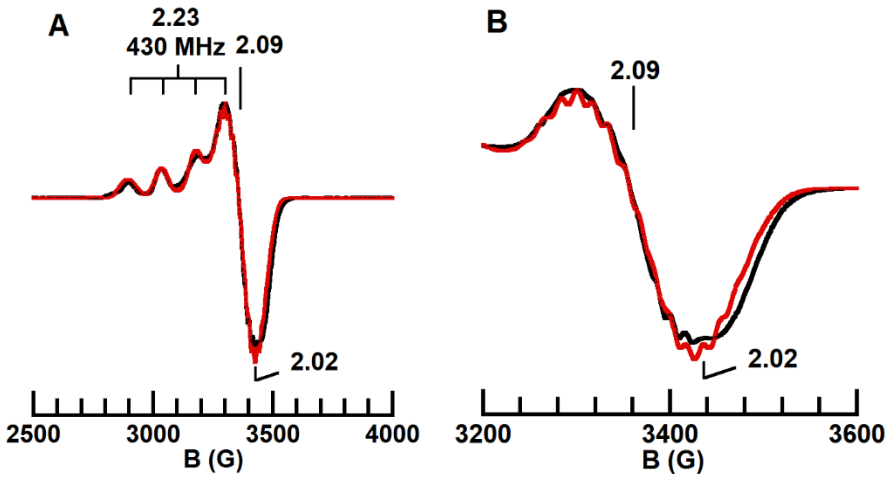

Figure 3. X-Band perpendicular-mode EPR spectrum of $Cu^{II}H_2$dippy (black) collected in 1:1 DMF/THF at 77 K and the simulation of the corresponding spectrum (red). Full spectrum (A) and zoom-in of the high field region (B).

N-hyperfine is subtly apparent in the EPR spectrum, primarily at the peak and trough of the derivative feature. Fitting of the spectrum based on the coupling constants of a related system ($A_{N,pyridine} = 40$ MHz, $A_{N,amide} = 53$ MHz) produced reasonable fits with a seven-line splitting pattern form [NNN] coordination.[21] Crystals suitable for X-ray diffraction studies were serendipitously grown in dichloromethane solution in the presence of tetraethylammonium chloride layered under diethyl ether. This crystal contained two distinct molecules in the asymmetric unit, both pentacoordinate copper(II) complexes, and two molecules of diethyl ether (Figure 5). These two molecules differ primarily in orientation of the carbonyl groups with respect to the [NNN] plane (Table 1). This orientation was measured by τ, which is a description of a five-coordinate geometry on a spectrum between purely square pyramidal (τ = 0) and purely trigonal bipyramidal (τ = 1). The two molecules were calculated to have τ = 0.20 and τ = 0.32, indicating distorted square pyramidal geometry.

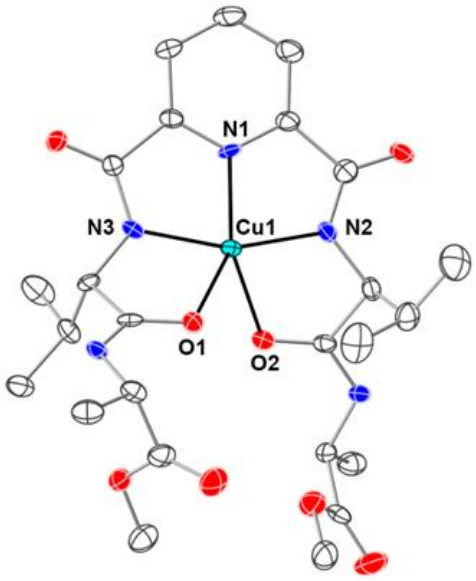

Table 1. Selected metrical parameters for $Cu^{II}H_2$dippy. The two molecules are distinguished by the † symbol.

Bond	Distance (Å)
Cu(1)–N(1)	1.942(2)
Cu(1) –N(2)	1.941(2)
Cu(1) –N(3)	1.987(4)
Cu(1) –O(1)	2.280(3)
Cu(1) –O(2)	2.177(7)
Cu(1†)–O(1†)	2.429(1)
Cu(1†)–O(2†)	2.051(4)
Bond Angle	**Degrees (°)**
N(1)-Cu(1)-O(2)	140.18
N(2)-Cu(1)-N(3)	159.52
N(1†)-Cu(1†)-O(2†)	148.53
N(2†)-Cu(1†)-N(3†)	160.05

Figure 4. Thermal ellipsoid plot of $Cu^{II}H_2$dippy. Ellipsoids are shown at the 50% probability level. Hydrogens and solvent molecules are removed for clarity. Only one molecule is shown for clarity. Bond lengths and bond angles of interest are included in the corresponding **Table 1**.

Electrochemical analysis of $Cu^{II}H_2$dippy (Figure 6) revealed an oxidative event at 0.010 V vs $[FeCp_2]^{+/0}$ at room temperature in THF (ΔE_p = 130 mV, $|i_{pa}/i_{pc}|$ = 2.0).

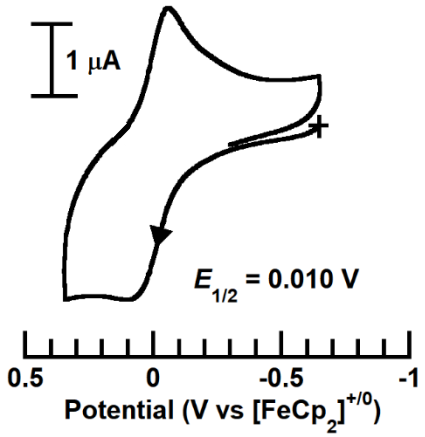

Figure 5. Cyclic voltammogram of $Cu^{II}H_2$dippy collected in THF with 0.1 M NBu_4PF_6 at 100 mV/s scan rate

Preparation and Characterization of [NBu_4][$Cu^{II}H_2$dippy(N_3)].

Addition of azide to $Cu^{II}H_2$dippy results in the *d-d* band in the visible region red-shifting slightly to λ_{max} = 654 nm (sh), and the formation of a charge transfer band at λ_{max} = 398 nm

(ε_M = 1100 M^{-1} cm^{-1}). These changes are consistent with previous work on copper azide species.[9,22] The EPR spectrum of [NBu_4][$Cu^{II}H_2$dippy(N_3)] was fit as a rhombic S = ½ system with g_1 = 2.040, g_2 = 2.058, g_3 = 2.213, and A_{Cu} = 555 MHz (Figure 7).

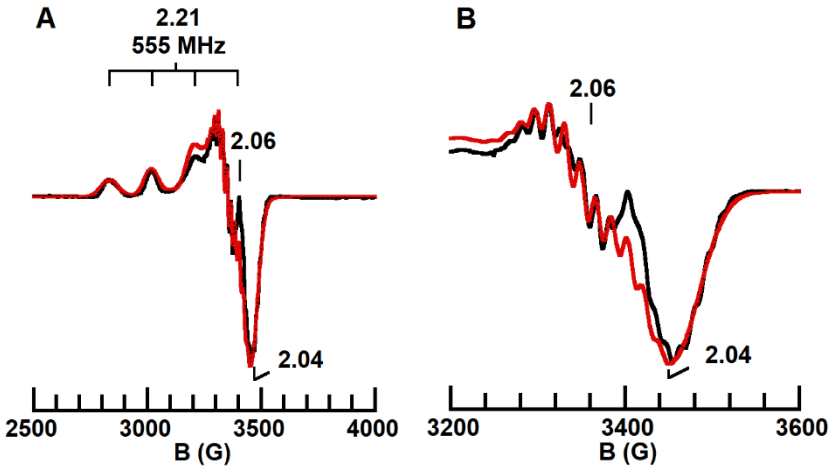

Figure 6. X-Band perpendicular-mode EPR spectrum of [NBu_4][$Cu^{II}H_2$dippy(N_3)] (black) and simulation of the corresponding spectrum (blue). Full spectrum (A) and zoom-in of the high field region (B).

Fitting of the high-field region in the EPR spectrum is consistent with a [NNNN] primary coordination sphere.

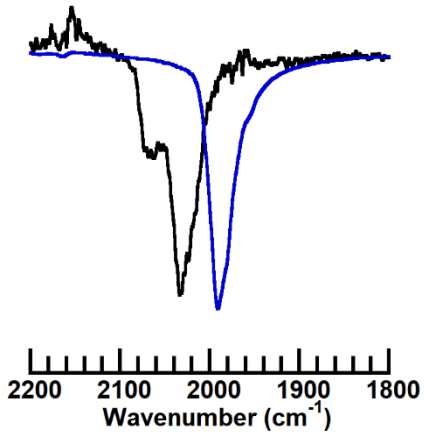

Figure 7. Overlaid solid-state IR spectra of [NBu_4][$Cu^{II}H_2$dippy(N_3)] (black) and NBu_4N_3 (blue).

The IR spectrum of [NBu_4][$Cu^{II}H_2$dippy(N_3)] contains an intense feature at ν = 2032 cm^{-1} attributed to an azide stretch based on comparison to the starting NBu_4N_3: this feature is shifted to higher energy by 42 cm^{-1}, from 1990 cm^{-1} for NBu_4N_3 (Figure 8).

Preparation of a Putative Copper(II) Hydroxido Complex

Addition of hydroxide to $Cu^{II}H_2$dippy results in the *d-d* band in the visible region blue-shifting to λ_{max} = 531 nm (ε_M = 110 M^{-1} cm^{-1}). The EPR spectrum of $[NMe_4][Cu^{II}H_2dippy(OH)]$ was preliminarily fit as a rhombic S = ½ system with g_1 = 2.029, g_2 = 2.060, g_3 = 2.174, and A_{Cu} = 590 MHz, and more extensive simulation work is needed to fit the splitting observed in the high-field region (Figure 9A). The IR spectrum of $[NMe_4][Cu^{II}H_2dippy(OH)]$ contains a shoulder feature at ν = 3392 cm^{-1}, which is not apparent in the IR spectrum of the precursor copper complex (Figure 9B). This result is consistent with previous work done in the Borovik group on a copper(II) hydroxide complex: the IR spectrum of $[HTBD][NBu_4][Cu^{II}ibaps(OH)]$ contains a feature at ν = 3300 cm^{-1} attributed to a hydroxide stretching mode.

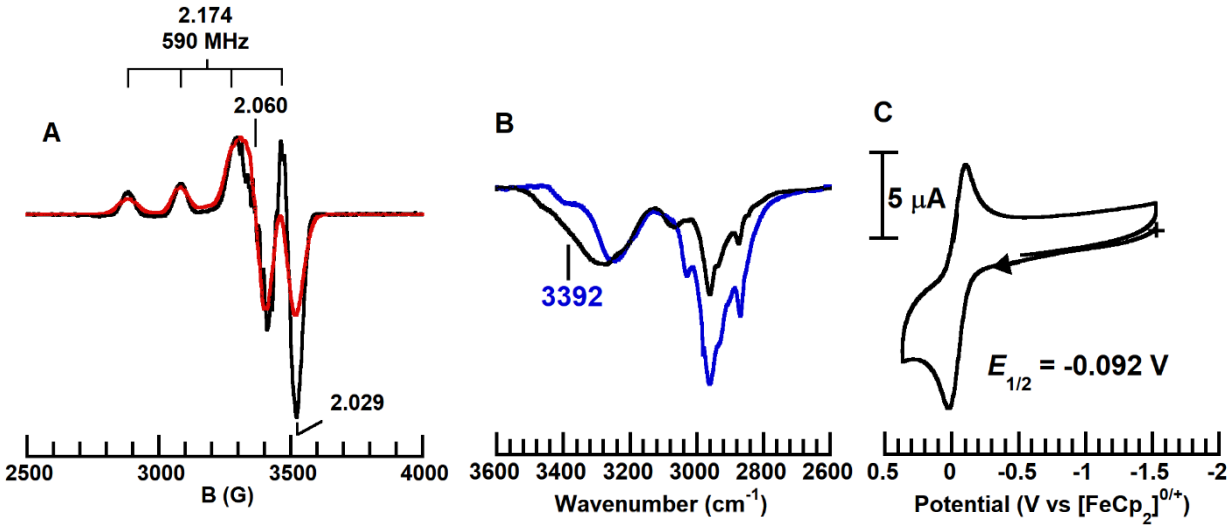

Figure 8. (A) X-band perpendicular-mode EPR spectrum (black) and simulation of the corresponding spectrum (red). (B) Overlaid solid-state IR spectra of $Cu^{II}H_2$dippy (black) and after the addition of hydroxide (blue). (C) Cyclic voltammogram collected in THF with 0.1 M NBu_4PF_6 at 100 mV/s scan rate.

Further work, especially isotopic labelling studies, will be required to confirm the identity of this feature. Electrochemical analysis (Figure 9C) was performed on $[NMe_4][Cu^{II}H_2dippy(OH)]$ and revealed an oxidative event at -0.092 V vs $[FeCp_2]^{0/+}$ at room

temperature in THF (ΔE_p = 125 mV, $|i_{pa}/i_{pc}|$ = 1.3). The sum of these observations support binding of an exogenous ligand, but further characterization will be needed to confirm both the identity of the ligand and the binding mode.

Reactivity of $Cu^{II}H_2$dippy with Oxidants.

The reactivity of $Cu^{II}H_2$dippy with aqueous H_2O_2 in dimethylformamide was studied through UV-vis and EPR spectroscopies (Figure 10). A starting blue solution of $Cu^{II}H_2$dippy (λ_{max} = 640 nm) was treated with ten equivalents of aqueous H_2O_2. The solution turns yellow-brown and the spectrum changes to reveal a shoulder near 420 nm. Aliquots taken from the stock solution and the final reaction mixture were studied by EPR spectroscopy.

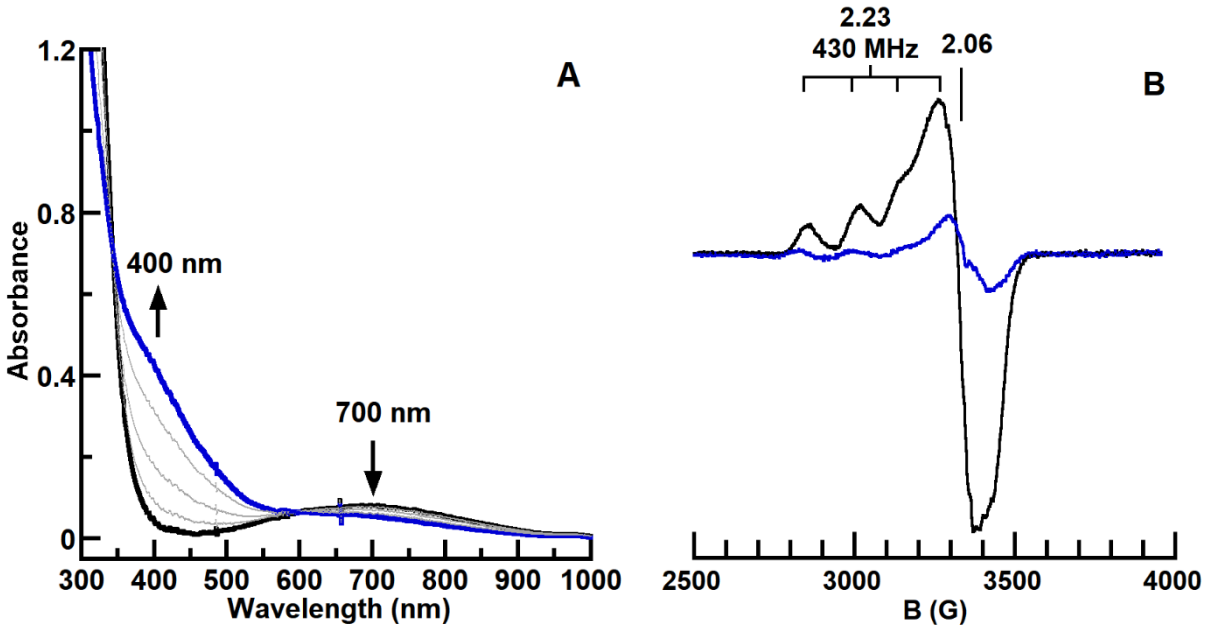

Figure 9. UV-vis spectra (A) and perpendicular-mode EPR spectra (B) of the reaction between $Cu^{II}H_2$dippy and H_2O_2 in DMF at 0 °C. Black (initial) and blue (final) spectra.

The perpendicular-mode EPR spectrum of $Cu^{II}H_2$dippy contains centered at g = 2 (Figure 10B: black trace). After treatment with H_2O_2, the signal centered at g = 2 is at significantly lower intensity (Figure 10B: blue trace). While the UV-vis spectral changes are consistent with previous reports of formation of copper peroxido complexes in non-acidic solution and the

spectral features of [NBu_4][$Cu^{II}H_2$dippy(N_3)], the loss of intensity in the perpendicular-mode EPR spectrum is inconsistent with formation of a monometallic copper(II) peroxido complex. Moreover, in the presence of base, no reaction is observed between $Cu^{II}H_2$dippy and H_2O_2, further suggesting that these spectral changes are not due to a bridging dicopper(II) peroxido complex. One explanation consistent with these observations is the formation of a formally Cu^{III} complex: the d^8 metal center would be expected to have square-planar geometry and be diamagnetic; the shoulder at 400 nm is similar to previously reported work on copper(III)-tripeptide complexes.[16]

Evan's method samples were prepared for $Cu^{II}H_2$dippy and $Cu^{II}H_2$dippy with 10 equivalents H_2O_2 in MeCN-d^3. The observed NMR shift for $Cu^{II}H_2$dippy is consistent with the expected S = ½ spin state (43.8 Hz observed; 42 Hz expected), while the observed NMR shift for the product of $Cu^{II}H_2$dippy and H_2O_2 was consistent with an S = 1 spin state (129.6 Hz observed; 129 Hz expected). This is inconsistent with the formation of a copper(III) species, which is expected to be square planar d^8 and diamagnetic. It is possible that the ligand is oxidized, rather than the metal center, which may be confirmed by X-ray absorption spectroscopy. The rising edge energy in the XANES region is related to the metal center oxidation state; small perturbations upon reaction with H_2O_2 less than 1 eV may indicate ligand-based oxidation, rather than metal-based oxidation.[23]

$Cu^{II}H_2$dippy was also reacted with acetylferrocenium tetrafluoroborate and examined by UV-vis and EPR spectroscopies (Figure 11). Upon addition of acetylferrocenium tetrafluoroborate to a solution of $Cu^{II}H_2$dippy in DCM at -80 °C, a new band with λ_{max} = 460 nm appears, which degrades quickly when warmed to room temperature.

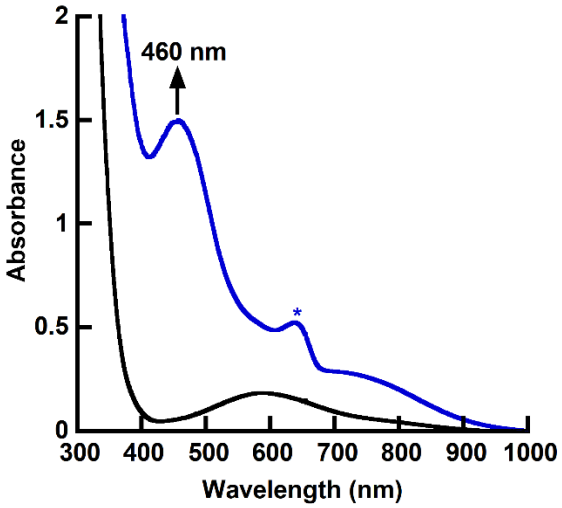

Figure 10. UV-vis spectra of the reaction between $Cu^{II}H_2$dippy and acetylferrocenium tetrafluoroborate in DCM at -80 °C. Black (initial) and blue (final) spectra. Asterisk indicates unreacted acetylferrocenium tetrafluoroborate.

This species gives a silent EPR spectrum in both the perpendicular and parallel mode. The distinct difference in temperature stability between this species and the product generated upon reaction with hydrogen peroxide indicates that the product of oxidation by acetylferrocenium is distinct from the product of reaction with hydrogen peroxide, and that hydrogen peroxide does not act as a simple one-electron oxidant with $Cu^{II}H_2$dippy.

Future Work

The binding modes of azide and hydroxide to $Cu^{II}H_2$dippy are currently unknown but may be uncovered through X-ray diffraction studies. The reaction product of $Cu^{II}H_2$dippy with H_2O_2 was characterized by Evan's method as an $S = 1$ species, while X-ray absorption spectroscopy may be used to probe the oxidation state of the copper center. While preliminary results have shown the ability to oxidize the putative hydroxide complex of $Cu^{II}H_2$dippy with ferrocenium and acetylferrocenium tetrafluoroborates, further studies are required to fully characterize these products. Finally, the ability of oxidized products of $Cu^{II}H_2$dippy to react with substrates such as substituted phenols and dihydroanthacene is of considerable interest.

Variants of the H_4dippy ligand platform have been proposed, particularly the inclusion of tyrosine or tryptophan amino acid residues to incorporate both redox non-innocent capabilities to the ligand as well as offer potential intramolecular substrates proximal to the oxidized metal center. Amino acid residues with hydrogen-bonding side-chains, such as the serine or asparagine amino acids thought to be important for substrate binding in LPMOs, are also of interest to poise substrates near the metal center.[24] Substrate binding in this way may be studied through circular dichroism spectroscopy, which is sensitive to the orientation of chiral species.

Experimental.

General Procedures. All reactions, unless otherwise noted, were performed under a nitrogen atmosphere in a dry box. All chemicals were purchased from commercial sources and used as received unless otherwise stated. Solvents were sparged with argon and dried over columns containing Q-5 and molecular sieves. Potassium hydride, as a 30% suspension in mineral oil, was filtered and washed with diethyl ether and pentane. Acetylferrocenium tetrafluoroborate was synthesized according to literature procedures.[25] Elementary analysis was not performed unless otherwise stated.

Synthesis of Ligand.

L-valyl-L-alanine methyl ester trifluoroacetate salt. The trifluoroacetate salt of L-valyl-L-alanine methyl ester was prepared by literature procedures with some modifications.[20,26,27] N-Boc-L-valine (3.00 g, 13.8 mmol) was added to a 250 mL flask under air in a fume hood and dissolved in dimethylformamide (60 mL) with stirring. Triethylamine (4.21 mL, 30.4 mmol) and pentafluorophenyl trifluoroacetate (2.85 mL, 16.6 mmol) were then added to the solution, accompanied with the solution rapidly changing color to pink. After 15 minutes, L-alanine methyl ester hydrochloride (1.93 g, 13.8 mmol) dissolved in dimethylformamide (30 mL) was

added to the solution and allowed to react for two hours. The final solution was yellow in color and was diluted with 450 mL ethyl acetate. This solution was then washed with water (3 x 200 mL) and brine (200 mL). The resulting organic fraction was dried over magnesium sulfate and concentrated on a rotary evaporator to give a yellow oil. This oil was diluted with dichloromethane (80 mL) and trifluoroacetic acid (20 mL) was added. This was reacted for four hours, at which point the solution was concentrated on a rotary evaporator and triturated with diethyl ether (100 mL) overnight, producing a white precipitate. Filtration over a glass frit produced L-valyl-L-alanine methyl ester trifluoroacetate salt (3.073 g, 9.716 mmol, 70% yield) as a white powder. ^{1}H NMR (500 MHz, CD_3CN): δ 7.25 (s, 1H, alanine amide), 4.44 (qd, 1H, J = 7.1, 7.2 Hz, alanine α-C), 3.78 (d, 1H, J = 4.8 Hz, valine α-C), 3.68 (s, 3H, methyl ester), 2.22 (m, valine side-chain methine), 1.37 (d, 3H, J = 7.5 Hz, alanine side-chain methyl), 1.02 (d, 3H, J = 7.2 Hz, valine side-chain methyl), 1.01 (d, 3H, J=7.0 Hz, valine side-chain methyl).

H_4dippy. 2,6-dicarbonyl-L-valyl-L-methylalanine pyridine was prepared by literature procedures with some modifications.[20] L-valyl-L-alanine methyl ester trifluoroacetate salt (3.07 g, 9.72 mmol) was dissolved in tetrahydrofuran (300 mL) with stirring. Triethylamine (3.37 mL, 24.3 mmol) was added, and the mixture was cooled to 0 °C. 2,6-dicarbonyl-pyridine dichloride (1.19 g, 5.83 mmol) dissolved in tetrahydrofuran (120 mL) was added to an addition funnel and added to the solution dropwise under nitrogen. The addition funnel was washed with additional tetrahydrofuran (30 mL) and this was also added dropwise under nitrogen to the reaction mixture. The ice bath was then removed, and the reaction warmed to room temperature, at which point it reacted for 24 hours. The solution was concentrated on a rotary evaporator, redissolved in ethyl acetate (350 mL) and washed with an NaOH solution (1 M, 3 x 75 mL), water (3 x 75 mL), and brine (75 mL). The organic fraction was dried over magnesium sulfate and

concentrated on a rotary evaporator to give H_4dippy as a white solid (2.398 g, 4.477 mmol, 92% yield) ^{1}H NMR (500 MHz, $CDCl_3$): δ 8.49 (d, 2H, J = 8.8 Hz, valine amide), 8.34 (d, 2H, J = 7.7 Hz, pyridine *m*-H), 8.05 (t, 1H, J = 7.7 Hz, pyridine *p*-H), 6.44 (d, 2H, J = 7.2 Hz, alanine amide), 4.61 (qd, 2H, J = 7.3, 7.2 Hz, alanine α-C), 4.44 (dd, 2H, J = 6.7, 8.9 Hz, valine α-C), 3.76 (s, 6H, methyl ester), 2.33 (m, 2H, J = 6.5, 6.8 Hz, valine methine), 1.42 (d, 6H, J = 7.2 Hz, alanine side-chain methyl), 1.07 (d, 6H, J = 6.5 Hz, valine side-chain methyl), 1.07 (d, 6H, J = 6.8 Hz, valine side-chain methyl).

Synthesis of Metal Complexes.

$Cu^{II}H_2$dippy. H_4dippy (100 mg, 0.187 mmol) was dissolved in tetrahydrofuran (10 mL) with stirring. KH (16 mg, 0.39 mmol) was added to the reaction mixed and allowed to react for 90 minutes. Gas evolution and a color change were observed. $Cu(OAc)_2$ (34 mg, 0.19 mmol) was added and allowed to react for a further three hours. The reaction mixture was then filtered on a glass frit to remove excess KH and precipitated KOAc, and the filtrate concentrated on a vacuum line to give a blue residue. This residue was redissolved in dichloromethane (5 mL) and filtered on a glass frit to remove excess $Cu(OAc)_2$. This filtrate was concentrated on a vacuum line to give $Cu^{II}H_2$dippy (107 mg, 0.179 mmol, 96% yield) as a blue solid. Blue crystals suitable for X-ray diffraction were grown in a dichloromethane solution in the presence of one equivalent of tetraethylammonium chloride layered under diethyl ether. λ_{max} (1:1 DMF/THF; ε_M, M^{-1} cm^{-1}) 640 nm (63). X-Band EPR (1:1 DMF/THF, 77K) $g_1 = 2.022$, $g_2 = 2.085$, $g_3 = 2.226$, $A_{Cu} = 430$ MHz, $A_N = 53, 40$ MHz. FTIR (ATR, selected bands cm^{-1}): 3266, 3058, 2961, 1741, 1655, 1582, 1517, 1444, 1378, 1206, 1159, 1052, 998, 977, 925, 844, 735.

[NBu_4][$Cu^{II}H_2$dippy(N_3)]. H_4dippy (134 mg, 0.250 mmol) was dissolved in tetrahydrofuran (10 mL) with stirring. Potassium hydride (21 mg, 0.52 mmol) was added to the reaction mixture and

allowed to react for 90 minutes. Gas evolution and a color change were observed. Copper(II) acetate (46 mg, 0.25 mmol) was added and allowed to react for a further three hours. Tetrabutylammonium azide (71 mg, 0.25 mmol) was added to the reaction mixture and allowed to react for two hours. This solution was filtered on a glass frit, concentrated on a vacuum line, and redissolved in dichloromethane (5 mL). This was filtered on a glass frit and concentrated on a vacuum line to give $[NBu_4][Cu^{II}H_2dippy(N_3)]$ as an orange-brown solid (181 mg, 0.205 mmol, 82% yield). λ_{max} (1:1 DMF/THF; ε_M, M^{-1} cm^{-1}) 398 nm (1100), 654 nm (sh). X-Band EPR (1:1 DMF/THF, 77 K) $g_1 = 2.040$, $g_2 = 2.058$, $g_3 = 2.213$, $A_{Cu} = 555$ MHz, $A_N = 53, 50, 40$ MHz. FTIR (ATR, selected bands cm^{-1}): 3230, 2961, 2873, 2061, 2032, 1738, 1663, 1577, 1515, 1456, 1376, 1205, 1155.

$[NMe_4][Cu^{II}H_2dippy(OH)]$. $Cu^{II}H_2dippy$ (55 mg, 0.092 mmol) was dissolved in tetrahydrofuran (5 mL) with stirring, and tetramethylammonium hydroxide (9 mg, 0.09 mmol) was added. This solution was allowed to react for one hour and concentrated on a vacuum line. The residue was washed with diethyl ether (5 mL) to remove excess tetramethylammonium hydroxide and produce $[NMe_4][Cu^{II}H_2dippy(OH)]$ as a purple solid (63 mg, 0.092 mmol, quantitative). λ_{max} (1:1 DMF/THF; ε, M^{-1} cm^{-1}) 531 nm (110). X-Band EPR (1:1 DMF/THF, 77 K) $g_1 = 2.029$, $g_2 = 2.060$, $g_3 = 2.174$, $A_{Cu} = 590$ MHz. FTIR (ATR, selected bands cm^{-1}): 3392, 3245, 3028, 2958, 1729, 1656, 1569, 1520, 1448, 1379, 1206, 1158, 1058, 1000.

Physical Methods. Electronic absorption spectra were collected on a Cary 60 spectrophotometer or an Agilent UV-vis spectrophotometer equipped with a Unisoku Unispeks cryostat in either a 1 cm quartz cuvette or a 1 mm thin cell quartz cuvette. X-Band (9.28 GHz) EPR spectra were collected as frozen solutions using a Bruker EMX spectrometer equipped with an ER041XG microwave bridge and the data was analyzed using SpinCount and fit using the EasySpin toolbox

for MATLAB.[28] Solid-state infrared spectra were collected on a Thermo Scientific Nicolet iS5 FT-IR spectrometer equipped with an iD5 ATR accessory. A Bruker SMART APEX-II diffractometer was used to collect crystallographic data. NMR spectra were collected on a Bruker DRX500 spectrometer.

Temperature-Controlled Reactivity Studies by UV-Vis Spectroscopy. For a standard experiment, a stock solution of the metal complex was prepared by dissolution in solvent. Solution (3 mL) was transferred to a 1 cm quartz cuvette equipped with a stirbar. The cuvette was then sealed with a rubber septum and transferred to a UV-vis spectrophotometer and allowed to thermally equilibrate for 15 minutes. Additional reagents were then added via gas-tight syringe. In certain cases, aliquots were removed to prepare samples for EPR spectroscopy.

Evan's Method Studies. For these studies, a capillary filled with acetonitrile was placed into an NMR tube along with a known amount of a solution of the compound of interest in d^3-acetonitrile. NMR spectra were collected on a Bruker DRX500 spectrometer, and the difference in frequency between the two intense acetonitrile solvent peaks was measured and compared to the frequency difference expected based on spin-only magnetic susceptibility.

References

(1) Beeson, W. T.; Vu, V. V; Span, E. A.; Phillips, C. M.; Marletta, M. A. Cellulose Degradation by Polysaccharide Monooxygenases. *Annu. Rev. Biochem* **2015**, *84*, 923–946.

(2) Kjaergaard, C. H.; Qayyum, F.; Wong, S. D.; Xu, F.; Hemsworth, G. R.; Walton, D. J.; Young, N. A.; Davies, G. J.; Walton, P. H.; Johansen, K. S.; et al. Spectroscopic and Computational Insight into the Activation of O_2 by the Mononuclear Cu Center in Polysaccharide Monooxygenases. *Proc. Natl. Acad. Sci.* **2014**, *111* (24), 8797–8802.

(3) Bissaro, B.; Rohr, A. K.; Muller, G.; Chylenski, P.; Skaugen, M.; Forsberg, Z.; Horn, S.

J.; Vaaje-Kolstad, G.; Eijsink, V. G. H. Oxidative Cleavage of Polysaccharides by Monocopper Enzymes Depends on H_2O_2. *Nat. Chem. Biol.* **2017**, *13*, 1123–1128.

(4) Wang, B.; Johnston, E. M.; Li, P.; Shaik, S.; Davies, G. J.; Walton, P. H.; Rovira, C. QM/MM Studies into the H_2O_2-Dependent Activity of Lytic Polysaccharide Monooxygenases: Evidence for the Formation of a Caged Hydroxyl Radical Intermediate. *ACS Catal.* **2018**, *8*, 1346–1351.

(5) Hedegård, E. D.; Ryde, U. Molecular Mechanism of Lytic Polysaccharide Monooxygenases. *Chem. Sci.* **2018**, *9*, 3866–3880.

(6) Hangasky, J. A.; Iavarone, A. T.; Marletta, M. A.; Karlin, K. D.; Stubbe, J. Reactivity of O_2 versus H_2O_2 with Polysaccharide Monooxygenases. *Proc. Natl. Acad. Sci.* **2018**, *115* (19), 4915–4920.

(7) Melník, M.; Kabešová, M.; Dunaj-Jurčo, M.; Holloway, C. E. Copper(II) Coordination Compounds: Classification and Analysis of Crystallographic and Structural Data I. Mononuclear Tetra- and Pentacoordinate Compounds. *J. Coord. Chem.* **1997**, *41* (2), 35–182.

(8) Melník, M.; Kabešová, M.; Macášková, Ľ.; Holloway, C. E. Copper(II) Coordination Compounds: Classification and Analysis of Crystallographic and Structural Data II. Mononuclear-, Hexa-, Hepta- and Octacoordinate Compounds. *J. Coord. Chem* **1998**, *45*, 31–145.

(9) Bhadra, M.; Yoon, J.; Lee, C.; Cowley, R. E.; Kim, S.; Siegler, M. A.; Solomon, E. I.; Karlin, K. D. Intramolecular Hydrogen Bonding Enhances Stability and Reactivity of Mononuclear Cupric Superoxide Complexes. *J. Am. Chem. Soc* **2018**, *140*, 9042–9045.

(10) Kobayashi, Y.; Ohkubo, K.; Nomura, T.; Kubo, M.; Fujieda, N.; Sugimoto, H.; Fukuzumi, S.; Goto, K.; Ogura, T.; Itoh, S. Copper(I)-Dioxygen Reactivity in a Sterically Demanding Tripodal Tetradentate Tren Ligand: Formation and Reactivity of a Mononuclear Copper(II) End-On Superoxo Complex. *Eur. J. Inorg. Chem.* **2012**, *2012* (29), 4574–4578.

(11) Maiti, D.; Sarjeant, A. A. N.; Karlin, K. D. Copper-Hydroperoxo-Mediated N-Debenzylation Chemistry Mimicking Aspects of Copper Monooxygenases. *Inorg. Chem.* **2008**, *47*, 8736–8747.

(12) Kunishita, A.; Ishimaru, H.; Nakashima, S.; Ogura, T.; Itoh, S. Reactivity of Mononuclear Alkylperoxo Copper(II) Complex. O-O Bond Cleavage and C-H Bond Activation. *J. Am. Chem. Soc.* **2008**, *130*, 4244–4245.

(13) Donoghue, P. J.; Tehranchi, J.; Cramer, C. J.; Sarangi, R.; Solomon, E. I.; Tolman, W. B. Rapid C—H Bond Activation by a Monocopper(III)—Hydroxide Complex Chart. *J. Am. Chem. Soc* **2011**, *133*, 26.

(14) Dhar, D.; Tolman, W. B. Hydrogen Atom Abstraction from Hydrocarbons by a Copper(III)-Hydroxide Complex. *J. Am. Chem. Soc.* **2015**, *137* (3), 1322–1329.

(15) Dhar, D.; Yee, G. M.; Spaeth, A. D.; Boyce, D. W.; Zhang, H.; Dereli, B.; Cramer, C. J.; Tolman, W. B. Perturbing the Copper(III)-Hydroxide Unit through Ligand Structural Variation. *J. Am. Chem. Soc.* **2016**, *138* (1), 356–368.

(16) Kirksey, S. T. J.; Neubecker, T. A.; Margerum, D. W. Thermally Stable Copper(III)- and Nickel(III)-Tripeptide Complexes and Their Photochemical Decomposition in Acid Solution. *J. Am. Chem. Soc.* **1979**, *101* (6), 1631–1633.

(17) Diaddario, L. L.; Robinson, W. R.; Margerum, D. W. Crystal and Molecular Structure of the Copper(III)-Tripeptide Complex of Tri-α-Aminoisobutyric Acid. *Inorg. Chem* **1983**, *22* (7), 1021–1025.

(18) Kawamoto, T.; Prakash, O.; Ostrander, R.; Rheingold, A. L.; Borovik, A. S. Metallohelices: Effects of Weak Interactions on Helical Morphology. *Inorg. Chem.* **1995**, *34*, 4294–4295.

(19) Kawamoto, T.; Hammes, B. S.; Haggerty, B.; Yap, G. P. A.; Rheingold, A. L.; Borovik, A. S. Synthesis and Structure of Helical Supramolecular Arrays. *J. Am. Chem. Soc.* **1996**, *118*, 285–286.

(20) Yu, Q.; Baroni, T. E.; Liable-Sands, L.; Yap, G. P. A.; Rheingold, A. L.; Borovik, A. S. Hydrogen Bonded Antiparallel β-Strand Motifs Promoted by 2,6-Bis(Carbamoylpeptide)Pyridine. *Chem. Commun.* **1999**, *53* (16), 1467–1468.

(21) Tehranchi, J.; Donoghue, P. J.; Cramer, C. J.; Tolman, W. B. Reactivity of (Dicarboxamide)M^{II}-OH (M = Cu, Ni) Complexes - Reaction with Acetonitrile to Yield M^{II}-Cyanomethides. *Eur. J. Inorg. Chem.* **2013**, *2013* (22–23), 4077–4084.

(22) Mann, S. I.; Heinisch, T.; Ward, T. R.; Borovik, A. S. Coordination Chemistry within a Protein Host: Regulation of the Secondary Coordination Sphere. *Chem. Commun* **2018**, *54*, 4413.

(23) Lim, H.; Thomas, K. E.; Hedman, B.; Hodgson, K. O.; Ghosh, A.; Solomon, E. I. X-Ray Absorption Spectroscopy as a Probe of Ligand Noninnocence in Metallocorroles: The Case of Copper Corroles. *Inorg. Chem.* **2019**, *58* (10), 6722–6730.

(24) Bertini, L.; Breglia, R.; Lambrughi, M.; Fantucci, P.; De Gioia, L.; Borsari, M.; Sola, M.; Bortolotti, C. A.; Bruschi, M. Catalytic Mechanism of Fungal Lytic Polysaccharide Monooxygenases Investigated by First-Principles Calculations. *Inorg. Chem* **2018**, *57*, 0.

(25) Connelly, N. G.; Geiger, W. E. Chemical Redox Agents for Organometallic Chemistry. *Chem. Rev.* **1996**, *96* (2), 877–910.

(26) Green, M.; Berman, J. Preparation of Pentafluorophenyl Esters of FMOC Protected Amino Acids with Pentafluorophenyl Trifluoroacetate. *Tetrahedron Lett.* **1990**, *31* (41), 5851–5852.

(27) Hartwig, S.; Nguyen, M. M.; Hecht, S. Exponential Growth of Functional Poly(Glutamic Acid) Dendrimers with Variable Stereochemistry. *Polym. Chem* **2010**, *1*, 69–71.

(28) Stoll, S.; Schweiger, A. EasySpin, a Comprehensive Software Package for Spectral Simulation and Analysis in EPR. **2005**.

Chapter 3

Investigation of a Cobalt(II) Complex of a Redox-Active Phosphinamide Ligand

Abstract

C–H bond activation and small molecule activation are synthetically difficult reactions that involve multiple electrons. Many organometallic catalysts used to perform these reactions contain second- and third-row transition metals because of their ability to readily undergo two-electron processes. The more earth-abundant first row transition metals, however, are often limited to one-electron oxidations and reductions. Redox-active ligands which can act as redox sources or sinks in coordination with metal-based oxidation or reduction have been developed to enable a first-row transition metal complex to readily undergo multi-electron chemistry. In this report, a Co(II) complex of a new phosphonamide bis(aminophenyl)amine ligand is studied, with optical features consistent with a $[Co_2N_2]$ diamond core structure. The cyclic voltammetry reveals two low-lying oxidative events at -0.80 V and -0.57 V vs $[FeCp_2]^{+/0}$. These were probed with chemical oxidants, generating species with spectroscopic characteristics characteristic of ligand oxidation and maintenance of a dinuclear complex.

Introduction

Many chemical transformations occur through two-electron chemistry, such as C–H bond activation, olefin metathesis, and hydrogenation. Metal catalysts have been developed to perform this chemistry both selectively and in high yields, but these tend to use second- and third-row transition metals such as platinum,[1] ruthenium,[2] and iridium,[3] which face a high risk of supply restriction.[4,5] While second- and third-row transition metal complexes readily undergo two-electron oxidation and reduction reactions, first-row transition metal complexes tend to undergo one-electron oxidation and reduction reactions. These one-electron redox steps promote radical

pathways, which are inherently less selective because of the propensity for radicals to engage in unproductive side reactions.

One recent synthetic approach has focused on the development of redox active ligands which can act as electron sources or sinks in coordination with a first-row or early transition metal (Figure 1).[6] The Heyduk group has pioneered the use of redox-active ligands to enable redox chemistry for d^0 metal complexes, such as zirconium(IV) and tantalum(V). A zirconium(IV) bis(amidophenyl)amide complex was prepared which reduces aryl azides to give a zirconium(IV) imido product which acts as a nitrene transfer reagent to isonitrile.[7] A tantalum(V) bis(amidophenyl)amide complex was also observed to reduce aryl azides to generate the analogous tantalum(V) imido product.[8,9] Recently, the Heyduk group has also reported a bis(phenylthiolato)amine nickel(II) complex which exhibited hydrogen atom non-innocence, where the N–H bond of the ligand was homolytically cleaved by TEMPO•, as well as a bis(2-phenol)amine-derived iron(III) quinonate complex which oxidatively coupled thiols to disulfides.[10,11]

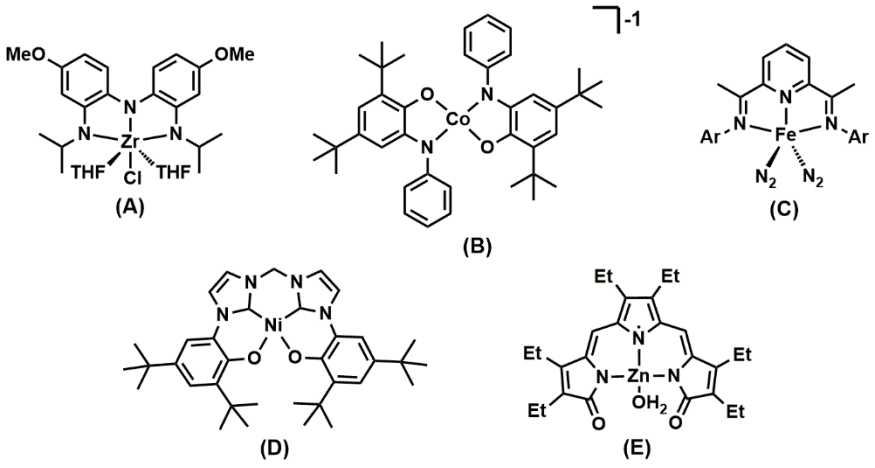

Scheme 1. Example complexes of redox-active ligands. (A) A Zr(IV) complex from the Heyduk group.[7] (B) A cobalt(III) complex from the Soper group.[12] (C) An Fe(II) complex from the Chirik group.[13] (D) A Ni(II) complex from the Thomas group.[14] (E) A Zn(II) complex from the Tomat group.[15]

The Soper group has also investigated a cobalt bis-iminophenolate complex which reductively couples alkyl halides and organozinc reagents, among others.[12,16,17] The Chirik group has developed an iron pyridinediimine complex which enables C–C bond formation with dienes, enynes, and diynes.[13,18] The Thomas group has developed a bis(phenol)-N-heterocyclic carbene nickel(II) complex which undergoes two ligand-based oxidations but experiences a redox tautomerization when pyridine is added to the one-electron product, generating a novel N-heterocyclic carbene Ni(III) complex.[14] The Tomat group has reported a Zn(II) tripyrrindione radical complex which exhibits fluorescence at room temperature.[15]

A variant of the bis(aminophenyl)amine ligand has been studied by Macbeth, incorporating amide functional groups, and was shown to generate dinuclear diamond-core cobalt(II) complexes[19–21]. These complexes were able to catalytically oxidize triphenylphosphine to triphenylphosphine oxide in the presence of dioxygen through the formation of a monometallic ligand radical-cobalt(II)-superoxido complex, as well as catalyze intramolecular C—H amination of aryl azides. Cook also investigated two sulfonamide variants of this ligand, exploring the unexpected metal binding properties of a tolyl sulfonamide ligand, H_3tbaps and a tris-isopropylphenyl sulfonamide ligand, H_3ibaps.[22] The dicopper complex of H_3tbaps exhibited an EPR spectrum characteristic of an $S = ½$ complex in both the solid state and in solution, suggesting a lack of magnetic coupling despite the short Cu—Cu distance of 2.53 Å. The diiron complex of H_3tbaps, however, exhibited ferromagnetic coupling with an $S = 4$ ground state, while the dicobalt complex of H_3tbaps exhibited anti-ferromagnetic coupling. This report aims to study the properties of metal complexes with a new phosphonamide bis(aminophenyl)amine ligand. Based on the work done on related tripodal systems, metal complexes may be supported

in higher oxidation states with phosphonamide-based ligands than are observed with sulfonamide-based ligands.[23,24]

Results and Discussion

Generation and Characterization of Cobalt Complexes of H_3tap.

The synthesis of the pre-ligand, H_3tap, was based on a modified version of a previous preparation,[22] and involved reacting the triamine, 2,2'-diamino-diphenylamine, with two equivalents of diphenylphosphinic chloride to give the final product, 2,2'-bis(diphenylphosphinamido)-diphenylamine (H_3tap). This product has been characterized by ^{1}H, ^{13}C, and ^{31}P NMR spectroscopies, as well as electrospray ionization mass spectrometry (ESI-MS) and Fourier transform infrared spectroscopy (FTIR). All expected resonances were observed in the ^{13}C and ^{31}P NMR spectra, while in the ^{1}H NMR spectrum the resonances due to N—H bonds were absent. This may be due to D_2O contamination of d^6-DMSO used as the NMR solvent: D_2O exchanges with acidic protons on NMR-active compounds, leading to lowered intensity. H_3tap is detected by ESI-MS as the sodium adduct, $[H_3tap + Na]^+$, at 622.1789 m/z. Finally, the FTIR spectrum of H_3tap contains broad, moderately intense peaks at 2850 and 2580 cm^{-1} (Figure 1). The triamine, 2,2'-diphenylamino-diphenylamine, has strong vibrational absorptions at ν = 3413, 3374, and 3344 cm^{-1}, associated with the N–H stretching vibration of an arylamine.[19] These features are missing in the FTIR spectrum of H_3tap: the broadness of these features, as well as their significant shifts to lower energies, supports the formation of strong hydrogen bonding interactions in the ligand precursor. Moreover, the vibrational absorptions at 1166 and 1124 cm^{-1} are consistent with P—O bond stretching modes.[25]

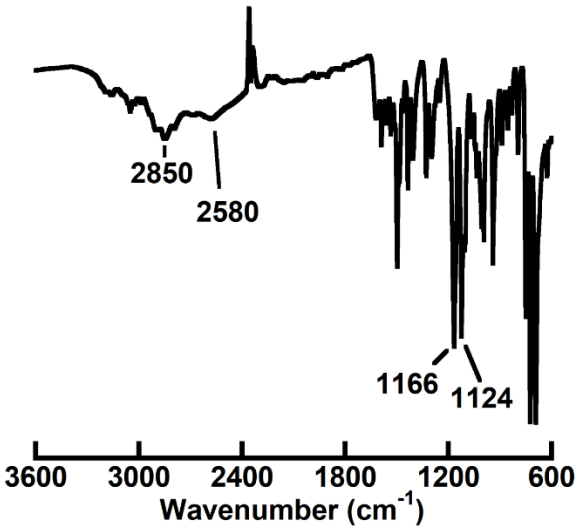

Figure 1. FTIR spectrum of H_3tap.

When generating the Co(II) complex of $[tap]^{-3}$, both the potassium salt and the tetraethylammonium salt have been used. To generate the potassium salt, H_3tap was dissolved in dimethylacetamide (DMA), deprotonated with three equivalents of potassium hydride and metalated with cobalt bromide. To generate the tetraethylammonium salt, H_3tap was instead deprotonated with three equivalents of sodium hydride and metalated with cobalt bromide, followed by cation metathesis using tetraethylammonium bromide. In both cases, the solution was then filtered and purified by layering under diethyl ether. The resulting mother liquor was concentrated by vacuum and layered under a pentane-diethyl ether mixture to give the metal complex as a powder in moderate yield (50—54 %). The Co(II) complexes were characterized by UV-vis and FTIR spectroscopies, as well as cyclic voltammetry.

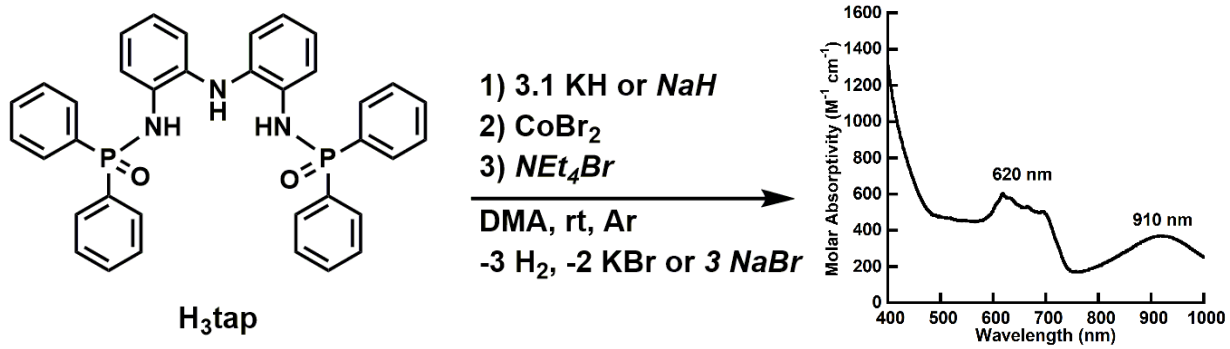

Figure 2. Synthetic procedure for generation of a Co(II) complex of $[tap]^{-3}$ and optical spectrum of the product, shown as the tetraethylammonium salt. Italics represent synthetic procedures for the tetraethylammonium salt.

The optical spectrum of the tetraethylammonium salt Co(II) complex contains two features with λ_{max} ($\varepsilon_{M,}$ M^{-1} cm^{-1}) = 620 (600) and 910 nm (400) (Figure 2). The potassium salt Co(II) complex has nearly identical features (λ_{max} = 615 and 910 nm). The relatively intense bands in the visible region of the optical spectrum for the Co(II) complex of $[tap]^{-3}$ are consistent with formation of a non-centrosymmetric Co(II) complex. Compared to centrosymmetric complexes, which tend to have molar extinction coefficients below 100 M^{-1} cm^{-1} for d-d transitions, non-centrosymmetric complexes are not constrained by the Laporte selection rule, exhibiting more intense d-d transitions.[26] The features at λ_{max} = 620 and 910 nm, having a molar absorptivity on the order of 500 M^{-1} cm^{-1}, are consistent with this principle. Moreover, this spectrum is analogous to the optical spectra of the dinuclear complexes prepared by MacBeth and Cook, which had relatively intense d-d transitions near λ_{max} = 600 and 925 nm.[19,22]

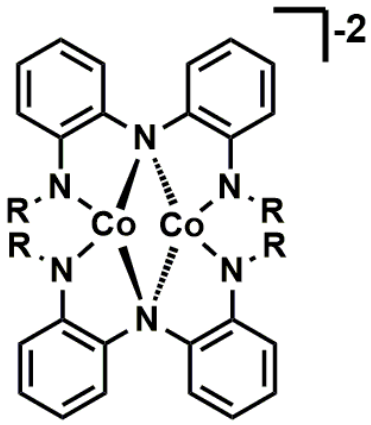

Figure 3. [Co_2N_2] diamond core structure observed by MacBeth and Cook.[19,22]

The FTIR spectrum of the Co(II) complex does not exhibit the strong features at 2850 and 2580 cm^{-1} found for H_3tap, and only exhibits one intense feature near 1100 cm^{-1}, consistent with deprotonation of the N—H groups and fully equivalent P=O bonds, unlike in H_3tap.

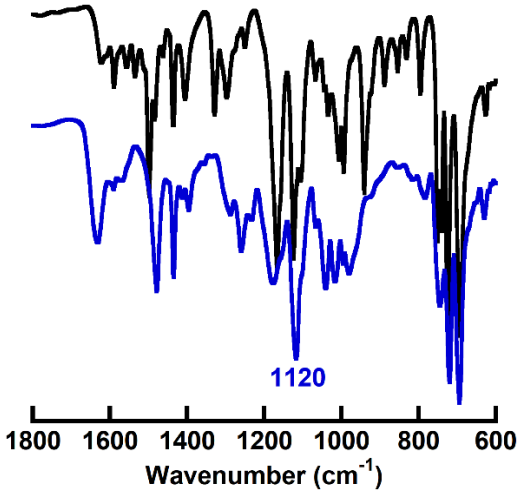

Figure 4. Overlaid FTIR spectrum of H_3tap (black) and the potassium salt of the Co(II) complex (blue).

The EPR and NMR spectra of this species are both featureless. While a silent EPR spectrum in the perpendicular mode is inconclusive, as both integer-spin systems and diamagnetic systems will not be observed, the silent NMR spectrum indicates that the Co(II) complex is paramagnetic. Finally, the cyclic voltammogram of this complex reveals rich electrochemistry, with a total of six oxidative events at -0.804 V, -0.567 V, -0.014 V, + 0.174 V,

+ 0.435 V, and + 0.834 V vs $[FeCp_2]^{+/0}$ (Figure 5). The overall appearance of this cyclic voltammogram is similar to the spectrum observed by Macbeth, which contains many overlapping oxidative events.[19] The monometallic complexes prepared by both Macbeth and Cook contain three well-resolved, reversible oxidative events.[19,22]

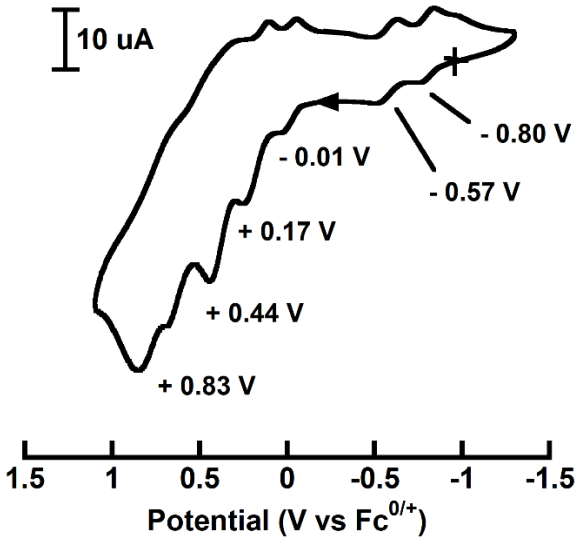

Figure 5. Cyclic voltammetry of the tetraethylammonium salt of the Co(II) complex with 0.1 M NBu_4PF_6 in MeCN, 2 mM concentration, 100 mV/s scan rate.

Oxidation Chemistry of Cobalt(II) Complexes of [tap]$^{-3}$.

The oxidative chemistry of these complexes was investigated, both with dioxygen and ferrocenium tetrafluoroborate. The reaction product with dioxygen was isolated as a solid by evaporation and the redissolved sample has spectroscopic features matching samples generated *in situ*.

Addition of one equivalent of ferrocenium tetrafluoroborate to the Co(II) complex generates new bands with λ_{max} (ε_M, M^{-1} cm^{-1}) = 600 (3000) and 800 nm (2000) (Figure 6). The perpendicular-mode EPR spectrum gives two features with g_1 = 2.05, g_2 = 1.98, and A_{Co} = 80 MHz. Addition of a second equivalent of ferrocenium tetrafluoroborate generates new features in

the UV-vis spectrum, with λ_{max} (ε_M, M^{-1} cm^{-1}) = 415 (6000), 610 (4000), and 900 nm (2000). This product, however, gives a silent perpendicular-mode EPR spectrum. Addition of a third equivalent of ferrocenium tetrafluoroborate does not generate any new features in the UV-vis spectrum.

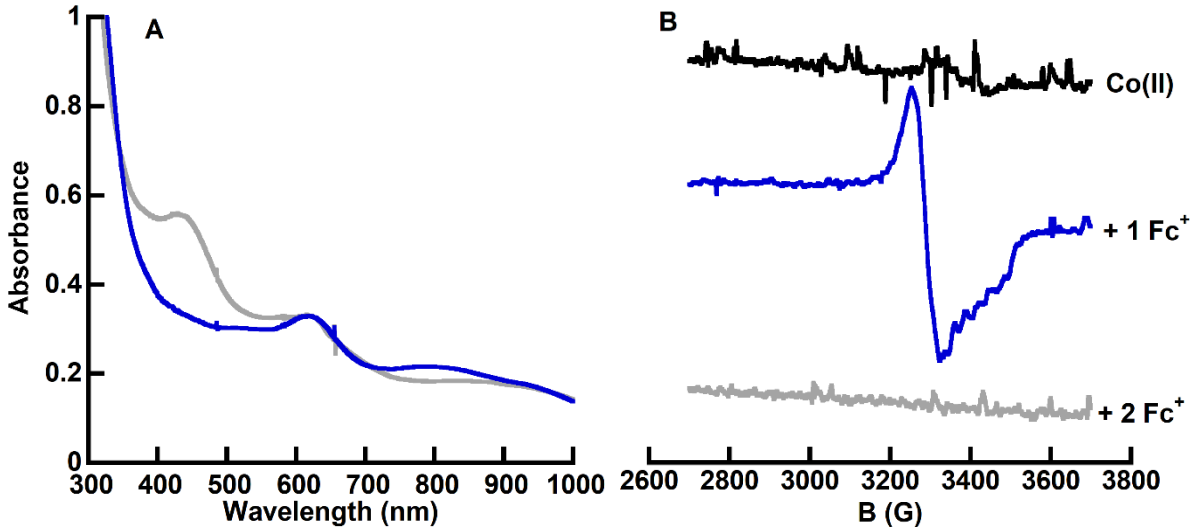

Figure 6. (A) Overlaid optical spectra of the product of one equivalent of $FcBF_4$ (black) and two equivalents of $FcBF_4$ (blue). (B) Overlaid perpendicular-mode EPR spectra collected at 77 K of the Co(II) complex (black), the product of one equivalent of $FcBF_4$ (blue), and two equivalents of $FcBF_4$ (grey).

When the Co(II) complex is exposed to dioxygen, the optical spectrum contains similar features at λ_{max} = 520, 620, and 810 nm (ε_M ~ 3000, 3000, 2000 M^{-1} cm^{-1}) (Figure 7). The perpendicular-mode EPR spectrum of this complex also contains similar features to the product of oxidation with one equivalent of ferrocenium tetrafluoroborate, with g_1 = 2.05 and g_2 = 1.97 (A_{Co} = 85 MHz).

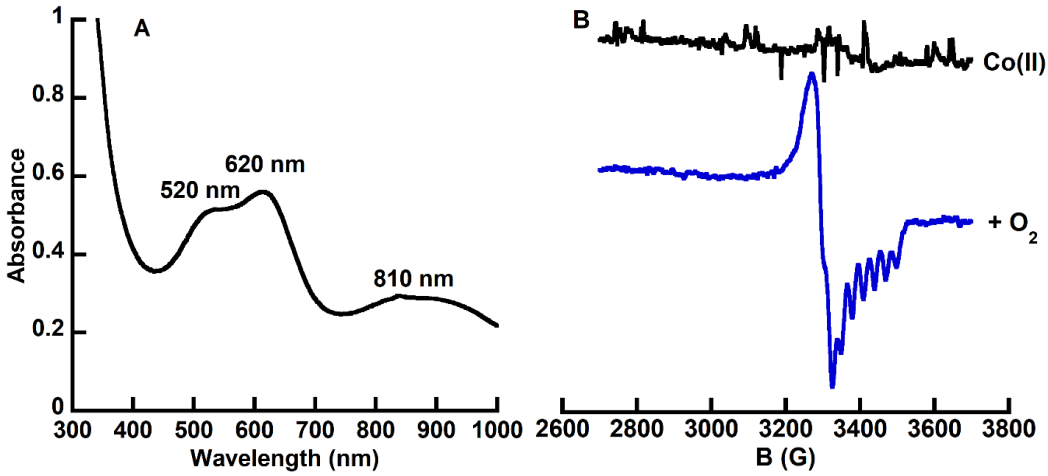

Figure 7. (A) Optical spectrum of product of oxidation by O_2 in THF, approximately 2 mM concentration in a 1 mm cuvette. (B) Overlaid perpendicular-mode EPR spectra collected at 77 K of the Co(II) complex (black) and the product upon addition of O_2 (blue).

Bulk synthesis of the product of oxidation by dioxygen on the Co(II) complex was carried out in tetrahydrofuran. This product was concentrated by evaporation, also removing any excess O_2, giving a dark purple solid.

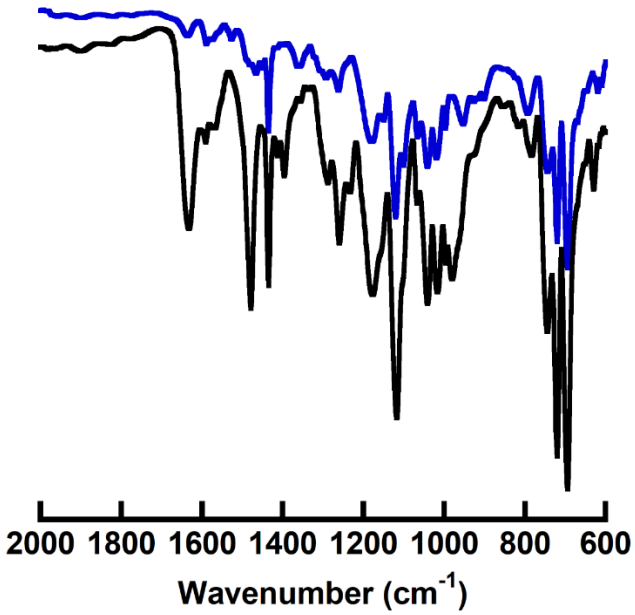

Figure 8. Overlaid FTIR spectra for the Co(II) complex of $[tap]^{-3}$ (black) and the product of oxidation by O_2 (blue).

This solid could be reconstituted in tetrahydrofuran and displayed spectroscopic characteristics identical to *in situ* generated product. This product was analyzed by FTIR spectroscopy and exhibited a strong feature at 1140 cm^{-1} consistent with a P—O stretching vibration (Figure 8).

The intense absorptions in the optical spectrum of all three oxidation products of the Co(II) complex of $[tap]^{-3}$ supports the generation of a ligand radical, leading to the observation of intense charge transfer bands akin to that observed for the oxidized metal complexes of the related $[ibaps]^{-3}$ ligand.[22,27] Formation of a Co(III) complex would result in the observation of new d-d transitions with extinction coefficients below 1000 M^{-1} cm^{-1} because the ligand field transition is symmetry forbidden. For example, several cobalt(III) complexes with tetradentate Schiff base ligands observed ligand field transitions with extinction coefficients no greater than 820 M^{-1} cm^{-1}.[28] Moreover, the EPR spectra obtained for the product of one equivalent of ferrocenium tetrafluoroborate, defined as the one-electron oxidized product, can be assigned as an S = ½ signal, inconsistent with formation of a monometallic Co(III) complex which would be expected to be integer spin. This is also not consistent with a ligand oxidation of a monometallic cobalt species, which would give an S = 1 signal with anti-ferromagnetic coupling, or an S = 2 signal with ferromagnetic coupling. A second oxidation would result in a half-integer signal observable by perpendicular-mode EPR spectroscopy.[22] This is, however, consistent with oxidation of a bimetallic cobalt complex. Finally, the low value for the eight-line hyperfine due to cobalt, 85 MHz, is consistent with a ligand-centered radical adjacent to a spin-active cobalt nucleus.[29] The return to a silent EPR spectrum with the addition of a second equivalent of ferrocenium further supports this hypothesis.

The addition of O_2 to the dinuclear cobalt(II) complexes studied by Macbeth was proposed to generate a monometallic ligand radical-cobalt(II)-superoxide species based on EXAFS data, EPR, and IR spectroscopies.[20] This pathway is not operative for the Co(II) complex of $[tap]^{-3}$ because the oxidation product by dioxygen appears to be the same as the oxidation product by ferrocenium, with qualitatively similar UV-vis and perpendicular-mode EPR spectra. Moreover, there are no additional peaks in the FTIR spectrum of the dioxygen-oxidized product in the region between 1000 and 1250 cm^{-1} consistent with formation of a cobalt superoxido complex.[20,30] This suggests that dioxygen acts as a one-electron outer sphere oxidant to the Co(II) complex of $[tap]^{-3}$.

Future Work

Based on these data, the Co(II) complex of $[tap]^{-3}$ is most likely a dinuclear cobalt complex in tetrahedral or pseudo-tetrahedral geometry, similar to the complexes prepared by Macbeth and Cook. One-electron oxidation of this complex likely generates a stable, ligand radical species which remains a dinuclear Co(II) species. Additional experiments need to be performed to understand the identify of the complex generated by the second oxidation.

If these assessments are true, they can be verified by an X-ray diffraction study. The C–C and C–N bond metrics in the ligand backbone will change upon ligand-based oxidation, whereas they would be relatively unchanged if the oxidation is metal-centered. Moreover, study by X-ray absorption spectroscopy, and analysis of the XANES region should reveal that the rising edge energy, which is related to the oxidation state of the metal under investigation, changes less than 1 eV in the one-electron oxidized product. This result would be consistent with a ligand-based oxidation, rather than a metal-based oxidation.[31] Further study by EPR spectroscopy in the

parallel-mode to investigate integer-spin products will help to identify both the starting dinuclear Co(II) complex, as well as the two-electron oxidized product.

Further studies into coupling the low-lying oxidation states with chemical reactivity are proposed: aryl azides may be reduced by this species, generating a two-electron oxidized cobalt-imido species which may further undergo intramolecular C—H amination analogous to work by Heyduk and Cook.[7,22] Furthermore, oxo-transfer reactions such as iodosobenzene or isopropyl iodoxybenzoate may oxidize the putative dicobalt(II) species to a cobalt-oxido or cobalt-hydroxido species able to perform H-atom abstraction chemistry on substrates such as tri-tert-butyl phenol or dihydroanthacene.[32]

Experimental

General Procedures. All reactions, unless otherwise noted, were performed under an argon atmosphere in a dry box. All chemicals were purchased from commercial sources and used as received unless otherwise stated. Solvents were sparged with argon and dried over columns containing Q-5 and molecular sieves. Potassium hydride and sodium hydride, as a 30% suspension in mineral oil, was filtered and washed with diethyl ether and pentane. The ligand precursors, 2,2'-dinitro-diphenylamine and 2,2'-diamino-diphenylamine, were prepared according to literature procedures.[19] Ferrocenium tetrafluoroborate was prepared according to literature procedures.[33] Elementary analysis was not performed unless otherwise stated.

H_3tap. A solution of 2,2'-diamino-diphenylamine (1.50 g, 7.53 mmol) and triethylamine (3.13 mL, 22.6 mmol) was prepared in tetrahydrofuran (15 mL) in a round-bottomed flask under an argon atmosphere. Another solution of diphenylphosphinic chloride (3.74 g, 15.8 mmol) in tetrahydrofuran (60 mL) was added by addition funnel dropwise, causing an immediate precipitation. The addition funnel was then washed with additional tetrahydrofuran (20 mL), and

the reaction left for twelve hours. The mixture was then removed from the dry box, filtered, and concentrated on a rotary evaporator, giving a dark brown oil. This residue was dissolved in ethyl acetate (150 mL) and watched with saturated ammonium chloride (5 x 75 mL), water (4 x 75 mL, and brine (100 mL). The organic fraction was separated and dried over $MgSO_4$. This fraction was then concentrated by rotary evaporation and triturated in 1:1 ethyl acetate:hexane, giving a white solid which was washed with hexanes (2 x 100 mL), dried under vacuum, and brought under argon to give H_3tap as a white solid (2.942 g, 65 % yield). ^{1}H NMR (500 MHz, DMSO): δ 6.53 – 7.33 (m, 8H, triamine H), 7.46 – 7.88 (m, 20H, phosphinic phenyl H). ^{31}P NMR (162 MHz, DMSO): δ 19.7, 24.6. ^{31}P NMR (162 MHz, MeOH): δ 21.6. ^{13}C NMR (126 MHz, THF): δ 116.2, 117.6, 119.8, 123.8, 124.7, 125.8, 128.9 (app dd), 131.9 (app d), 132.1 (app d), 132.3 (app d), 133.1 (app d). FTIR (ATR; selected bands cm^{-1}): 2850, 2580, 1166, 1124. HRMS (ES+): Exact mass calcd (found) for [M + Na]: 622.1789 (622.1815)

Co(II) Complex of [tap]$^{-3}$ – Tetraethylammonium Salt. H_3tap (164 mg, 0.273 mmol) was dissolved in dimethylacetamide (3 mL) with stirring. Sodium hydride (20 mg, 0.85 mmol) was added, followed by immediate gas evolution. Once gas evolution ceased, cobalt(II) bromide was added (60 mg, 0.27 mmol), causing an immediate color change from orange to a dark green-brown. This reacted for two hours, then tetraethylammonium bromide (57 mg, 0.27 mmol) was added to remove sodium. The solution was filtered to remove sodium bromide (51 mg, 0.50 mmol) and purified by layering under ether to precipitate residual sodium bromide. The colored mother liquor was concentrated by evaporation and extracted into tetrahydrofuran. This solution was filtered, removing any residual sodium bromide (27 mg, 0.26 mmol) and concentrated by evaporation to give the product as a dark green solid, tentatively $(Net_4)_2[Co_2tap_2]$ (201 mg, 54% yield). λ_{max} (THF; ε_M M^{-1} cm^{-1}) 620 nm (600), 910 nm (400).

Co(II) Complex of [tap]$^{-3}$ – Potassium Salt. H_3tap (145 mg, 0.242 mmol) was dissolved in dimethylacetamide (3 mL) with stirring. Potassium hydride (30 mg, 0.75 mmol) was added and allowed to react until gas evolution ceased. Cobalt(II) bromide was then added (53 mg, 0.24 mmol), producing an immediate color change from orange to green-brown. After two hours of reaction, the reaction mixture was filtered to remove potassium bromide and purified by layering under ether. The colored mother liquor was concentrated by evaporation and extracted into tetrahydrofuran. This solution was filtered and concentrated by evaporation to give a dark green solid, tentatively $K_2[Co_2tap_2]$ (167 mg, 50% yield) . λ_{max} (THF; ε_M M^{-1} cm^{-1}) 615 nm (600), 910 nm (400). FTIR (ATR, selected bands cm^{-1}): 1120 cm^{-1}.

Bulk Oxidation of a Co(II) Complex of [tap]$^{-3}$. A solution of $K_2[Co_2tap_2]$ (55 mg, 0.040 mmol) was prepared in tetrahydrofuran (15 mL) in a Schlenk flask. This was sealed with a rubber septum and charged with excess O_2 (10 mL, 0.45 mmol). This reacted for five hours, changing in color from green to dark purple. The solvent was removed by evaporation and the Schlenk flask was returned to a dry box where it was reconstituted in tetrahydrofuran, concentrated by evaporation, and used without further purification. λ_{max} (THF; ε_M M^{-1} cm^{-1}) 520 nm (3000), 600 nm (3000), 800 nm (2000). X-Band EPR (1:1 THF/DCM, 77K) $g_1 = 2.05$, $g_2 = 1.97$, $A_{Co} = 85$ MHz. FTIR (ATR, selected bands cm^{-1}): 1140 cm^{-1}.

Physical Methods

Electronic absorption spectra were collected on a Cary 60 spectrophotometer or an Agilent UV-vis spectrophotometer equipped with a Unisoku Unispeks cryostat in either a 1 cm quartz cuvette or a 1 mm thin cell quartz cuvette. X-Band (9.4 GHz) EPR spectra were collected as frozen solutions using a Bruker EMX spectrometer equipped with an ER041XG microwave bridge and the data was analyzed using SpinCount. Solid-state infrared spectra were collected on a Thermo

Scientific Nicolet iS5 FT-IR spectrometer equipped with an iD5 ATR accessory. NMR spectra were collected on a Bruker DRX500 or DRX400 spectrometer.

References

(1) Periana, R. A.; Taube, D. J.; Gamble, S.; Taube, H. Ligated Platinum Group Metal Catalyst Complex and Improved Process for Catalytically Converting Alkanes to Esters and Derivatives Thereof. 98/50333, 1998.

(2) Schwab, P.; France, M. B.; Ziller, J. W.; Grubbs, R. H. A Series of Well-Defined Metathesis Catalysts–Synthesis of $[RuCl_2(=CHR')(PR_3)_2]$ and Its Reactions. *Angew. Chemie Int. Ed. English* **1995**, *34* (18), 2039–2041.

(3) Suggs, J. W.; Cox, S. D.; Crabtree, R. H.; Quirk, J. M. Facile Homogeneous Hydrogenations of Hindered Olefins with $[Ir(Cod)Py(PCy_3)]PF_6$. *Tetrahedron Lett.* **1981**, *22* (4), 303–306.

(4) Eggert, R. G.; Carpenter, A. S.; Freiman, S. W.; Graedel, T. E.; Meyer, D. A.; McNulty, T. P.; Moudgil, B. M.; Poulton, M. M.; Surges, L. J.; Eide, E. A.; et al. *Minerals, Critical Minerals, and the U.S. Economy*; Washington, D.C., 2008.

(5) Jones, R. T. JOM World Nonferrous Smelter Survey, Part II: Platinum Group Metals. *JOM* **2004**, *56* (12), 59–63.

(6) Chirik, P. J.; Wieghardt, K. Radical Ligands Confer Nobility on Base-Metal Catalysts. *Science (80-.).* **2010**, *327* (5967), 794–795.

(7) Nguyen, A. I.; Zarkesh, R. A.; Lacy, D. C.; Thorson, M. K.; Heyduk, A. F. Catalytic Nitrene Transfer by a Zirconium(IV) Redox-Active Ligand Complex. *Chem. Sci.* **2011**, *2* (1), 166–189.

(8) Nguyen, A. I.; Blackmore, K. J.; Carter, S. M.; Zarkesh, R. A.; Heyduk, A. F. One- and Two-Electron Reactivity of a Tantalum(V) Complex with a Redox-Active Tris(Amido) Ligand. *J. Am. Chem. Soc.* **2009**, *131* (9), 3307–3316.

(9) Munhá, R. F.; Zarkesh, R. A.; Heyduk, A. F. Tuning the Electronic and Steric Parameters of a Redox-Active Tris(Amido) Ligand. *Inorg. Chem.* **2013**, *52* (19), 11244–11255.

(10) Rosenkoetter, K. E.; Wojnar, M. K.; Charette, B. J.; Ziller, J. W.; Heyduk, A. F. Hydrogen-Atom Noninnocence of a Tridentate [SNS] Pincer Ligand. *Inorg. Chem.* **2018**, *57* (16), 9728–9737.

(11) Wong, J. L.; Sánchez, R. H.; Logan, J. G.; Zarkesh, R. A.; Ziller, J. W.; Heyduk, A. F. Disulfide Reductive Elimination from an Iron(III) Complex. *Chem. Sci.* **2013**, *4*, 1906–1910.

(12) Smith, A. L.; Hardcastle, K. I.; Soper, J. D. Redox-Active Ligand-Mediated Oxidative Addition and Reductive Elimination at Square Planar Cobalt(III): Multielectron Reactions for Cross-Coupling. *J. Am. Chem. Soc.* **2010**, *132* (41), 14358–14360.

(13) Sylvester, K. T.; Chirik, P. J. Diynes : Evidence for Bis (Imino) Pyridine Ligand Participation. *J. Am. Chem. Soc.* **2009**, *131*, 8772–8774.

(14) Kunert, R.; Philouze, C.; Jarjayes, O.; Thomas, F. Stable M(II)-Radicals and Nickel(III) Complexes of a Bis(Phenol) N-Heterocyclic Carbene Chelated to Group 10 Metal Ions. *Inorg. Chem.* **2019**, *58* (12), 8030–8044.

(15) Gautam, R.; Petritis, S. J.; Astashkin, A. V.; Tomat, E. Paramagnetism and Fluorescence of Zinc(II) Tripyrrindione: A Luminescent Radical Based on a Redox-Active Biopyrrin.

Inorg. Chem. **2018**, *57* (24), 15240–15246.

(16) Dzik, W. I.; Van Der Vlugt, J. I.; Reek, J. N. H.; De Bruin, B. Ligands That Store and Release Electrons during Catalysis. *Angew. Chemie - Int. Ed.* **2011**, *50* (15), 3356–3358.

(17) Smith, A. L.; Clapp, L. A.; Hardcastle, K. I.; Soper, J. D. Redox-Active Ligand-Mediated Co-Cl Bond-Forming Reactions at Reducing Square Planar Cobalt(III) Centers. *Polyhedron* **2010**, *29* (1), 164–169.

(18) Bouwkamp, M. W.; Bowman, A. C.; Lobkovsky, E.; Chirik, P. J. Iron-Catalyzed [2π + 2π] Cycloaddition of α,ω-Dienes: The Importance of Redox-Active Supporting Ligands. *J. Am. Chem. Soc.* **2006**, *128* (41), 13340–13341.

(19) Sharma, S. K.; May, P. S.; Jones, M. B.; Lense, S.; Hardcastle, K. I.; MacBeth, C. E. Catalytic Dioxygen Activation by Co(II) Complexes Employing a Coordinatively Versatile Ligand Scaffold. *Chem. Commun.* **2011**, *47* (6), 1827–1829.

(20) Corcos, A. R.; Villanueva, O.; Walroth, R. C.; Sharma, S. K.; Bacsa, J.; Lancaster, K. M.; MacBeth, C. E.; Berry, J. F. Oxygen Activation by Co(II) and a Redox Non-Innocent Ligand: Spectroscopic Characterization of a Radical-Co(II)-Superoxide Complex with Divergent Catalytic Reactivity. *J. Am. Chem. Soc.* **2016**, *138* (6), 1796–1799.

(21) Villanueva, O.; Weldy, N. M.; Blakey, S. B.; MacBeth, C. E. Cobalt Catalyzed Sp^3 C-H Amination Utilizing Aryl Azides. *Chem. Sci.* **2015**, *6* (11), 6672–6675.

(22) Cook, S. A. Principles of Molecular Design in the Development of Ligand Frameworks That Control the Primary and Secondary Coordination Spheres of Metal Ions, University of California, Irvine, 2015.

(23) Oswald, V. F.; Weitz, A. C.; Biswas, S.; Ziller, J. W.; Hendrich, M. P.; Borovik, A. S. Manganese-Hydroxido Complexes Supported by a Urea/Phosphinic Amide Tripodal Ligand. *Inorg. Chem.* **2018**, *57* (21), 13341–13350.

(24) Oswald, V. F. Tripodal Phosphoryl Amide Farmeworks: Investigating the Relationship Between High Valent Metal-Oxido and Metal-Hydroxido Complexes., University of California, Irvine, 2018.

(25) Stegmann, H. B.; Dumm, H. V.; Burmester, A.; Scheffler, K. Umwandlung Von 2.2-Diphenyl-2-Fluor-2.3-Dihydro-1.3.2 Λ^5-Benzoxazaphospholen II. *Phosphorus Sulfur Relat. Elem.* **1980**, *9* (1), 99–106.

(26) Cotton, F. A.; Goodgame, D. M. L.; Goodgame, M. The Electronic Structures of Tetrahedral Cobalt(II) Complexes. *J. Am. Chem. Soc.* **1961**, *83* (23), 4690–4699.

(27) Cook, S. A.; Bogart, J. A.; Levi, N.; Weitz, A. C.; Moore, C.; Rheingold, A. L.; Ziller, J. W.; Hendrich, M. P.; Borovik, A. S. Mononuclear Complexes of a Tridentate Redox-Active Ligand with Sulfonamido Groups: Structure, Properties, and Reactivity. *Chem. Sci.* **2018**, *9* (31), 6540–6547.

(28) Amirnasr, M.; Vafazadeh, R.; Mahmoudkhani, A. H. Synthesis, Structure, and Electrochemistry of Cobalt(III) Complexes with Bis(Benzoylacetone)-Ethylenediimine Schiff Base. *Can. J. Chem.* **2002**, *80*, 1196–1203.

(29) Anson, C. W.; Ghosh, S.; Hammes-Schiffer, S.; Stahl, S. S. Co(Salophen)-Catalyzed Aerobic Oxidation of *p* -Hydroquinone: Mechanism and Implications for Aerobic Oxidation Catalysis. *J. Am. Chem. Soc.* **2016**, *138* (12), 4186–4193.

(30) Jones, R. D.; Summerville, D. A.; Basolo, F. Synthetic Oxygen Carriers Related to Biological Systems. *Chem. Rev.* **1979**, *79* (2), 139–179.

(31) Lim, H.; Thomas, K. E.; Hedman, B.; Hodgson, K. O.; Ghosh, A.; Solomon, E. I. X-Ray Absorption Spectroscopy as a Probe of Ligand Noninnocence in Metallocorroles: The Case of Copper Corroles. *Inorg. Chem.* **2019**, *58* (10), 6722–6730.

(32) Goldsmith, C. R.; Daniel, T.; Stack, P. Hydrogen Atom Abstraction by a Mononuclear Ferric Hydroxide Complex: Insights into the Reactivity of Lipoxygenase. *Inorg. Chem.* **2006**, *45*, 6048–6055.

(33) Connelly, N. G.; Geiger, W. E. Chemical Redox Agents for Organometallic Chemistry. *Chem. Rev.* **1996**, *96* (2), 877–910.

Chapter 4

Efforts towards Generation of High-Valent Iron-Thiolate Complexes in Redox-Active Bis(amidophenyl)amide Ligands

Abstract

The reactive mechanism of cytochrome P450 has been proposed to proceed through a high-valent Fe=O species, named compound I. Further studies have characterized this species as an iron(IV)-ligand radical species. Synthetic redox-active ligands have been studied which are able to act as redox sources or sinks in coordination with metal-based oxidation or reduction to increase the stability of high valent metal centers. In this report, iron(III) complexes of redox-active ligands, a phosphonamide bis(aminophenyl)amine ligand and a sulfonamide bis(aminophenyl)amine ligand, have been studied. Furthermore, the installation of an exogenous thiolato ligand was investigated, and the reactivity of these species with the oxo-transfer reagent isopropyl iodoxybenzoate was studied by UV-vis and EPR spectroscopies. Finally, the ability of these oxidized species to react with substates was investigated.

Introduction

Hemeproteins, proteins which contain an Fe(II/III) center coordinated to a substituted porphyrin unit via four pyrrole rings are found in all living organisms.[1,2] There are three major classes of hemeproteins: gas-carrying hemeproteins, such as hemoglobin and myoglobin; enzymes, such as cytochrome P450 and horse radish peroxidase; and electron-transfer proteins, such as cytochrome c. The iron center is further associated with the protein through coordination to various amino acids, providing a fifth and occasionally sixth ligand. While the electron

transfer proteins typically contain six-coordinate iron cofactors, the gas-carrying and enzymatic hemeproteins use five-coordinate iron cofactors to permit the binding of exogenous ligands.

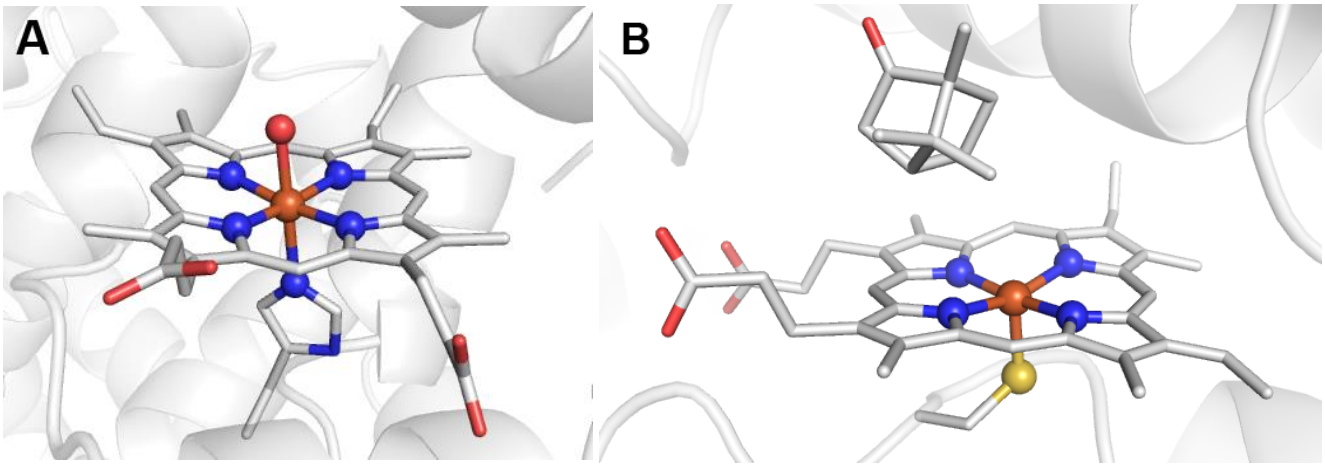

Figure 1. (A) Aquo-met state of the heme B cofactor in T-state *H. sapiens* hemoglobin (PDB: 1VWT). (B) Camphor-bound met state of the heme B cofactor in *P. putida* cytochrome $P450_{cam}$ (PDB: 5CP4).

Hemoglobin, for example, has a similar primary coordination sphere to cytochrome P450 with the exception of the apical ligand: hemoglobin uses a histidine as the apical ligand, and binds dioxygen without further activation, while cytochrome P450 uses a cysteine as the apical ligand, and activates dioxygen to affect the hydroxylation of C—H bonds in substrates (Figure 1).[3,4] Cytochrome P450 breaks the O—O bond in dioxygen, generating an Fe^{IV}=O ligand radical complex referred to as Compound I (Figure 2). Notably, when Compound I is reduced, cytochrome P450 and a small number of others generate a Lewis basic hydroxoiron(IV) complex.[3–11]

Cytochrome P450 undergoes two-electron chemistry through H-atom abstraction by Compound I from the substrate to generate Compound II, followed by rebound of the hydroxido ligand to the substrate radical and reduction of the iron center to iron(III).[12,13] The basic thiolate ligand found in cytochrome P450 is thought to increase the pKa of the compound II state, enabling this system to proceed through this two-electron process.[5,12,13] While the Compound I

state is formally an iron(V) species, it is more properly described as an iron(IV)-ligand radical, where the porphyrin ligand and thiolate atom bear part of the oxidative load to stabilize this reactive intermediate.

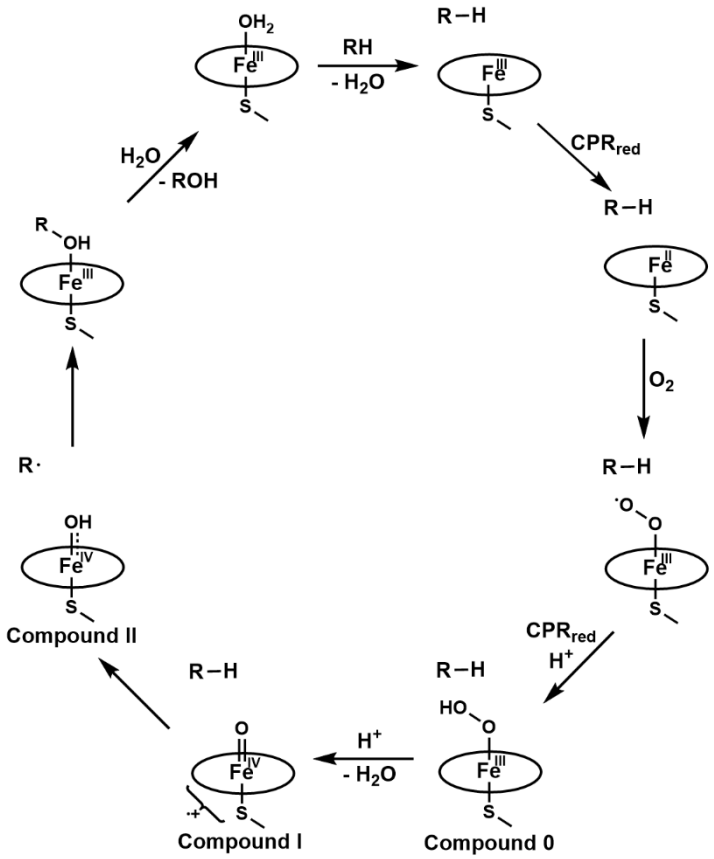

Figure 2. Consensus mechanism of reaction for the reaction of Cytochrome P450 with substrate. CPR_{red} refers to the reduced form of cytochrome P450 reductase, which acts as an electron shuttle from NADPH to cytochrome P450.[14]

A number of model systems have been developed to study the properties of the active site in cytochrome P450. Most of these synthetic models rely on decorated porphyrins, installing steric bulk about the active site, apical binding motifs, and hydrogen-bonding groups poised above the metal center.

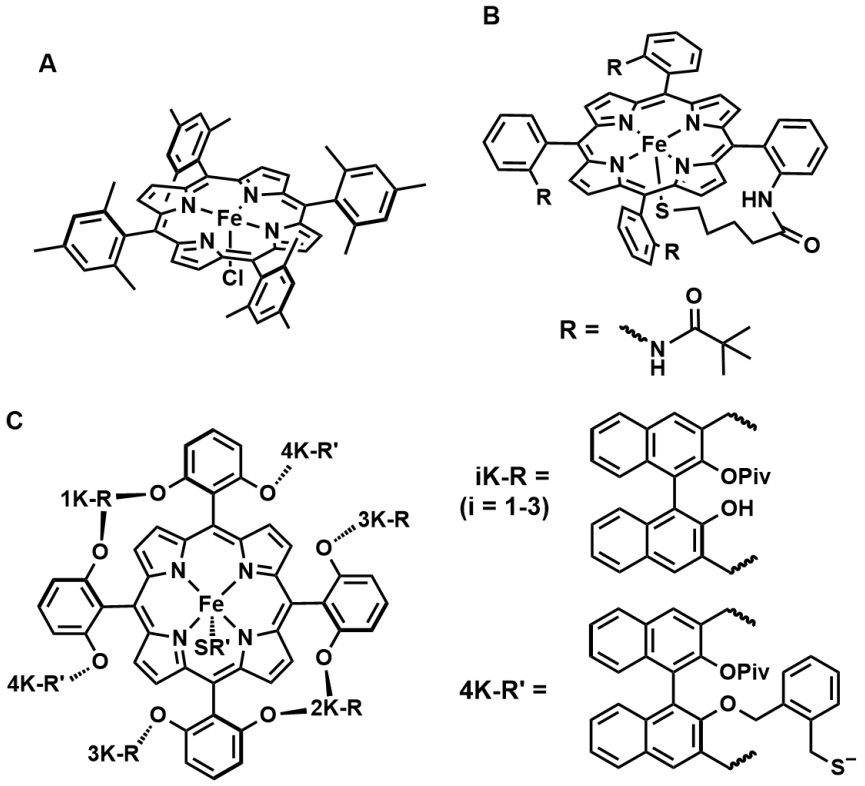

Figure 3. (A) Fe(TMP)Cl reported by Groves.[15] (B) Bulky aliphatic thiolate-decorated porphorinato iron(III) complex described by Dey.[16] (C) TCP-TB, reported by Tani and Naruta.[17]

For example, Groves reported a (tetramesityl-porphyrin)iron chloride complex which reacted with metachloroperbenzoic acid to generate a formally oxoiron(V) species which they described as a (porphyrin-radical cation)oxoiron(IV) complex based on the Mössbauer parameters, which were similar to the reported values for the Compound I state of HRP, and an absorbance spectrum consistent with a porphyrin radical cation (Figure 3).[15] Naruta and Tani, synthesized a shielded "twin coronet porphyrin" which incorporated binaphthyl groups for steric bulk, a thiolate group poised to coordinate to the iron center, and hydroxyl groups to provide hydrogen-bonding interactions (Figure 3).[17] They were able to synthesize the iron(III) porphyrinate complex, which bound superoxide at –80 °C. This superoxido ligand was displaced under a CO atmosphere and the resonance Raman spectrum exhibited a strong line at 1137 cm^{-1} assigned to the O—O stretching vibration.

Recently, Dey has studied the redox-activity of the thiolate in Cytochrome P450 synthetic models through a decorated porpyrinate iron(III) system, similar to the mercapto-tailed porphyrin system developed by Collman and Groh, which exhibits valence tautomerism between iron(III)-thiolate and iron(II)-thiyl radical forms (Figure 3).[16,18] The resonance Raman spectra of these species at low temperatures showed the expected structure-sensitive Raman bands at 1361 cm^{-1} and 1554 cm^{-1} which is assigned to the high-spin iron(III) species. When the sample is warmed to room temperature, new bands appear at 1343 cm^{-1} and 1540 cm^{-1}, assigned to a high-spin iron(II) species. In the perpendicular-mode EPR spectra of these complexes, spectra taken in non-coordinating solvents at low temperatures were consistent with a high-spin iron(III) complex while the spectra taken at room temperature had only a g = 2 signal which accounted for 50 % of the total sample by spin quantification.

Variable temperature studies for resonance Raman, EPR, and visible spectroscopies showed reversible and continuous interconversion between the assigned iron(III)-thiolate and iron(II)-thiyl radical species. Based on these studies, Dey reported that the iron(III)-thiolate was enthalpically favored while the iron(II)-thiyl radical was entropically favored. While the non-bulky porphyrin thiolates are susceptible to oxidation by dioxygen, Dey found that the addition of 0.5 % H_2O shifted the equilibrium so that only the iron(III) state was observed and prevented oxidation under air. He proposes that hydrogen-bonding to the thiolate ligand prevents inadvertent degradation in oxygenated environments by generation of superoxide.

Redox-active ligands have been mentioned in Chapter 3; the H_3ibaps framework developed by Cook is particularly important to this work. This framework combines steric bulk from the triisopropyl-phenyl substituents with the strongly donating trianionic backbone when deprotonated.[19] She reported monomeric cobalt(II) and iron(II) complexes with exogenous

bipyridine ligands which exhibited rich and reversible electrochemistry, both with three oxidative events corresponding to the attainment of a formally pentavalent state. Further studies into these complexes showed that the $[Fe^{II}(ibaps)bpy]^-$ complex is reactive with aryl azides and promotes intramolecular C—H bond amination.[20] Based on comparison of the electrochemical properties of the $[Fe^{II}(ibaps)bpy]^-$ to the analogous $[Ga^{III}(ibaps)bpy]$ complex, Bogart determined that the initial oxidative event was metal-centered, while the second and third oxidative events were ligand-based. Despite this, inconsistencies in the spectroscopic measurements for the singly oxidized $[Fe(ibaps)bpy]^0$ (Mössbauer spectroscopy indicated a ferric center, while the optical spectrum resembled the expected quinonate state of the ibaps ligand) lead to some ambiguity on the balance between metal and ligand oxidation.

Previous work in the Heyduk group has studied a bis(2-phenol)amine-derived iron(III) quinonate complex which oxidatively couples thiols to disulfides in the presence of pyridine.[21] Notable, this reaction generates a two-electron reduced iron(III) catecholate product whereby the ligand is reduced, rather than the metal center.

Bogart also synthesized an iron(III) thiolate complex in the $[ibaps]^{-3}$ ligand through synthesis of the $K_2[Fe^{II}ibaps(pyCH_2S)]$ followed by oxidation with ferrocenium tetrafluoroborate. This putative $[Fe^{III}ibaps(pyCH_2S)]^-$ species was characterized as having a S = 5/2 ground state by perpendicular-mode EPR spectroscopy and exhibited two features in the visible spectrum at λ_{max} = 485 nm and 675 nm. This species was reactive with O_2 and was also noted to react with IBX-^{i}Pr, generating a complex with an intense feature in the visible spectrum at λ_{max} = 980 nm and an intense EPR feature at g = 2. This report aims to further investigate the properties of this iron(III)-thiolate complex and to compare them with the properties of the analogous complex prepared in the H_3tap ligand framework.

Results and Discussion

Generation and Characterization of Ferric Complexes of H_3ibaps

The pre-ligand, H_3ibaps, was prepared according to previous synthetic routes.[22]

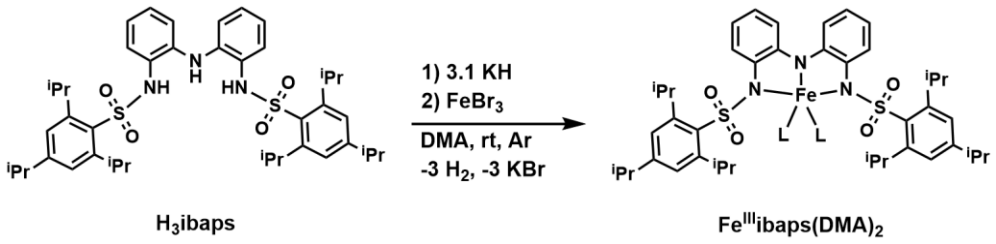

Scheme 1. Preparation of Fe^{III}ibaps$(DMA)_2$.

To prepare the Fe(III) bis(dimethylacetamide) complex of $[ibaps]^{3-}$, H_3ibaps is dissolved in dimethylacetamide (DMA), deprotonated with three equivalents of potassium hydride, and metalated with ferric bromide according to the procedure developed by Bogart.[22] The solution was then concentrated by vacuum and triturated with diethyl ether. This mixture was then filtered and the ether solution concentrated by vacuum to give the metal complex as the previously characterized bis(dimethylacetamide) complex in good yield (81 %).

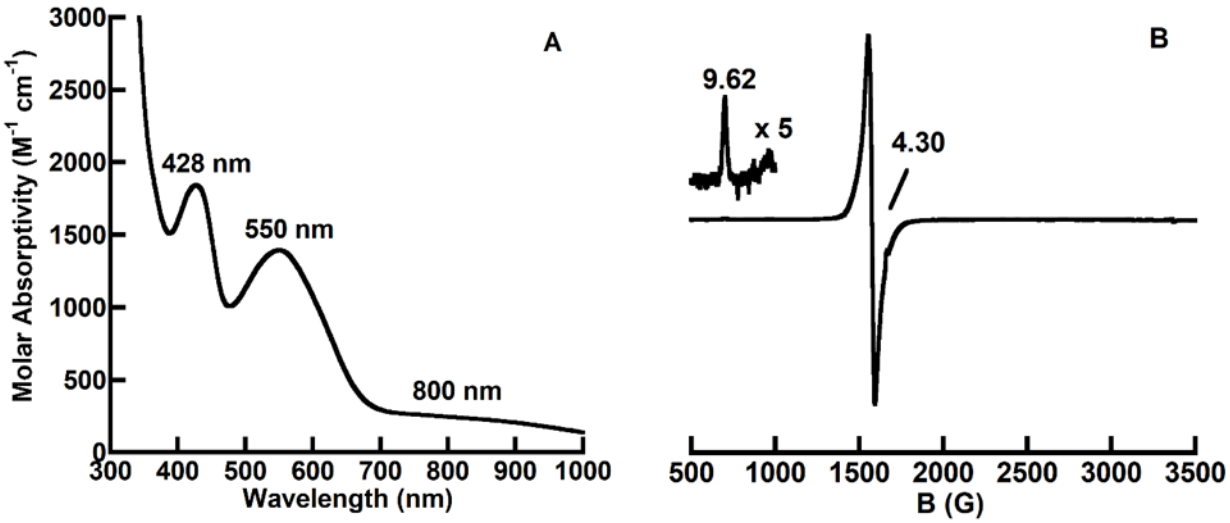

Figure 4. Characterization of $[Fe^{III}$ibaps$(DMA)_2]$ by (A) optical spectroscopy in THF/Et2O at 25 °C and (B) perpendicular-mode EPR spectroscopy at 10 mM in toluene at 77 K.

This complex was characterized through UV-vis and EPR spectroscopies (Figure 4). The optical spectrum of [Fe^{III}ibaps$(DMA)_2$] is solvent-dependent: a tetrahydrofuran-diethyl ether solution gives features with λ_{max} = 428 nm (1800 M^{-1} cm^{-1}), 550 nm (1400 M^{-1} cm^{-1}), and 800 nm (240 M^{-1} cm^{-1}), while a toluene solution gives λ_{max} = 385 nm (4000 M^{-1} cm^{-1}), 524 nm (2900 M^{-1} cm^{-1}), 800 nm (1200 M^{-1} cm^{-1}). Perpendicular mode EPR spectroscopy of [Fe^{III}ibaps$(DMA)_2$] gave an rhombic spectrum indicated of a *S* = 5/2 spin state with g = 9.62, 4.30.

The cyclic voltammogram of [Fe^{III}ibaps$(DMA)_2$] reveals rich electrochemistry, with four oxidative events at – 0.25 V, 0.00 V, + 0.58 V, and + 0.85 V vs [$FeCp_2^{0/+}$] (Figure 5).

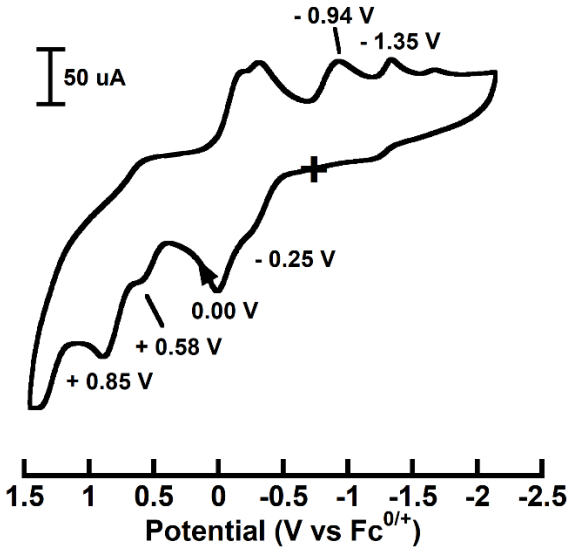

Figure 5. Cyclic voltammogram of [Fe^{III}ibaps$(DMA)_2$] with 0.1 M NBu_4PF_6 in MeCN, 1 mM concentration, 400 mV/s scan rate.

Once generated *in situ*, the [Fe^{III}ibaps$(DMA)_2$] complex is reacted with a slight excess of potassium pyridinemethylthiolate to generate the putative [Fe^{III}ibaps$(PyCH_2S)]^-$ moiety, then 18-crown-6 was added to bind the potassium ion. The resulting solution is then concentrated by vacuum, washed with a mixed of pentane-diethyl ether to remove excess [Fe^{III}ibaps$(DMA)_2$], and redissolved in tetrahydrofuran. After filtering, this solution was evaporated and washed with

diethyl ether. This putative [K(18-c-6)][Fe^{III}ibaps(PyCH$_2$S)] complex was studied by UV-vis and EPR spectroscopies. The optical spectrum collected in MeCN has λ_{max} = 400 nm (sh), 500 nm (3000 M^{-1} cm^{-1}), 750 nm (sh) (Figure 5A). The two higher energy features are consistent with a S → Fe^{III} LMCT, which have been found in several model complexes to lie between 400 – 600 nm.[23–25] The perpendicular mode EPR spectrum gives a complicated spectrum which may correspond to a slightly rhombic S = 5/2 spin system with g = 7.74, 4.29, 2.00 (Figure 6B).

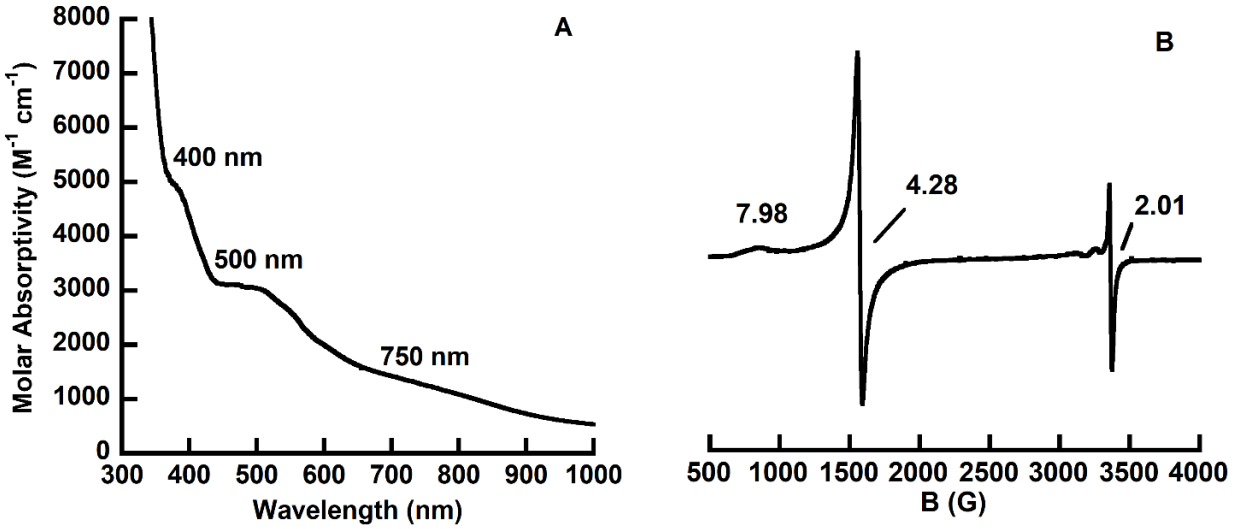

Figure 6. Characterization of [K(18-c-6)][Fe^{III}ibaps(pyCH$_2$S)] by (A) optical spectroscopy in MeCN at – 30 °C and (B) perpendicular-mode EPR spectroscopy at 10 mM in MeCN at 77 K.

The electrochemistry of the putative [K(18-c-6)][Fe^{III}ibaps(pyCH$_2$S)] complex was investigated through cyclic voltammetry, revealing a similar distribution of features to [Fe^{III}ibaps(DMA)$_2$] (Figure 7). In contrast to the electrochemistry of [Fe^{III}ibaps(DMA)$_2$], the cyclic voltammogram of [K(18-c-6)][Fe^{III}ibaps(pyCH$_2$S)] exhibits less reversible and prominent redox events.

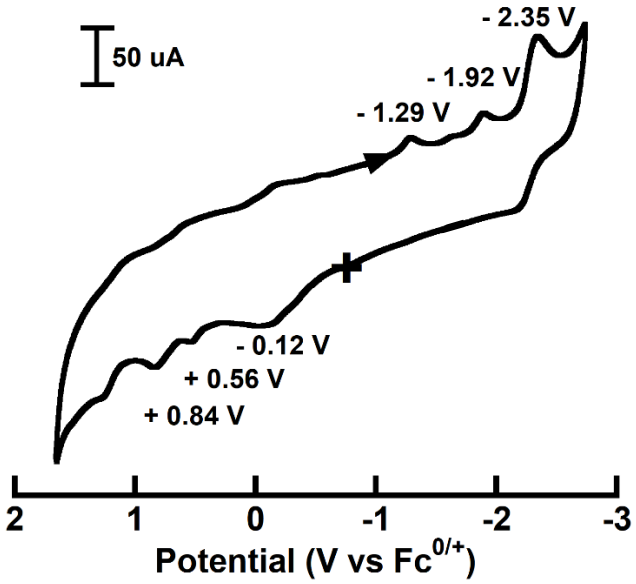

Figure 7. Cyclic voltammogram of [K(18-c-6)][Fe^{III}ibaps(pyCH_2S)] with 0.1 M NBu_4PF_6 in MeCN, 1 mM concentration, 400 mV/s scan rate.

Oxidative Reactivity of a Ferric Thiolate Complex in H_3ibaps

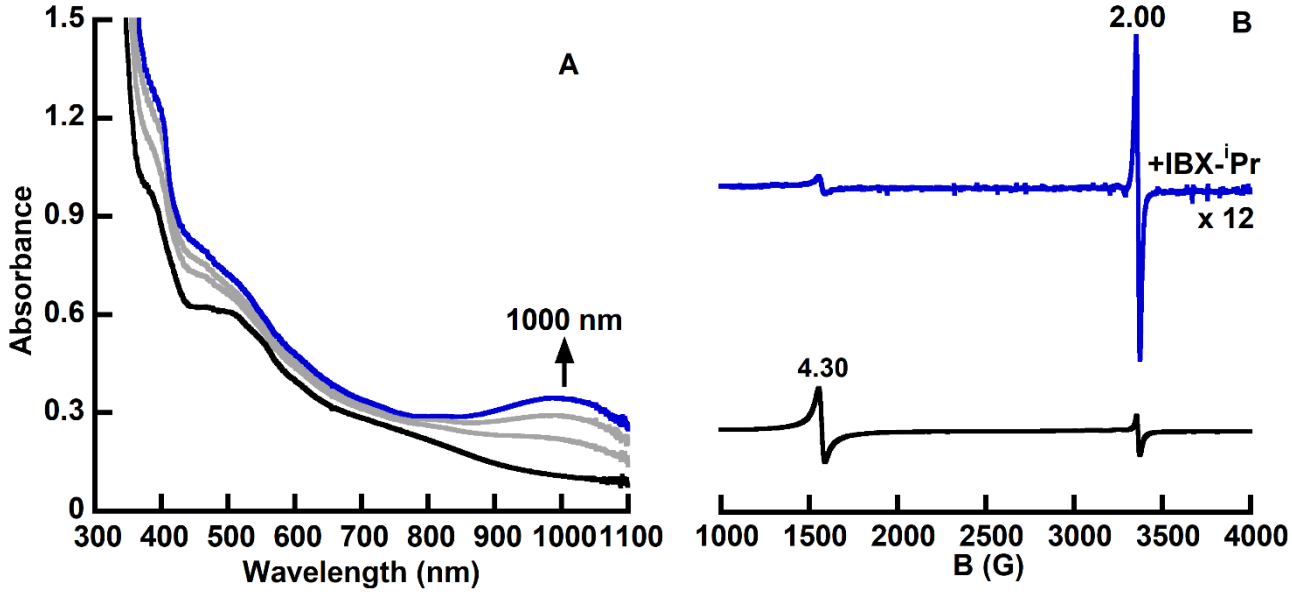

Figure 8. (A) UV-vis spectral traces of the reaction between [K(18-c-6)][Fe(pyCH_2S)ibaps] and IBX-^{i}Pr at -30 °C in MeCN. (B) Stacked perpendicular-mode EPR spectra of the reaction between [K(18-c-6)][Fe^{III}ibaps(pyCH_2S)] and IBX-^{i}Pr in MeCN at 77 K, scaled to adjust for concentration differences between the two samples.

To examine the oxidative capabilities of the putative [K(18-c-6)][Fe^{III}ibaps($PyCH_2S$)] complex, the reaction between this complex and isopropyl iodoxybenzoate (IBX-^{i}Pr), an oxo-transfer reagent, was performed. Reactions of metal complexes with oxo-transfer reagents, such as IBX-^{i}Pr and iodosobenzene are well-known to proceed through two-electron oxidation of the metal center and concomitant formation of a metal-oxo complex.[26,27] Upon addition of IBX-^{i}Pr at -30 °C in MeCN, new features are observed in the UV-vis spectrum at λ_{max} = 1000 nm (Figure 8A.). This is associated with the formation of a strong feature at g = 2 in the perpendicular-mode EPR spectrum (Figure 8B.).

The ability of this oxidized species to react with weak X—H bonds was explored using phenolic substrates, which are known to react with metal-oxo and metal-hydroxo complexes through hydrogen-atom transfer to generate phenoxyl radicals.[26,28–31]

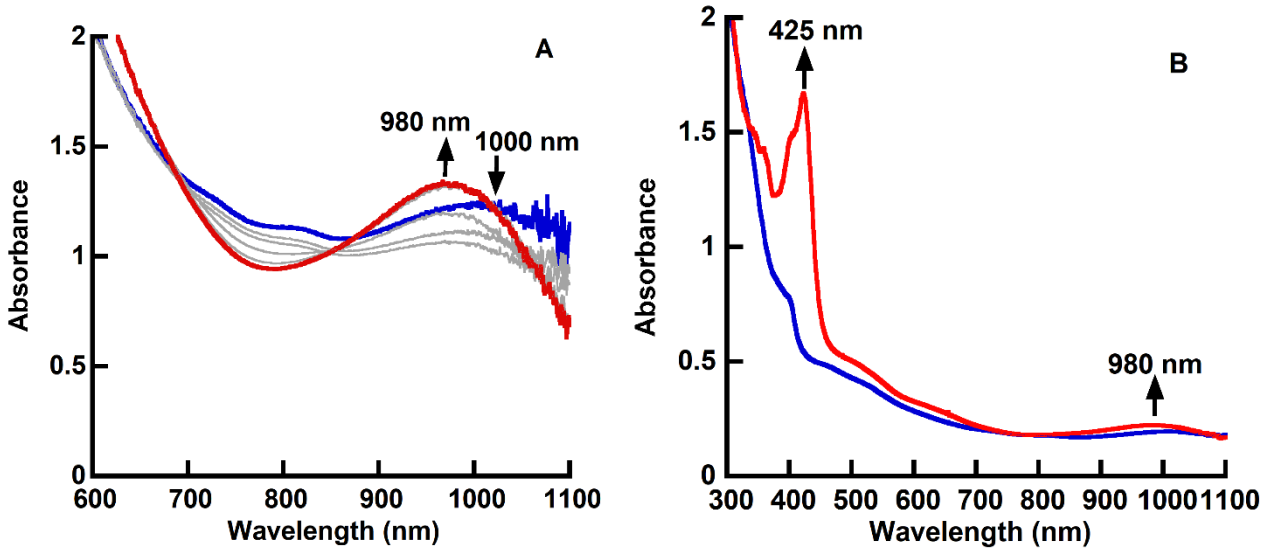

Figure 9. (A) UV-vis spectral traces of the reaction upon addition of 10 equivalents of $^{t}Bu_3PhOH$ to the product of [K(18-c-6)][Fe^{III}ibaps($pyCH_2S$)] and IBX-^{i}Pr at -30 °C in MeCN, zoomed into the low-energy region. (B) Stacked traces of before and after addition of 10 equivalents of $^{t}Bu_3PhOH$.

This oxidized species is reactive with 2,4,6-tri-tert-butyl phenol, leading to the observation of a strong feature at λ_{max} = 425 nm, corresponding to the phenoxy radical, and a moderately strong feature at λ_{max} = 980 nm (Figure 9).[32]

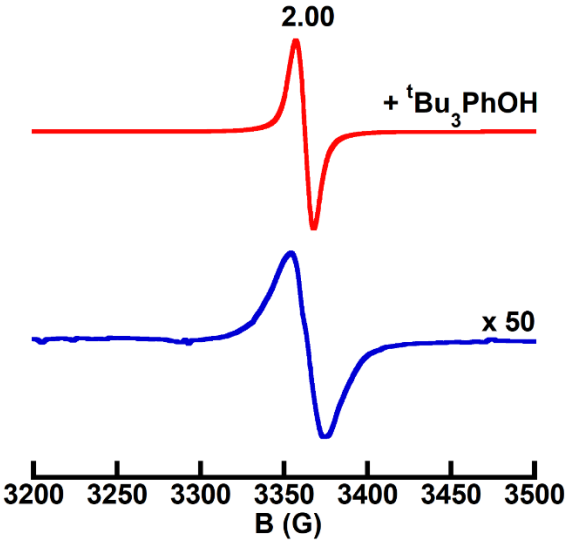

Figure 10. Stacked perpendicular-mode EPR spectra collected at 77 K of product of [K(18-c-6)][Fe^{III}ibaps(pyCH_2S)] and IBX-^{i}Pr at -30 °C in MeCN (blue), and the product upon addition of 10 equivalents of ^{t}Bu$_3$PhOH (red), scaled to similar heights.

Addition of a phenolic substrate, when studied by perpendicular-mode EPR spectroscopy, generates the sharp, intense g = 2 signal expected for a phenoxy radical (Figure 10).

Generation and Characterization of a Ferric Complex of H_3tap

When preparing the Fe(III) complex of $[tap]^{3-}$, H_3tap is dissolved in DMA, deprotonated with three equivalents of potassium hydride, and metalated with ferric bromide. Potassium pyridinemethylthiolate is then added in a minimal amount of DMA , followed by the addition of [2.2.2]-cryptand. This solution is concentrated by vacuum to a volume of approximately 1 mL and a 9:1 mixture of pentane:diethyl ether is added to precipitate out the putative [K(222-crypt)][Fe^{III}tap(pyCH_2S)] complex (Scheme 2). Further washing steps with pentane:diethyl ether and pure diethyl ether were required to remove all traces of DMA, giving the metal complex as a

brown solid in moderate yield (70%). This complex was then characterized by UV-vis and EPR spectroscopy (Figure 11).

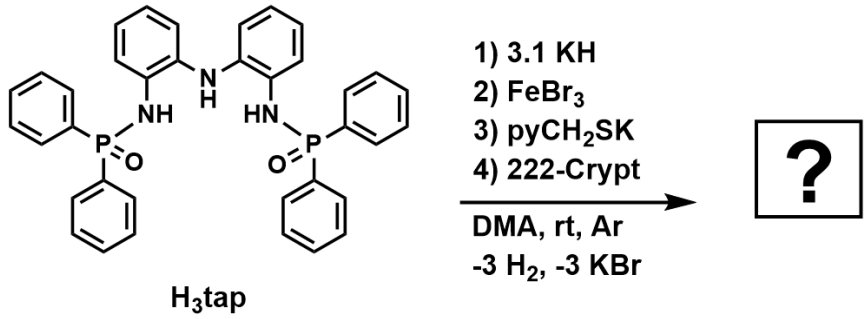

Scheme 2. Preparation of the putative [K(222-crypt)][Fe^{III}tap($pyCH_2S$)] complex.

The optical spectrum of [K(222-crypt)][Fe($pyCH_2S$)tap] was measured in tetrahydrofuran, with λ_{max} = 410 nm (1700 M^{-1} cm^{-1}), 510 nm (1100 M^{-1} cm^{-1}), 680 nm (600 M^{-1} cm^{-1}), and 785 nm (400 M^{-1} cm^{-1}). The perpendicular mode EPR spectrum of [K(222-crypt)][Fe^{III}tap($pyCH_2S$)] at 10 K exhibits a complicated pattern centered around g = 2 which is not obviously assignable.

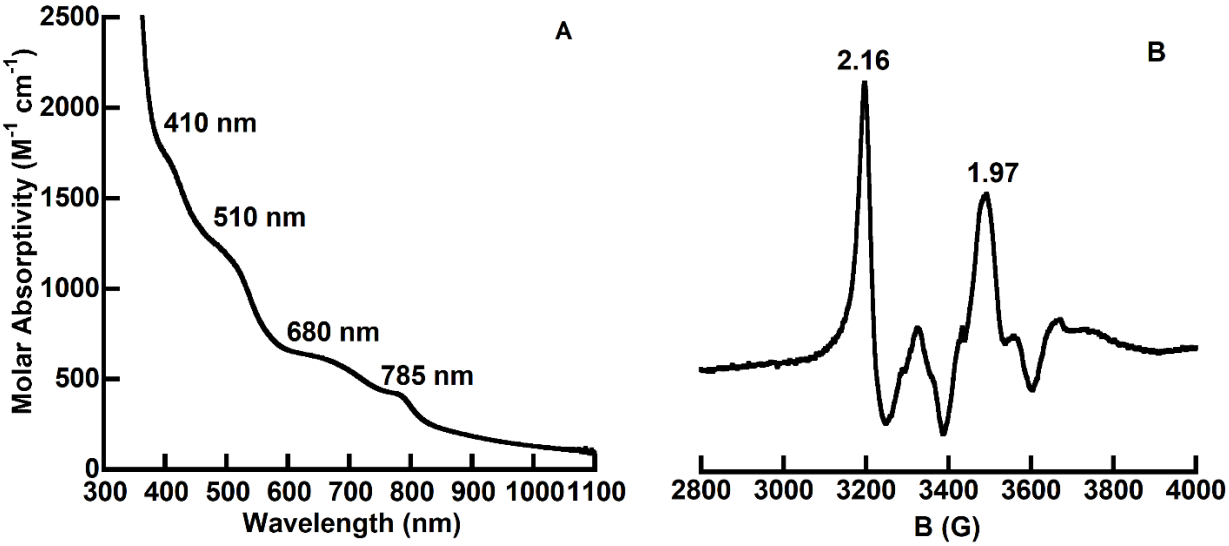

Figure 11. Characterization of [K(222-crypt)][Fe^{III}tap($pyCH_2S$)] by (A) optical spectroscopy collected at -20 °C in THF and (B) perpendicular-mode EPR spectrum collected at 10K in DMF/THF.

Organic carbon and nitrogen radicals present with significalntly smaller linewidths than are observed for [K(222-crypt)][Fe^{III}tap(pyCH_2S)], and the splitting pattern observed is not consistent with the small hyperfine coupling constants observed for nitrogenous radicals.[33,34] Moreover, while thiyl radicals have been observed with axial *g*-anisotropy, their linewidths are generally significantly smaller than those observed here.[35,36]

The electrochemistry of the putative [K(222-crypt)][Fe^{III}tap(pyCH_2S)] complex was investigated through cyclic voltammetry, revealing three oxidative events at – 0.47 V, + 0.34 V, and + 0.65V (Figure 12). In contrast to the electrochemistry of [K(18-c-6)][Fe^{III}ibaps(pyCH_2S)] the first oxidation event for [K(222-crypt)][Fe^{III}tap(pyCH_2S)] lies at a significantly more negative potential, supporting the stabilization of the higher oxidation state by a more strongly donating phosphonamido ligand.

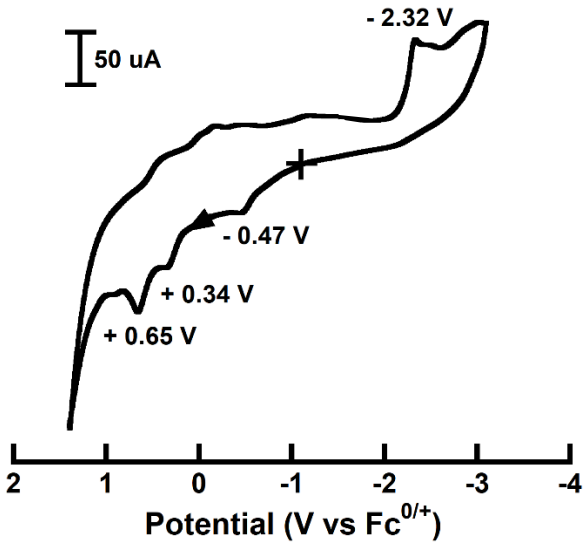

Figure 12. Cyclic voltammogram of [K(222-crypt)][Fe^{III}tap(pyCH_2S)] with 0.1 M NBu_4PF_6 in MeCN, 1 mM concentration, 400 mV/s scan rate.

Upon the addition of one equivalent of IBX-^{i}Pr at -20 °C in THF, new features were observed in the optical spectrum at λ_{max} = 520 nm and 960 nm. This is associated with a strong,

g = 2 signal with a complicated splitting pattern. The increased intensity of this feature compared to the starting [K(222-crypt)][Fe^{III}tap($pyCH_2S$)] species suggests ligand oxidation, however the linewidth of the g = 2.01 feature (peak-to-peak separation of 29 G) is significantly larger than that expected for an organic radical (see Figure 10, about 12 G peak-to-peak separation). This may be due to delocalization of significant spin density over multiple nuclei, as was proposed by Bogart for [Fe^{III}ibaps(bpy)].

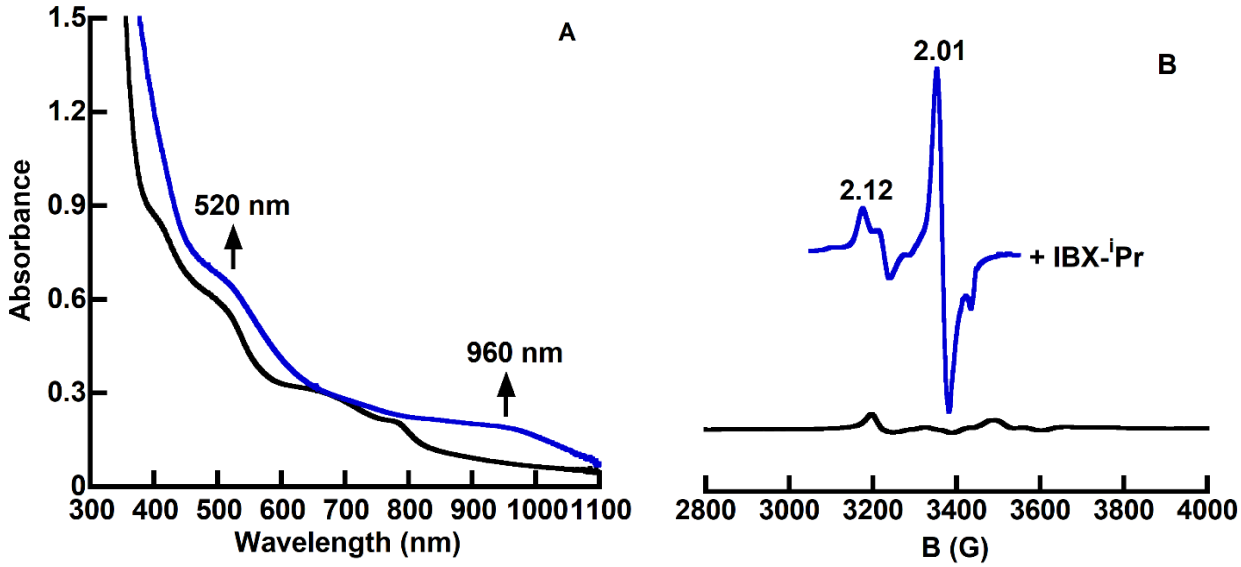

Figure 13. (A) UV-vis spectra of the reaction between [K(222-crypt)][Fe^{III}tap($pyCH_2S$)] and IBX-^{i}Pr at -20 °C in THF. (B) Stacked perpendicular-mode EPR spectra collected at 77 K of the reaction between [K(222-crypt)][Fe^{III}tap($pyCH_2S$)] and IBX-^{i}Pr in THF.

Future Plans

The identity of the product of the reaction between [K(18-c-6)][Fe^{III}ibaps($pyCH_2S$)] or [K(222-crypt)][Fe^{III}tap($pyCH_2S$)] and IBX-^{i}Pr remains largely unknown. While IBX-^{i}Pr is canonically a two-electron oxidant with coordinate O-atom transfer, which would suggest a formally [Fe^{V}(O)] product. Because the [ibaps]$^{-3}$ and [tap]$^{-3}$ ligands are redox-active, this product may also be more properly described as an iron(IV)-ligand radical or iron(III)-ligand diradical species. This distinction would need to be explored through careful study with a combination of

Mössbauer, EXAFS, and low-temperature EPR spectroscopies with computational methods, which may be able to distinguish the metal oxidation state and overall spin-state. Moreover, the secondary product formed upon reaction of this oxidized product with phenolic substrates, potentially a formal [Fe^{IV}(OH)] species, but also possibly an iron(III)-ligand radical or iron(II)-ligand diradical species, would need to be explored through the same methods.

To explicate the mechanism behind this observed reactivity, more detailed studies on the possible intermediates in these reactions will need to be undertaken. While these reactions undertaken at –30 °C are suggestive of the broad understanding of the reaction, we are unable to reject the possibility of intermediates which react too quickly to be detected at these temperatures. Low temperature studies at –80 °C may provide stronger evidence to reject potential intermediates if none are observed. While C—H bond activation was not observed for DHA, and phenolic substrates were reactive, further studies with more varied substrates may permit a thermodynamic exploration of this reaction.

Experimental

General Procedures. All reactions, unless otherwise noted, were performed under a nitrogen atmosphere in a dry box. All chemicals were purchased from commercial sources and used as received unless otherwise stated. Solvents were sparged with argon and dried over columns containing Q-5 and molecular sieves. Potassium hydride, as a 30% suspension in mineral oil, was filtered and washed with diethyl ether and pentane. H_3ibaps was prepared by literature procedures.[22] Elementary analysis was not performed unless otherwise stated.

[Fe^{III}ibaps(DMA)$_2$]. [Fe^{III}ibaps(DMA)$_2$] was prepared by modification to literature procedure.[22] H_3ibaps (132 mg, 0.180 mmol) was dissolved in dimethylacetamide (3 mL) with stirring. KH (22 mg, 0.558 mmol) was added to the reaction mixture and allowed to react for 90 minutes,

resulting in gas evolution and a color change. $FeBr_3$ (53 mg, 0.180 mmol) was added and allowed to react for two hours. The reaction mixture was then concentrated by vacuum and triturated with diethyl ether. This mixture was then filtered, and the ether solution concentrated by vacuum to give the [Fe^{III}ibaps(DMA)$_2$] (140 mg, 0.146 mmol, 81 % yield) as a dark, purple solid. λ_{max} (1:1 THF/Et_2O; ε_M, M^{-1} cm^{-1}) = 428 nm (1800), 550 nm (1400), 800 nm (240). λ_{max} (toluene; ε_M, M^{-1} cm^{-1}) = 385 nm (4000), 524 nm (2900), 800 nm (1200). X-Band EPR (toluene, 77K) g = 9.62, 4.30.

[K(18-c-6)][Fe^{III}ibaps(pyCH_2S)]. H_3ibaps (166 mg, 0.227 mmol) was dissolved in dimethylacetamide (3 mL) with stirring. KH (29 mg, 0.723 mmol) was added to the reaction mixture and allowed to react for 90 minutes, resulting in gas evolution and a color change. $FeBr_3$ (67 mg, 0.227 mmol) was added and allowed to react for two hours. A solution of potassium pyridinemethylthiolate (41 mg, 0.250 mmol) in a minimal amount of DMA was added and allowed to react for one hour. 18-crown-6 (60 mg, 0.227 mmol) was then added and allowed to react for one additional hour. The resulting solution is then concentrated by vacuum, washed with a mixed of pentane-diethyl ether to remove excess [Fe^{III}ibaps(DMA)$_2$], and redissolved in tetrahydrofuran. After filtering, this solution was evaporated and washed with diethyl ether to remove K[Fe^{III}ibaps(pyCH_2S)], leaving [K(18-c-6)][Fe^{III}ibaps(pyCH_2S)] (202 mg, 0.167 mmol, 74 % yield) as a dark red-brown solid. λ_{max} (MeCN; ε_M, M^{-1} cm^{-1}) = 400 nm (sh), 500 nm (3000), 750 nm (sh). X-Band EPR (MeCN, 77K) g = 7.74, 4.29, 2.00.

[K(222-crypt)][Fe^{III}tap(pyCH_2S)]. H_3tap (370 mg, 0.617 mmol) was dissolved in DMA (3 mL) with stirring. KH (77 mg, 1.92 mmol) was added to the reaction mixture, and allowed to react for 90 minutes. $FeBr_3$ (182 mg, 0.617 mmol) was added and allowed to react for two hours. Potassium pyridinemethylthiolate (101 mg, 0.617 mmol) was then added in a minimal amount

of DMA, followed by the addition of [2.2.2]-cryptand (232 mg, 0.617 mmol). This solution was concentrated by vacuum to a volume of approximately 1 mL and a 9:1 mixture of pentane:diethyl ether was added to precipitate out the putative [K(222-crypt)][Fe^{III}tap(pyCH_2S)] complex. Further washing steps with pentane:diethyl ether and pure diethyl ether were required to remove all traces of DMA, giving [K(222-crypt)][Fe^{III}tap(pyCH_2S)] (514 mg, 0.430 mmol, 70%) as a brown solid. λ_{max} (THF; ε_M, M^{-1} cm^{-1}) = 410 nm (1700), 510 nm (1100), 680 nm (600), 785 nm (400). X-Band EPR (1:1 DMF/THF, 77K) g = 2.16, 1.97.

Physical Methods. Electronic absorption spectra were collected on a Cary 60 spectrophotometer or an Agilent UV-vis spectrophotometer equipped with a Unisoku Unispeks cryostat in either a 1 cm quartz cuvette or a 1 mm thin cell quartz cuvette. X-Band (9.28 GHz) EPR spectra were collected as frozen solutions using a Bruker EMX spectrometer equipped with an ER041XG microwave bridge and the data was analyzed using SpinCount. Solid-state infrared spectra were collected on a Thermo Scientific Nicolet iS5 FT-IR spectrometer equipped with an iD5 ATR accessory. A Bruker SMART APEX-II diffractometer was used to collect crystallographic data. NMR spectra were collected on a Bruker DRX500 spectrometer. Cyclic voltammograms were collected at 400 mV/s to optimize reversibility.

Temperature-Controlled Reactivity Studies by UV-Vis Spectroscopy. For a standard experiment, a stock solution of the metal complex was prepared by dissolution in solvent. Solution (3 mL) was transferred to a 1 cm quartz cuvette equipped with a stirbar. The cuvette was then sealed with a rubber septum and transferred to a UV-vis spectrophotometer and allowed to thermally equilibrate for 15 minutes. Additional reagents were then added via gas-tight syringe. In certain cases, aliquots were removed to prepare samples for EPR spectroscopy.

References

(1) Hersleth, H.-P.; Uchida, T.; Røhr, Å. K.; Teschner, T.; Schü, V.; Kitagawa, T.; Trautwein,

A. X.; Gö Rbitz, C. H.; Andersson, K. K. Crystallographic and Spectroscopic Studies of Peroxide-Derived Myoglobin Compound II and Occurrence of Protonated Fe. *J. Biol. Chem.* **2007**, *282* (32), 23372–23386.

(2) Stone, K. L.; Behan, R. K.; Green, M. T. X-Ray Absorption Spectroscopy of Chloroperoxidase Compound I: Insight into the Reactive Intermediate of P450 Chemistry. *Proc. Natl. Acad. Sci. U. S. A.* **2005**, *102* (46), 16563–16565.

(3) Behan, R. K.; Green, M. T. On the Status of Ferryl Protonation. *J. Inorg. Biochem.* **2006**, *100* (4), 448–459.

(4) Zeng, W.; Barabanschikov, A.; Zhang, Y.; Zhao, J.; Sturhahn, W.; Alp, E. E.; Sage, J. T. Synchrotron-Derived Vibrational Data Confirm Unprotonated Oxo Ligand in Myoglobin Compound II. *J. Am. Chem. Soc.* **2008**, *130*, 1816–1817.

(5) Yosca, T. H.; Langston, M. C.; Krest, C. M.; Onderko, E. L.; Grove, T. L.; Livada, J.; Green, M. T. Spectroscopic Investigations of Catalase Compound II: Characterization of an Iron(IV) Hydroxide Intermediate in a Non-Thiolate-Ligated Heme Enzyme. *J. Am. Chem. Soc.* **2016**, *138* (49), 16016–16023.

(6) Penner-Hahn, J. E.; Smith Eble, K.; McMurry, T. J.; Mark Renner, L.; Balch, A. L.; Groves, J. T.; Dawson, J. H.; Hodgson, K. O.; In Cytochrome P-, J. E.; Implications, E.; et al. Structural Characterization of Horseradish Peroxidase Using EXAFS Spectroscopy. Evidence for Fe=0 Ligation in Compounds I and II. *J. Am. Chem. Soc.* **1986**, *108*, 7819–7825.

(7) Kincaid, J. R.; Zheng, Y.; Al-Mustafa, J.; Czarnecki, K. Resonance Raman Spectra of Native and Mesoheme-Reconstituted Horseradish Peroxidase and Their Catalytic

Intermediates. *J. Biol. Chem.* **1996**, *271* (46), 28805–28811.

(8) Casadei, C. M.; Gumiero, A.; Metcalfe, C. L.; Murphy, E. J.; Basran, J.; Concilio, M. G.; Teixeira, S. C. M.; Schrader, T. E.; Fielding, A. J.; Ostermann, A.; et al. Neutron Cryo-Crystallography Captures the Protonation State of Ferryl Heme in a Peroxidase. *Science (80-.).* **2014**, *345* (6193), 193–197.

(9) Stone, K. L.; Hoffart, L. M.; Behan, R. K.; Krebs, C.; Green, M. T. Evidence for Two Ferryl Species in Chloroperoxidase Compound II. *J. Am. Chem. Soc.* **2006**, *128*, 6147–6153.

(10) Behan, R. K.; Hoffart, L. M.; Stone, K. L.; Krebs, C.; Green, M. T. Evidence for Basic Ferryls in Cytochromes P450. *J. Am. Chem. Soc.* **2006**, *128* (35), 11471–11474.

(11) Sitter, A. J.; Reczek, C. M.; Terner, J. Heme-Linked Ionization of Horseradish Peroxidase Compound II Monitored by the Resonance Raman Fe(IV)=O Stretching Vibration. *J. Biol. Chem.* **1985**, *260* (12), 7515–7522.

(12) Yosca, T. H.; Rittle, J.; Krest, C. M.; Onderko, E. L.; Silakov, A.; Calixto, J. C.; Behan, R. K.; Green, M. T. Iron(IV)Hydroxide PKa and the Role of Thiolate Ligation in C-H Bond Activation by Cytochrome P450. *Science (80-.).* **2013**, *342* (6160), 825–829.

(13) Yosca, T. H.; Ledray, A. P.; Ngo, J.; Green, M. T. A New Look at the Role of Thiolate Ligation in Cytochrome P450. *J. Biol. Inorg. Chem.* **2017**, *22*, 209–220.

(14) Lu, A. Y.; Junk, K. W.; Coon, M. J. Resolution of the Cytochrome P-450-Containing Omega-Hydroxylation System of Liver Microsomes into Three Components. *J. Biol. Chem.* **1969**, *244* (13), 3714–3721.

(15) Groves, J. T.; Haushalter, R. C.; Nakamura, M.; Nemo, T. E.; Evans, B. J. High-Valent Iron-Porphyrin Complexes Related to Peroxidase and Cytochrome P-450. *J. Am. Chem. Soc.* **1981**, *103* (10), 2884–2886.

(16) Das, P. K.; Samanta, S.; Mcquarters, A. B.; Lehnert, N.; Dey, A. Valence Tautomerism in Synthetic Models of Cytochrome P450. *Proc. Natl. Acad. Sci.* **2016**, *113* (24), 6611–6616.

(17) Tani, F.; Matsu-ura, M.; Nakayama, S.; Naruta, Y. Synthetic Models for the Active Site of Cytochrome P450. *Coord. Chem. Rev.* **2002**, *226*, 219–226.

(18) Collman, J. P.; Groh, S. E. "Mercaptan-Tail" Porphyrins: Synthetic Analogues for the Active Site of Cytochrome P-4501. *J. Am. Chem. Soc* **1982**, *104*, 1391–1403.

(19) Cook, S. A. Principles of Molecular Design in the Development of Ligand Frameworks That Control the Primary and Secondary Coordination Spheres of Metal Ions, University of California, Irvine, 2015.

(20) Cook, B. J.; Pink, M.; Pal, K.; Caulton, K. G. Electron and Oxygen Atom Transfer Chemistry of Co(II) in a Proton Responsive, Redox Active Ligand Environment. *Inorg. Chem.* **2018**, *57* (10), 6176–6185.

(21) Wong, J. L.; Sánchez, R. H.; Logan, J. G.; Zarkesh, R. A.; Ziller, J. W.; Heyduk, A. F. Disulfide Reductive Elimination from an Iron(III) Complex. *Chem. Sci.* **2013**, *4*, 1906–1910.

(22) Cook, S. A.; Bogart, J. A.; Levi, N.; Weitz, A. C.; Moore, C.; Rheingold, A. L.; Ziller, J. W.; Hendrich, M. P.; Borovik, A. S. Mononuclear Complexes of a Tridentate Redox-Active Ligand with Sulfonamido Groups: Structure, Properties, and Reactivity. *Chem. Sci.*

2018, *9* (31), 6540–6547.

(23) Shearer, J.; Scarrow, R. C.; Kovacs, J. A. Synthetic Models for the Cysteinate-Ligated Non-Heme Iron Enzyme Superoxide Reductase: Observation and Structural Characterization by XAS of an Fe^{III}-OOH Intermediate. *J. Biol. Inorg. Chem* **1998**, *16* (4), 9.

(24) Kitagawa, T.; Dey, A.; Lugo-Mas, P.; Benedict, J. B.; Kaminsky, W.; Solomon, E.; Kovacs, J. A. A Functional Model for the Cysteinate-Ligated Non-Heme Iron Enzyme Superoxide Reductase (SOR). *J. Am. Chem. Soc.* **2006**, *128*, 14448–14449.

(25) Fischer, A. A.; Miller, J. R.; Jodts, R. J.; Ekanayake, D. M.; Lindeman, S. V; Brunold, T. C.; Fiedler, A. T. Spectroscopic and Computational Comparisons of Thiolate-Ligated Ferric Nonheme Complexes to Cysteine Dioxygenase: Second-Sphere Effects on Substrate (Analogue) Positioning. **2020**, *22*, 55.

(26) Goldsmith, C. R.; Daniel, T.; Stack, P. Hydrogen Atom Abstraction by a Mononuclear Ferric Hydroxide Complex: Insights into the Reactivity of Lipoxygenase. *Inorg. Chem.* **2006**, *45*, 6048–6055.

(27) Widger, L. R.; Davies, C. G.; Yang, T.; Siegler, M. A.; Troeppner, O.; Jameson, G. N. L.; Ivanović-, I. I.-; Burmazović, B.; Goldberg, D. P. Dramatically Accelerated Selective Oxygen-Atom Transfer by a Nonheme Iron(IV)-Oxo Complex: Tuning of the First and Second Coordination Spheres. *J. Am. Chem. Soc.* **2014**, *136*, 2699–2702.

(28) Wijeratne, G. B.; Corzine, B.; Day, V. W.; Jackson, T. A. Saturation Kinetics in Phenolic O−H Bond Oxidation by a Mononuclear Mn(III)−OH Complex Derived from Dioxygen. *Inorg. Chem* **2014**, *53*, 17.

(29) Altwicker, E. R. The Chemistry of Stable Phenoxy Radicals. *Chem. Rev.* **1967**, *67* (5), 475–531.

(30) Borovik, A. S. Role of Metal-Oxo Complexes in the Cleavage of C—H Bonds. *Chem. Soc. Rev.* **2011**, *40*, 1870–1874.

(31) Usharani, D.; Lacy, D. C.; Borovik, A. S.; Shaik, S. Dichotomous Hydrogen Atom Transfer vs Proton-Coupled Electron Transfer During Activation of X−H Bonds (X = C, N, O) by Nonheme Iron−Oxo Complexes of Variable Basicity. *J. Am. Chem. Soc.* **2013**, *135*, 17090–17104.

(32) Manner, V. W.; Markle, T. F.; Freudenthal, J. H.; Roth, J. P.; Mayer, J. M. The First Crystal Structure of a Monomeric Phenoxyl Radical: 2,4,6-Tri-Tert-Butylphenoxyl Radical. *Chem. Commun.* **2008**, No. 2, 256–258.

(33) Reddy, T. J.; Iwama, T.; Halpern, H. J.; Rawal, V. H. General Synthesis of Persistent Trityl Radicals for EPR Imaging of Biological Systems. *J. Org. Chem.* **2002**, *67*, 4635–4639.

(34) Mitchell, D. G.; Quine, R. W.; Tseitlin, M.; Eaton, S. S.; Eaton, G. R. X-Band Rapid-Scan EPR of Nitroxyl Radicals. *J. Magn. Reson.* **2012**, *214*, 221–226.

(35) Lassmann, G.; Kolberg, M.; Bleifuss, G.; Gräslund, A.; Sjöberg, B.-M.; Lubitz, W. Protein Thiyl Radicals in Disordered Systems: A Comparative EPR Study at Low Temperaturey. *Phys. Chem. Chem. Phys.* **2003**, *5*, 2442–2453.

(36) Bergene, R.; Sagstuen, E. International Journal of Radiation Biology and Related Studies in Physics, Chemistry and Medicine Studies of Sulphur-Substituted Pyrimidines 2-Thio-5-

Carboxyuracil at 77 K. *Int. J. Radiat. Biol.* **1975**, *28* (2), 137–146.

Appendix

Table 1. Crystal data and structure refinement for $Cu^{II}H_2$dippy.

Empirical formula	$C_{29}\ H_{45}\ Cu\ N_5\ O_9$	
Formula weight	671.24	
Temperature	133(2) K	
Wavelength	0.71073 Å	
Crystal system	Monoclinic	
Space group	$P2_1$	
Unit cell dimensions	a = 13.141(3) Å	α = 90°.
	b = 17.777(4) Å	β = 102.461(3)°.
	c = 15.787(4) Å	γ = 90°.
Volume	3600.9(15) $Å^3$	
Z	4	
Density (calculated)	1.238 Mg/m^3	
Absorption coefficient	0.659 mm^{-1}	
F(000)	1420	
Crystal color	blue	
Crystal size	0.406 x 0.390 x 0.182 mm^3	
Theta range for data collection	1.321 to 28.826°	
Index ranges	$-17 \le h \le 16, 0 \le k \le 23, 0 \le l \le 21$	
Reflections collected	8740	
Independent reflections	8740 [R(int) = MERGED]	
Completeness to theta = 25.500°	99.9 %	
Absorption correction	Semi-empirical from equivalents	
Max. and min. transmission	0.745790 and 0.632088	
Refinement method	Full-matrix least-squares on F^2	
Data / restraints / parameters	8740 / 1 / 797	
Goodness-of-fit on F^2	1.134	
Final R indices [I>2sigma(I) = 8033 data]	R1 = 0.0578, wR2 = 0.1471	
R indices (all data, 0.74 Å)	R1 = 0.0685, wR2 = 0.1550	
Absolute structure parameter	0.088(14)	
Extinction coefficient	n/a	
Largest diff. peak and hole	1.265 and -1.016 $e.Å^{-3}$	

Table 2. Atomic coordinates (x 10^4) and equivalent isotropic displacement parameters ($Å^2$x 10^3) for $Cu^{II}H_2$dippy. U(eq) is defined as one third of the trace of the orthogonalized U^{ij} tensor.

	x	y	z	U(eq)
Cu(1)	10066(1)	5165(1)	9973(1)	17(1)
O(1)	8688(4)	5921(3)	10052(3)	20(1)
O(2)	8852(4)	4384(3)	9363(3)	22(1)
O(3)	6016(5)	6092(4)	10318(4)	34(1)
O(4)	6199(4)	6459(3)	8993(3)	24(1)
O(5)	11537(4)	6999(3)	9239(3)	22(1)
O(6)	5619(4)	2857(4)	8955(4)	40(2)
O(7)	6268(4)	3980(3)	9427(4)	31(1)
O(8)	11757(4)	3462(3)	11252(3)	25(1)
N(1)	11575(4)	5249(3)	10270(4)	18(1)
N(2)	10284(4)	6089(3)	9328(4)	18(1)
N(3)	10388(4)	4298(3)	10731(4)	18(1)
N(4)	8057(4)	7087(3)	9661(4)	18(1)
N(5)	8180(4)	3246(4)	9617(4)	20(1)
C(1)	12028(5)	5827(4)	9980(4)	18(1)
C(2)	13113(5)	5896(4)	10176(5)	22(1)
C(3)	13676(5)	5328(4)	10678(5)	30(2)
C(4)	13192(6)	4719(4)	10961(5)	28(2)
C(5)	12099(5)	4695(4)	10739(5)	21(1)
C(6)	11241(5)	6375(4)	9460(4)	16(1)
C(7)	9391(5)	6548(4)	8953(4)	18(1)
C(8)	8678(5)	6499(4)	9604(4)	17(1)
C(9)	7298(5)	7037(4)	10208(4)	21(1)
C(10)	6441(5)	6459(5)	9855(5)	25(2)
C(11)	5436(6)	5901(5)	8596(5)	31(2)
C(12)	8822(5)	6231(4)	8056(4)	22(1)
C(13)	9598(6)	6169(6)	7471(5)	36(2)
C(14)	7895(5)	6721(5)	7627(4)	25(2)
C(15)	6794(6)	7802(5)	10269(5)	29(2)
C(16)	11385(5)	4081(4)	10943(4)	21(1)
C(17)	9588(5)	3732(4)	10716(4)	19(1)
C(18)	8833(5)	3821(4)	9818(4)	17(1)
C(19)	7369(5)	3214(4)	8806(4)	22(1)
C(20)	6303(5)	3322(4)	9061(5)	24(2)
C(21)	5342(6)	4133(5)	9746(6)	36(2)

C(22)	8995(6)	3813(5)	11454(5)	27(2)
C(23)	9748(8)	3691(6)	12327(6)	43(2)
C(24)	8412(8)	4567(5)	11408(6)	43(2)
C(25)	7428(6)	2484(5)	8320(5)	28(2)
Cu(2)	4903(1)	5446(1)	4928(1)	29(1)
O(9)	5062(4)	6344(3)	6110(3)	29(1)
O(10)	4184(4)	4765(3)	5671(3)	25(1)
O(11)	5046(5)	8434(4)	8274(4)	41(2)
O(12)	4075(4)	7420(3)	7835(4)	33(1)
O(13)	4326(5)	7366(3)	3523(4)	37(1)
O(14)	4137(5)	4639(3)	7725(4)	34(1)
O(15)	2502(4)	4835(3)	6992(4)	37(1)
O(16)	6692(5)	3828(4)	4216(4)	36(1)
N(6)	5434(5)	5578(4)	3891(4)	31(2)
N(7)	5845(5)	4596(4)	5040(4)	28(1)
N(8)	4133(5)	6372(4)	4447(4)	33(2)
N(9)	4329(5)	3639(4)	6348(4)	23(1)
N(10)	4587(5)	7559(4)	6264(4)	27(1)
C(26)	6060(7)	5045(5)	3693(5)	33(2)
C(27)	6381(7)	5094(6)	2917(5)	41(2)
C(28)	6072(8)	5700(6)	2377(6)	46(2)
C(29)	5434(8)	6247(5)	2594(5)	42(2)
C(30)	5106(7)	6169(5)	3384(5)	38(2)
C(31)	6259(6)	4417(5)	4370(5)	31(2)
C(32)	5757(6)	4037(5)	5703(5)	25(2)
C(33)	4687(6)	4170(4)	5895(4)	22(2)
C(34)	3342(5)	3741(4)	6634(4)	22(1)
C(35)	3397(6)	4456(4)	7168(5)	26(2)
C(36)	2491(8)	5519(6)	7496(8)	52(3)
C(37)	6611(6)	4103(5)	6550(5)	30(2)
C(38)	7696(7)	3946(8)	6354(7)	58(3)
C(39)	6574(7)	4865(5)	6978(6)	39(2)
C(40)	3165(6)	3068(4)	7178(5)	27(2)
C(41)	4462(7)	6704(5)	3791(5)	34(2)
C(42)	3678(6)	6851(6)	5014(5)	35(2)
C(43)	4499(6)	6895(5)	5856(5)	27(2)
C(44)	5353(5)	7714(5)	7055(5)	25(2)
C(45)	4817(5)	7909(4)	7786(5)	25(2)
C(46)	3536(8)	7564(6)	8535(7)	47(2)
C(47A)	2595(17)	6675(15)	5207(14)	44(5)

C(47B)	2669(12)	6395(11)	5132(10)	22(3)
C(48A)	2218(18)	7113(15)	5904(15)	47(6)
C(48B)	2189(14)	6873(11)	5736(12)	29(4)
C(49A)	1760(20)	6711(17)	4306(17)	62(6)
C(49B)	1891(15)	6307(12)	4229(12)	37(4)
C(50)	6109(6)	8342(6)	6913(6)	35(2)
O(17)	10922(5)	2745(4)	7958(4)	37(1)
C(51)	10378(7)	3306(5)	8334(6)	38(2)
C(52)	10847(8)	4055(5)	8253(6)	41(2)
C(53)	10407(7)	2042(6)	7834(7)	42(2)
C(54)	10978(9)	1525(6)	7364(8)	56(3)
O(18)	1507(7)	2719(6)	5226(6)	73(2)
C(55)	549(19)	3012(15)	4994(17)	135(8)
C(56)	185(17)	3417(13)	5711(14)	120(7)
C(57A)	1894(18)	2372(15)	4573(16)	47(5)
C(57B)	1750(20)	2120(19)	4720(20)	67(8)
C(58A)	3131(12)	2165(9)	4877(10)	19(3)
C(58B)	2867(16)	1957(13)	4958(14)	40(5)

Table 3. Bond lengths [Å] and angles [°] for $Cu^{II}H_2$dippy.

Cu(1)-N(3)	1.942(6)
Cu(1)-N(1)	1.942(5)
Cu(1)-N(2)	1.985(6)
Cu(1)-O(2)	2.177(5)
Cu(1)-O(1)	2.280(5)
O(1)-C(8)	1.246(9)
O(2)-C(18)	1.235(9)
O(3)-C(10)	1.204(9)
O(4)-C(10)	1.328(9)
O(4)-C(11)	1.453(9)
O(5)-C(6)	1.250(8)
O(6)-C(20)	1.205(9)
O(7)-C(20)	1.310(10)
O(7)-C(21)	1.440(10)
O(8)-C(16)	1.259(9)
N(1)-C(1)	1.318(9)
N(1)-C(5)	1.330(9)
N(2)-C(6)	1.330(8)

N(2)-C(7)	1.447(9)
N(3)-C(16)	1.338(9)
N(3)-C(17)	1.451(9)
N(4)-C(8)	1.342(9)
N(4)-C(9)	1.456(8)
N(5)-C(18)	1.328(9)
N(5)-C(19)	1.480(8)
C(1)-C(2)	1.397(9)
C(1)-C(6)	1.526(9)
C(2)-C(3)	1.394(11)
C(3)-C(4)	1.379(11)
C(4)-C(5)	1.404(9)
C(5)-C(16)	1.519(9)
C(7)-C(8)	1.535(9)
C(7)-C(12)	1.557(9)
C(9)-C(15)	1.525(10)
C(9)-C(10)	1.537(10)
C(12)-C(13)	1.520(10)
C(12)-C(14)	1.532(10)
C(17)-C(22)	1.540(10)
C(17)-C(18)	1.553(9)
C(19)-C(25)	1.518(11)
C(19)-C(20)	1.550(10)
C(22)-C(23)	1.529(12)
C(22)-C(24)	1.538(12)
Cu(2)-N(6)	1.927(6)
Cu(2)-N(7)	1.937(7)
Cu(2)-N(8)	1.995(8)
Cu(2)-O(10)	2.052(5)
Cu(2)-O(9)	2.430(6)
O(9)-C(43)	1.242(10)
O(10)-C(33)	1.258(10)
O(11)-C(45)	1.207(10)
O(12)-C(45)	1.321(9)
O(12)-C(46)	1.458(10)
O(13)-C(41)	1.251(11)
O(14)-C(35)	1.206(10)
O(15)-C(35)	1.331(10)
O(15)-C(36)	1.454(11)
O(16)-C(31)	1.239(11)

N(6)-C(30)	1.335(12)
N(6)-C(26)	1.335(12)
N(7)-C(31)	1.329(10)
N(7)-C(32)	1.467(9)
N(8)-C(41)	1.341(10)
N(8)-C(42)	1.453(12)
N(9)-C(33)	1.330(9)
N(9)-C(34)	1.474(9)
N(10)-C(43)	1.337(11)
N(10)-C(44)	1.451(9)
C(26)-C(27)	1.381(10)
C(26)-C(31)	1.529(12)
C(27)-C(28)	1.380(15)
C(28)-C(29)	1.375(15)
C(29)-C(30)	1.412(11)
C(30)-C(41)	1.505(14)
C(32)-C(33)	1.519(10)
C(32)-C(37)	1.553(9)
C(34)-C(35)	1.519(10)
C(34)-C(40)	1.521(10)
C(37)-C(39)	1.520(12)
C(37)-C(38)	1.547(12)
C(42)-C(43)	1.523(10)
C(42)-C(47A)	1.55(2)
C(42)-C(47B)	1.599(18)
C(44)-C(45)	1.516(10)
C(44)-C(50)	1.543(11)
C(47A)-C(48A)	1.52(3)
C(47A)-C(49A)	1.60(3)
C(47B)-C(48B)	1.51(3)
C(47B)-C(49B)	1.57(2)
O(17)-C(53)	1.413(11)
O(17)-C(51)	1.429(10)
C(51)-C(52)	1.485(13)
C(53)-C(54)	1.482(15)
O(18)-C(55)	1.34(2)
O(18)-C(57A)	1.39(2)
O(18)-C(57B)	1.41(3)
C(55)-C(56)	1.50(3)
C(57A)-C(58A)	1.64(3)

C(57B)-C(58B)	1.46(4)

N(3)-Cu(1)-N(1)	80.6(2)
N(3)-Cu(1)-N(2)	159.5(2)
N(1)-Cu(1)-N(2)	78.9(2)
N(3)-Cu(1)-O(2)	78.9(2)
N(1)-Cu(1)-O(2)	140.2(2)
N(2)-Cu(1)-O(2)	118.3(2)
N(3)-Cu(1)-O(1)	120.3(2)
N(1)-Cu(1)-O(1)	136.3(2)
N(2)-Cu(1)-O(1)	75.2(2)
O(2)-Cu(1)-O(1)	83.42(19)
C(8)-O(1)-Cu(1)	111.5(4)
C(18)-O(2)-Cu(1)	111.4(4)
C(10)-O(4)-C(11)	115.7(6)
C(20)-O(7)-C(21)	115.8(6)
C(1)-N(1)-C(5)	123.5(5)
C(1)-N(1)-Cu(1)	119.3(5)
C(5)-N(1)-Cu(1)	117.2(4)
C(6)-N(2)-C(7)	120.3(6)
C(6)-N(2)-Cu(1)	118.1(4)
C(7)-N(2)-Cu(1)	118.8(4)
C(16)-N(3)-C(17)	118.2(6)
C(16)-N(3)-Cu(1)	117.0(5)
C(17)-N(3)-Cu(1)	118.7(4)
C(8)-N(4)-C(9)	119.7(6)
C(18)-N(5)-C(19)	122.9(6)
N(1)-C(1)-C(2)	120.5(6)
N(1)-C(1)-C(6)	112.3(5)
C(2)-C(1)-C(6)	127.1(6)
C(3)-C(2)-C(1)	116.9(6)
C(4)-C(3)-C(2)	121.9(6)
C(3)-C(4)-C(5)	117.5(7)
N(1)-C(5)-C(4)	119.7(6)
N(1)-C(5)-C(16)	112.4(6)
C(4)-C(5)-C(16)	127.8(6)
O(5)-C(6)-N(2)	129.5(6)
O(5)-C(6)-C(1)	120.1(6)
N(2)-C(6)-C(1)	110.4(6)
N(2)-C(7)-C(8)	104.7(5)

N(2)-C(7)-C(12)	110.9(5)
C(8)-C(7)-C(12)	110.2(5)
O(1)-C(8)-N(4)	122.5(6)
O(1)-C(8)-C(7)	119.6(6)
N(4)-C(8)-C(7)	117.9(6)
N(4)-C(9)-C(15)	110.1(6)
N(4)-C(9)-C(10)	111.6(6)
C(15)-C(9)-C(10)	108.9(6)
O(3)-C(10)-O(4)	125.5(7)
O(3)-C(10)-C(9)	122.8(7)
O(4)-C(10)-C(9)	111.5(6)
C(13)-C(12)-C(14)	110.3(6)
C(13)-C(12)-C(7)	109.0(6)
C(14)-C(12)-C(7)	112.1(6)
O(8)-C(16)-N(3)	128.8(6)
O(8)-C(16)-C(5)	120.3(6)
N(3)-C(16)-C(5)	110.9(6)
N(3)-C(17)-C(22)	114.0(6)
N(3)-C(17)-C(18)	105.2(5)
C(22)-C(17)-C(18)	110.7(6)
O(2)-C(18)-N(5)	125.3(6)
O(2)-C(18)-C(17)	121.6(6)
N(5)-C(18)-C(17)	113.1(6)
N(5)-C(19)-C(25)	111.4(6)
N(5)-C(19)-C(20)	107.0(6)
C(25)-C(19)-C(20)	112.6(6)
O(6)-C(20)-O(7)	125.3(7)
O(6)-C(20)-C(19)	124.6(7)
O(7)-C(20)-C(19)	110.1(6)
C(23)-C(22)-C(24)	112.7(8)
C(23)-C(22)-C(17)	109.5(7)
C(24)-C(22)-C(17)	111.9(6)
N(6)-Cu(2)-N(7)	80.3(3)
N(6)-Cu(2)-N(8)	79.8(3)
N(7)-Cu(2)-N(8)	160.1(3)
N(6)-Cu(2)-O(10)	148.5(3)
N(7)-Cu(2)-O(10)	81.5(2)
N(8)-Cu(2)-O(10)	116.5(3)
N(6)-Cu(2)-O(9)	125.8(2)
N(7)-Cu(2)-O(9)	119.6(2)

N(8)-Cu(2)-O(9)	72.7(2)
O(10)-Cu(2)-O(9)	85.5(2)
C(43)-O(9)-Cu(2)	108.9(5)
C(33)-O(10)-Cu(2)	112.2(5)
C(45)-O(12)-C(46)	114.5(7)
C(35)-O(15)-C(36)	114.9(7)
C(30)-N(6)-C(26)	123.6(7)
C(30)-N(6)-Cu(2)	118.4(6)
C(26)-N(6)-Cu(2)	117.9(5)
C(31)-N(7)-C(32)	120.9(7)
C(31)-N(7)-Cu(2)	118.6(6)
C(32)-N(7)-Cu(2)	116.5(5)
C(41)-N(8)-C(42)	117.5(8)
C(41)-N(8)-Cu(2)	115.8(7)
C(42)-N(8)-Cu(2)	119.4(5)
C(33)-N(9)-C(34)	120.9(6)
C(43)-N(10)-C(44)	123.6(6)
N(6)-C(26)-C(27)	119.0(9)
N(6)-C(26)-C(31)	112.0(7)
C(27)-C(26)-C(31)	128.8(9)
C(28)-C(27)-C(26)	119.5(9)
C(29)-C(28)-C(27)	120.8(8)
C(28)-C(29)-C(30)	118.0(9)
N(6)-C(30)-C(29)	119.1(9)
N(6)-C(30)-C(41)	112.3(7)
C(29)-C(30)-C(41)	128.5(9)
O(16)-C(31)-N(7)	130.0(8)
O(16)-C(31)-C(26)	119.7(7)
N(7)-C(31)-C(26)	110.1(7)
N(7)-C(32)-C(33)	104.8(6)
N(7)-C(32)-C(37)	114.2(6)
C(33)-C(32)-C(37)	110.2(6)
O(10)-C(33)-N(9)	121.6(7)
O(10)-C(33)-C(32)	121.9(6)
N(9)-C(33)-C(32)	116.5(7)
N(9)-C(34)-C(35)	109.5(6)
N(9)-C(34)-C(40)	109.1(6)
C(35)-C(34)-C(40)	109.9(6)
O(14)-C(35)-O(15)	123.6(8)
O(14)-C(35)-C(34)	124.3(7)

O(15)-C(35)-C(34)	111.9(7)
C(39)-C(37)-C(38)	111.6(8)
C(39)-C(37)-C(32)	111.3(7)
C(38)-C(37)-C(32)	109.9(7)
O(13)-C(41)-N(8)	128.9(9)
O(13)-C(41)-C(30)	120.1(7)
N(8)-C(41)-C(30)	110.9(8)
N(8)-C(42)-C(43)	105.0(7)
N(8)-C(42)-C(47A)	121.4(12)
C(43)-C(42)-C(47A)	110.2(10)
N(8)-C(42)-C(47B)	103.7(9)
C(43)-C(42)-C(47B)	111.9(8)
O(9)-C(43)-N(10)	123.9(7)
O(9)-C(43)-C(42)	120.1(9)
N(10)-C(43)-C(42)	115.9(7)
N(10)-C(44)-C(45)	110.4(6)
N(10)-C(44)-C(50)	111.2(6)
C(45)-C(44)-C(50)	111.4(7)
O(11)-C(45)-O(12)	123.9(7)
O(11)-C(45)-C(44)	124.7(7)
O(12)-C(45)-C(44)	111.4(7)
C(48A)-C(47A)-C(42)	119.8(19)
C(48A)-C(47A)-C(49A)	111(2)
C(42)-C(47A)-C(49A)	107.3(17)
C(48B)-C(47B)-C(49B)	110.4(15)
C(48B)-C(47B)-C(42)	104.9(14)
C(49B)-C(47B)-C(42)	109.7(12)
C(53)-O(17)-C(51)	114.1(7)
O(17)-C(51)-C(52)	109.6(7)
O(17)-C(53)-C(54)	109.8(8)
C(55)-O(18)-C(57A)	116.3(16)
C(55)-O(18)-C(57B)	117.3(18)
O(18)-C(55)-C(56)	114(2)
O(18)-C(57A)-C(58A)	112.4(16)
O(18)-C(57B)-C(58B)	110(2)

Table 4. Anisotropic displacement parameters ($Å^2 x\ 10^3$) for $Cu^{II}H_2$dippy. The anisotropic displacement factor exponent takes the form: $-2\pi^2[\ h^2\ a^{*2}U^{11} + ...\ + 2\ h\ k\ a^*\ b^*\ U^{12}\ ]$

	U^{11}	U^{22}	U^{33}	U^{23}	U^{13}	U^{12}
Cu(1)	11(1)	18(1)	22(1)	2(1)	1(1)	0(1)
O(1)	18(2)	20(2)	21(2)	3(2)	4(2)	2(2)
O(2)	16(2)	25(3)	25(3)	4(2)	1(2)	1(2)
O(3)	35(3)	45(3)	27(3)	1(3)	14(2)	-6(3)
O(4)	24(2)	25(3)	22(2)	1(2)	3(2)	-6(2)
O(5)	20(2)	17(2)	28(3)	2(2)	5(2)	-1(2)
O(6)	22(3)	40(4)	58(4)	-3(3)	11(3)	-8(2)
O(7)	26(3)	26(3)	42(3)	1(3)	10(2)	2(2)
O(8)	17(2)	22(3)	31(3)	2(2)	-3(2)	4(2)
N(1)	9(2)	18(3)	27(3)	-2(2)	6(2)	-3(2)
N(2)	14(3)	20(3)	17(3)	0(2)	-1(2)	4(2)
N(3)	19(3)	17(3)	16(3)	2(2)	-2(2)	0(2)
N(4)	12(3)	24(3)	18(3)	3(2)	3(2)	5(2)
N(5)	13(3)	26(3)	20(3)	3(2)	1(2)	-1(2)
C(1)	12(3)	21(3)	22(3)	-1(3)	4(2)	3(2)
C(2)	15(3)	25(4)	28(4)	-3(3)	6(3)	-6(3)
C(3)	13(3)	30(4)	45(4)	-6(3)	7(3)	0(3)
C(4)	19(3)	20(4)	42(4)	0(3)	3(3)	6(3)
C(5)	17(3)	15(3)	27(3)	-3(3)	-2(3)	-2(2)
C(6)	15(3)	19(3)	16(3)	1(2)	7(2)	4(2)
C(7)	11(3)	25(4)	20(3)	2(3)	7(2)	-3(2)
C(8)	8(3)	21(3)	19(3)	-7(3)	-1(2)	-4(2)
C(9)	16(3)	30(4)	17(3)	-2(3)	5(2)	6(3)
C(10)	18(3)	35(4)	25(3)	0(3)	10(3)	0(3)
C(11)	33(4)	36(4)	27(4)	-4(3)	11(3)	-10(3)
C(12)	24(3)	26(4)	15(3)	3(3)	0(2)	4(3)
C(13)	31(4)	55(6)	24(4)	1(4)	8(3)	16(4)
C(14)	17(3)	38(4)	21(3)	1(3)	3(2)	2(3)
C(15)	22(3)	33(4)	32(4)	-9(3)	7(3)	2(3)
C(16)	23(3)	16(3)	22(3)	-4(3)	2(3)	-2(3)
C(17)	21(3)	18(3)	18(3)	6(3)	4(2)	3(3)
C(18)	11(3)	16(3)	22(3)	-2(3)	3(2)	2(2)
C(19)	17(3)	27(4)	19(3)	6(3)	0(2)	-6(3)
C(20)	15(3)	33(4)	20(3)	7(3)	-5(2)	0(3)
C(21)	30(4)	36(5)	44(5)	13(4)	14(3)	4(3)

C(22)	31(4)	29(4)	24(4)	3(3)	12(3)	1(3)
C(23)	54(6)	46(5)	27(4)	0(4)	9(4)	-1(4)
C(24)	58(6)	44(5)	38(5)	-3(4)	32(4)	8(4)
C(25)	23(3)	36(4)	22(3)	-3(3)	3(3)	-4(3)
Cu(2)	28(1)	42(1)	16(1)	6(1)	3(1)	-10(1)
O(9)	28(3)	31(3)	23(3)	4(2)	-7(2)	-4(2)
O(10)	22(3)	37(3)	18(2)	8(2)	5(2)	-6(2)
O(11)	35(3)	45(4)	46(4)	-12(3)	14(3)	-11(3)
O(12)	30(3)	38(3)	35(3)	-7(3)	18(2)	-7(2)
O(13)	44(3)	39(3)	22(3)	6(3)	-3(2)	-14(3)
O(14)	39(3)	36(3)	24(3)	-4(2)	2(2)	-6(2)
O(15)	30(3)	34(3)	51(4)	-5(3)	16(3)	2(2)
O(16)	39(3)	43(3)	30(3)	-7(3)	17(2)	-14(3)
N(6)	44(4)	36(4)	12(2)	-3(3)	6(2)	-20(3)
N(7)	22(3)	40(4)	22(3)	7(3)	9(2)	-4(3)
N(8)	31(4)	47(4)	16(3)	6(3)	-5(2)	-9(3)
N(9)	21(3)	28(3)	21(3)	3(2)	10(2)	-5(2)
N(10)	17(3)	35(4)	28(3)	11(3)	2(2)	7(3)
C(26)	43(4)	37(5)	21(3)	-6(3)	10(3)	-20(4)
C(27)	53(5)	49(5)	27(4)	-16(4)	21(4)	-26(5)
C(28)	60(6)	57(6)	23(4)	-11(4)	14(4)	-37(5)
C(29)	60(6)	48(5)	16(3)	-2(3)	3(3)	-32(5)
C(30)	51(5)	43(5)	19(4)	-2(3)	3(3)	-28(4)
C(31)	27(4)	41(4)	27(4)	0(3)	11(3)	-15(3)
C(32)	22(4)	34(4)	22(3)	5(3)	8(3)	-5(3)
C(33)	19(3)	33(4)	12(3)	0(3)	-1(2)	-5(3)
C(34)	21(3)	29(4)	19(3)	0(3)	9(3)	-3(3)
C(35)	35(4)	27(4)	21(3)	3(3)	14(3)	-5(3)
C(36)	50(5)	39(5)	74(7)	-14(6)	27(5)	1(5)
C(37)	26(4)	41(4)	22(3)	1(3)	1(3)	-5(3)
C(38)	22(4)	109(10)	43(5)	-7(6)	3(4)	-4(5)
C(39)	38(5)	36(4)	36(4)	-4(4)	-7(3)	-12(4)
C(40)	26(4)	32(4)	25(4)	2(3)	10(3)	-7(3)
C(41)	37(4)	45(5)	16(3)	4(3)	-5(3)	-19(4)
C(42)	17(3)	65(6)	22(4)	12(4)	1(3)	-4(4)
C(43)	17(3)	36(4)	27(4)	15(3)	2(3)	-4(3)
C(44)	18(3)	30(4)	27(3)	5(3)	3(3)	6(3)
C(45)	18(3)	27(4)	30(4)	3(3)	6(3)	3(3)
C(46)	44(5)	52(6)	56(6)	-11(5)	35(4)	-13(4)
C(50)	18(3)	50(5)	39(5)	6(4)	10(3)	-6(3)

O(17)	31(3)	45(4)	38(3)	-6(3)	12(2)	-2(3)
C(51)	40(5)	41(5)	38(5)	7(4)	21(4)	13(4)
C(52)	59(6)	37(5)	32(4)	1(4)	19(4)	8(4)
C(53)	32(5)	45(5)	45(5)	5(4)	0(4)	-6(4)
C(54)	70(8)	39(5)	56(7)	-12(5)	5(5)	-4(5)

Table 5. Hydrogen coordinates (x 10^4) and isotropic displacement parameters (Å^{2}x 10^3) for $Cu^{II}H_2$dippy.

	x	y	z	U(eq)
H(4)	8107	7502	9369	22
H(5)	8232	2867	9983	24
H(2)	13451	6312	9976	27
H(3)	14415	5361	10829	35
H(4A)	13583	4330	11294	33
H(7)	9610	7080	8893	22
H(9A)	7666	6878	10804	25
H(11A)	5217	6002	7973	47
H(11B)	4828	5926	8862	47
H(11C)	5746	5398	8684	47
H(12)	8558	5716	8145	27
H(13A)	9826	6673	7343	54
H(13B)	9266	5919	6929	54
H(13C)	10202	5874	7765	54
H(14A)	7370	6718	7983	38
H(14B)	7589	6522	7049	38
H(14C)	8133	7238	7574	38
H(15A)	7331	8168	10521	43
H(15B)	6284	7761	10637	43
H(15C)	6442	7968	9688	43
H(17)	9915	3223	10751	23
H(19)	7480	3643	8426	26
H(21A)	4726	4051	9281	53
H(21B)	5355	4656	9944	53
H(21C)	5316	3795	10232	53
H(22)	8462	3403	11381	32
H(23A)	10135	3222	12309	64
H(23B)	9354	3659	12787	64

H(23C)	10238	4113	12445	64
H(24A)	8912	4982	11454	65
H(24B)	8047	4597	11886	65
H(24C)	7906	4603	10854	65
H(25A)	8092	2461	8134	41
H(25B)	6851	2463	7811	41
H(25C)	7379	2057	8702	41
H(9)	4687	3220	6479	27
H(10)	4157	7922	6040	33
H(27)	6812	4714	2757	50
H(28)	6302	5740	1848	55
H(29)	5220	6665	2223	51
H(32)	5780	3521	5455	30
H(34)	2755	3780	6115	27
H(36A)	1817	5771	7310	78
H(36B)	3049	5855	7406	78
H(36C)	2600	5391	8113	78
H(37)	6473	3708	6962	36
H(38A)	7701	3442	6103	87
H(38B)	8228	3975	6894	87
H(38C)	7844	4321	5942	87
H(39A)	6838	5252	6639	59
H(39B)	7008	4852	7567	59
H(39C)	5853	4983	7005	59
H(40A)	3105	2610	6824	41
H(40B)	2521	3141	7386	41
H(40C)	3754	3017	7675	41
H(42)	3494	7359	4755	42
H(42A)	3627	7366	4754	42
H(44)	5769	7246	7221	30
H(46A)	3191	8055	8447	70
H(46B)	4040	7561	9092	70
H(46C)	3013	7171	8537	70
H(47A)	2623	6136	5394	53
H(47B)	2871	5890	5396	27
H(48A)	2674	7009	6470	70
H(48B)	1504	6961	5913	70
H(48C)	2233	7652	5779	70
H(48D)	2653	6883	6312	44
H(48E)	1514	6660	5779	44

H(48F)	2087	7387	5507	44
H(49A)	1682	7233	4104	93
H(49B)	1090	6520	4387	93
H(49C)	2005	6401	3875	93
H(49D)	1940	6750	3871	56
H(49E)	1178	6261	4318	56
H(49F)	2071	5856	3936	56
H(50A)	6428	8207	6427	53
H(50B)	6655	8403	7439	53
H(50C)	5725	8815	6782	53
H(51A)	10420	3189	8954	45
H(51B)	9634	3310	8035	45
H(52A)	10833	4158	7641	62
H(52B)	11570	4059	8583	62
H(52C)	10448	4442	8481	62
H(53A)	9686	2113	7496	50
H(53B)	10372	1823	8403	50
H(54A)	11030	1751	6809	85
H(54B)	10602	1046	7258	85
H(54C)	11679	1436	7715	85
H(55A)	51	2602	4777	162
H(55B)	534	3368	4510	162
H(56A)	229	3961	5627	181
H(56B)	628	3276	6271	181
H(56C)	-539	3277	5702	181
H(57A)	1792	2710	4063	57
H(57B)	1494	1905	4394	57
H(57C)	1555	2252	4102	80
H(57D)	1356	1667	4821	80
H(58A)	3416	2059	4365	29
H(58B)	3214	1720	5254	29
H(58C)	3505	2590	5196	29
H(58D)	3077	1693	4478	60
H(58E)	3015	1639	5477	60
H(58F)	3257	2429	5076	60

X-ray Data Collection, Structure Solution and Refinement for $Cu^{II}H_2$dippy.

A blue crystal of approximate dimensions 0.406 x 0.390 x 0.182 mm was mounted in a cryoloop and transferred to a Bruker SMART APEX II diffractometer. The APEX2[1] program package and

the CELL_NOW[2] were used to determine the unit-cell parameters. Data was collected using a 60 sec/frame scan time for a sphere of diffraction data. The raw frame data was processed using SAINT[3] and TWINABS[4] to yield the reflection data file (HKLF 5 format)[4]. Subsequent calculations were carried out using the SHELXTL[5] program. The diffraction symmetry was 2/*m* and the systematic absences were consistent with the monoclinic space group $P2_1$ that was later determined to be correct.

The structure was solved by direct methods and refined on F^2 by full-matrix least-squares techniques. The analytical scattering factors[6] for neutral atoms were used throughout the analysis. There were two of the same molecules in different orientations per unit cell. Hydrogen atoms were included using a riding model.

Least-squares analysis yielded wR2 = 0.1550 and Goof = 1.134 for 797 variables refined against 8740 data (0.74 Å), R1 = 0.0578 for those 8033 with $I > 2.0\sigma(I)$. The structure was refined as a two-component twin, BASF[5] = 0.45001.

References

(1) APEX2 Version 2014.11-0, Bruker AXS, Inc.; Madison, WI 2014.

(2) Sheldrick, G. M. CELL_NOW, Version 2008/4, Bruker AXS, Inc.; Madison, WI 2008.

(3) SAINT Version 8.34a, Bruker AXS, Inc.; Madison, WI 2013.

(4) Sheldrick, G. M. TWINABS, Version 2012/1, Bruker AXS, Inc.; Madison, WI 2012.

(5) Sheldrick, G. M. SHELXTL, Version 2014/7, Bruker AXS, Inc.; Madison, WI 2014.

(6) International Tables for Crystallography 1992, Vol. C., Dordrecht: Kluwer Academic Publishers.

Definitions:

$wR2 = [\Sigma[w(F_o^2-F_c^2)^2] / \Sigma[w(F_o^2)^2]]^{1/2}$

$R1 = \Sigma||F_o|-|F_c|| / \Sigma|F_o|$

$Goof = S = [\Sigma[w(F_o^2-F_c^2)^2] / (n-p)]^{1/2}$ where n is the number of reflections and p is the total number of parameters refined.